UNIVERSITÀ DEGLI STUDI DI MILANO

SCUOLA DI DOTTORATO

SCIENZE BIOCHIMICHE, NUTRIZIONALI E METABOLICHE

DIPARTIMENTO DI SCIENZE VETERINARIE E SANITA' PUBBLICA

CORSO DI DOTTORATO DI RICERCA IN BIOCHIMICA CICLO XXV

TESI DI DOTTORATO DI RICERCA

PROTEIN TYROSINE NITRATION UNDER NORMAL PHYSIOLOGICAL CONDITIONS IN CELLULAR AND ANIMAL MODELS

Dott.ssa Elisa Margherita **MAFFIOLI**

Matricola n° R08818

Docente guida: Prof.ssa Gabriella TEDESCHI

Coordinatore: Prof. Francesco BONOMI

ANNO ACCADEMICO 2011-2012

To my family

Index

Summary

The significance of NO_2Tyr *in vivo* is highlighted by observations that nitrated proteins are markedly elevated in a broad range of human diseases and clinical disorders. The presence of nitrated tyrosine residues was detected in human fluids and pathological tissues such as atherosclerotic plaques of coronary vessels, amyotrophic lateral sclerosis, and Alzheimer's lesions, among many others.

Although the accumulation of nitrated proteins correlates well with many disease states and is considered a marker of oxidative stress under pathological conditions, substantial evidence has accrued that protein tyrosine nitration is a post-translational modification playing a role in physiological processes, including signal transduction, neuronal differentiation, and embryonic development.

On this regard, the aim of the research presented in this PhD thesis is to better understand the significance of protein nitration under normal physiological conditions focusing on differentiation and developmental processes.

The PhD thesis is divided in four parts. The first introductory part is dedicated to presenting the biological functions of nitric oxide and its cellular effects in biological system. Particular attention has been devoted to protein tyrosine nitration and its pathological and physiological significance. Two different experimental models (cells and organism) have been used to investigate this issue: (a) a cellular model (PC12 cells) to discuss the effects of micro- and nanoscale topography on neuronal proliferation and differentiation and (b) an animal model (*Ciona intestinalis*) for studying the role of oxidative stress and NO-derived reactive nitrogen species (RNS) during *Ciona* development and metamorphosis-related events. In particular, as far as the first model is concerned, my studies were directed to the characterization of PC12 cells behavior on nanostructured TiO_2 films in the presence and in the absence of the classical inducer of differentiation NGF. In the second part of the thesis I present the experimental procedures used. Proteomics techniques, including mono- and two-dimensional electrophoresis, electroblotting and immunostaining, and mass spectrometry (MALDI-TOF and LTQ-Orbitrap Velos) have been used to study both experimental models. In the third

part the results obtained are reported. Our findings suggest that tyrosine nitration is a physiological event not necessary related to pathological processes and that this NO-mediated post-translational modification of proteins may be regarded as a direct way to NO-signaling transduction. Finally, in the last part I resume the main conclusions and present future perspectives.

Part 1- Introduction

1.1 NITRIC OXIDE IN BIOLOGICAL SYSTEMS

Nitric oxide (NO) is a versatile diffusible signaling molecule involved in numerous physiological and pathophysiological processes such as neuronal communication, host defense, regulation of vascular tone, platelet aggregation, and angiogenesis [1]. It is a relatively stable radical that diffuses from the site of production and interacts with targets without the need for special transporter or receptor. Unlike most other endogenous chemical mediators, which are stored in vesicles or are secreted, NO is a diffusible gas that readily permeates cell membranes. Because NO cannot be stored, its signaling specificity must be controlled at the level of synthesis by nitric oxide synthase (NOS).

1.1.1 NO biosynthesis

NO is biosynthesised from the amino acid L-arginine [2] which is a semi-essential amino acid since it can be synthesized from glutamate or produced by recycling citrulline in the citrulline-NO cycle with arginosuccinate synthase and arginosuccinate lyase. The overall reaction, catalysed by a family of enzymes called nitric oxide synthase (NOS), is the result of a complete series of oxido/reductive events, involving a large number of cofactors which bind to the enzyme (Figure 1).

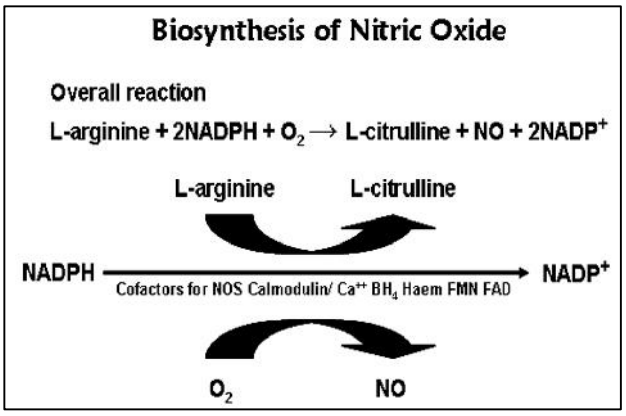

Figure 1. The biosynthesis of nitric oxide from L-arginine.

The co-factors for the reaction are not a side issue; their availability can be important for the activity of this pathway and therefore for NO formation.

Although NOS is the main NO source, in some special situations this molecule can be synthesized by other mechanisms. NO can be produced by the xanthine oxidase pathway or by H_2O_2 and L-arginine in a non-enzymatic way [3], or by the reduction of nitrites in acid and reducing conditions, as occurs in ischemic processes [4].

1.1.2 The nitric oxide synthases

Three isoforms were found: neuronal or nNOS, inducible or iNOS (macrophages) and endothelial or eNOS. Although these names are currently used, cells often express more than one isoforms. There is some evidence that another form of NOS may exist in the inner mitochondrial membrane (mNOS), at least in some tissue but not in all [5].

The enzyme consists of one oxygenase and one reductase domain. The oxygenase domain contains binding sites for haem, tetrahydrobiopterin (BH_4) and L-arginine and, it is linked, through a binding site for calmodulin (CaM), to the reductase domain which contains binding sites for flavin adenine dinucleotide (FAD), flavin mononucleotide (FMN) and nicotine adenine dinucleotide phosphate (NADP). In order to produce NO from L-arginine, the NOS isoforms require formation of dimers for full activity and the system needs to be fully coupled through BH_4. Any deficiency of BH_4 will lead to the formation of other products by reductase e.g. H_2O, H_2O_2 and superoxide anion ($O_2^{\bullet -}$), another free radical. Indeed, NOS enzymes are very versatile and can be switched from NO formation to the production of other reactive oxygen species, such as hydrogen peroxide, that have cell signaling properties and can even have similar physiological effects as NO.

NO has different physiological functions and therefore the enzymes are tailored for the location and stimuli where NO is required. The main areas are related to blood flow, neurotransmission and to non-specific immunity. The different NOS isoforms present similar activity in terms of NO production but they have different structural properties related to the various roles played by NO in the body.

eNOS is docked to the plasma membrane because it has hydrophobic anchors due to myristoylation and palmitoylation. It is located in regions of the plasma membrane associated with the accumulation of receptors for agents that regulate endothelial activity [6]. The most important physiological activation of eNOS occurs as the result of repeated stimulation by the pulsatile flow of the blood. With every heartbeat, small amounts of NO are produced in the endothelium to accommodate the increased blood flow by dilating the arteries.

nNOS is very similar to eNOS, but has no anchoring sites to hold the enzyme in the plasma membrane. It is expressed in population of developing and mature neurons [7] and has also been found in rat astrocytes [8]. nNOS and eNOS are Ca^{2+}-calmodulin-dependant enzymes constitutively expressed in mammalian cells [9] that produce NO at low levels in response to a stimulus lasting a few minutes. In contrast, iNOS is Ca^{2+}-calmodulin-independent and it is expressed following immunological or inflammatory stimulation in macrophages, astrocytes, microglia and other cells producing large amounts of NO.

1.2 CELLULAR EFFECTS OF NITRIC OXIDE

Because NO is involved in so many biological events, its synthesis, action and regulatory pathways have been studied by numerous investigators in numerous systems. Unfortunately, this has led to discrepancies in the literature and sometimes confusing results.

Two mechanisms of action for NO can be described:

(1) 3',5'-cyclic guanosine monophosphate (cGMP)-dependant, which involves the production of the second messenger, cGMP, following NO activation of NO-sensitive isoform of soluble guanylyl cyclase (sGC);

(2) cGMP-independent, which are mediated by reactive nitrogen species that are produced as a result of the interaction of NO with oxygen (O_2) or superoxide radicals ($O_2^{\bullet -}$) and lead to the direct modification of proteins such as S-

nitrosylation of reduced cysteine residues and the nitration of tryptophan and tyrosine residues.

1.2.1 Soluble guanylate cyclase activation

The soluble enzyme guanylyl cyclase (sGC) is a heme-containing protein that plays a key role within the NO/cGMP signaling cascade in vascular regulation and neurotransmission. The enzyme contains a prosthetic heme group that acts as the acceptor site for NO. High affinity binding of NO to the heme moiety produces a conformational change with the catalysis of guanosine-5'-triphosphate (GTP) in cGMP [10, 11]. cGMP, like cAMP, is a second messenger with important functions as intracellular signaling molecule in the regulation of various cellular events. Its formation is only the first step of the cascade of signaling mechanisms induced by NO. The cGMP produced can regulate a variety of specific protein kinases G (PKG), phosphodiesterase, cyclic AMP dependent kinases (PKA), and ion channels.

1.2.2 Nitric oxide and proteins modifications

Although the main NO cellular signaling pathway is the soluble guanylyl cyclase (sGC) activation, NO can also exert other cellular effects independent of sGC like the direct interaction with other reactive oxygen species. A particularly important result of these interactions is the modification of proteins with the concomitant alteration of protein function.

In particular, NO interacts with substances that have unpaired electrons in their molecular orbitals like metal complexes and oxygen species, namely O_2, $O_2^{\bullet-}$, which lead to multiple different effects [12].

When NO interacts with O_2 can produce NO^+, which in turn, interacts with thiols such as cysteine residues within proteins [13]. This can lead to S-nitrosylation of the thiols. Protein nitrosylation is a chemical reaction that has been demonstrated to affect the function of numerous proteins, including transcription factors and signaling molecules.

The DNA binding activities of both NF-kB and c-*Jun*, for instance, are inhibited when they are nitrosylated, affecting gene expression [14, 15]. Concurrent with the thought that to be an important regulatory event nitrosylation must be reversible, the laboratory of Stamler described a conserved de-nitrosylating enzyme [16].

NO can also interact with $O_2^{\bullet -}$. When this occurs, the strong oxidant peroxynitrite ($ONOO^-$) is formed [17] leading to nitration of tyrosine in proteins.

1.3 PROTEIN TYROSINE NITRATION

Tyrosine nitration is a covalent protein modification resulting from the addition of a nitro ($-NO_2$) group onto one of the two equivalent ortho carbons of the aromatic ring of tyrosine residues to produce the stable adduct 3-nitrotyrosine. The addition of the nitro group implies the formation of nitrating species, with nitric oxide providing the source of nitrogen [18]. *In vitro* and *in vivo* studies have indicated that several nitrating species, such as nitrogen dioxide, peroxynitrite, and nitrous acid can be formed *in vivo* either simultaneously or at different times depending on the cell type and the stimulus. For example, nitrite is a well-known substrate for hemeproteins [19-21] and its conversion to nitrogen dioxide could account for the nitration of tyrosine residues. Moreover, the formation of peroxynitrite by the reaction of nitric oxide and superoxide and, the subsequent reaction of peroxynitrite with CO_2 lead to the formation of an intermediate capable of nitrating tyrosine residues in proteins [22]. Another pathway is the formation of the nitrous acid by the acidification of nitrite [23]. Although this process requires a significant drop in pH, HNO_2 could nitrate protein slowly and indeed in some models the slow accumulation of nitrotyrosine has been observed without an apparent need for superoxide or hydrogen peroxide [24].

Overall, the data presented until now, do not confirm the existence of a single pathway but rather reaffirm previous speculations [18] that a multitude of biological reactions could be responsible for the nitration of tyrosine residues in proteins.

1.3.1 The formation of peroxynitrite

Although oxygen is itself a free radical, the body also makes other oxygen free radicals and reactive oxygen species such as hydrogen peroxide. In mitochondria about one percent of the oxygen is incompletely reduced to water and so tissues constantly produce a radical species called superoxide anion ($O_2^{\bullet -}$). Furthermore, there are a number of other enzymatic systems that generate superoxide and hydrogen peroxide. Since superoxide is a potentially damaging species, there are good enzymatic defence mechanisms to prevent its accumulation like the enzyme superoxide dismutase (SOD). It breaks down the superoxide anion to hydrogen peroxide which is turned into water by the action of catalase or glutathione peroxidase. However a non-enzymatic reaction between NO and superoxide anion has a reaction constant which is about four times greater and, potentially may yield a product known as peroxynitrite, a powerful oxidant since it is both a reactive oxygen and a reactive nitrogen species.
The chemistry of the reaction is the following:

$$NO + O_2^{\bullet -} \rightarrow ONOO^- + H^+ \rightarrow ONOOH$$

The protonated form of peroxynitrite readily decomposes at physiological pH to form several products including the free radicals nitrogen dioxide and hydroxyl radicals which are extremely reactive:

$$ONOOH \rightarrow OH^- + NO_2^+$$
$$ONOOH \rightarrow OH^{\bullet} + NO_2^{\bullet}$$

Peroxynitrite is a powerful oxidant: it attacks proteins, nucleic acids and lipids [25]. In particular, proteins can be modified in several ways by peroxynitrite, e.g. oxidation of thiols, nitration of aromatic amino acids such as tyrosine and also some aliphatic ones.

1.3.2 Selectivity of protein tyrosine nitration in vivo

Nitration of proteins has been detected under physiological conditions in most organ systems and in a number of cellular models. The majority of the studies, however, have been focused on pathological condition and nitrated proteins have been detected and quantified in several major human diseases [26, 27]. Utilizing immunoprecipitation and proteomic approaches many studies have identified specific proteins that are modified by nitration *in vivo* such as low density lipoprotein in human atherosclerotic lesions [28], prostacyclin synthase in bovine atherosclerotic lesions [29], actin in kidney and hepatic tissue of mice with sickle cell disease [30], and α-synuclein in 1-methyl-4-phenyl-1,2,3,6-tetrahydropyridine (MPTP) model of Parkinson's disease [31].

Furthermore, electron microscopic (EM) examination of tissues has revealed intriguing subcellular localization of nitrated proteins. In human Parkinson's disease nitrated α-synuclein was found to decorate almost exclusively Lewys bodies, the hallmark protein inclusions in Parkinson's disease and dystrophic neuritis [32]. In the brain, under physiological conditions, EM analysis of nitrated proteins revealed localization in the outer mitochondrial membranes in dendrites, within asymmetric synapses in dendritic spines, synaptic vesicles in axon terminals, and astrocytic processes [33].

Overall, these data have provided evidence that protein nitration is a rather selective process that modifies specific proteins *in vivo*. Several factors could explain this apparent selectivity:

- the proteins are in close proximity to the site of generation of nitrating agents;
- the proteins are the most abundant proteins and/or contain a large number of tyrosine residues;
- the proteins contain tyrosine residues in a specific primary sequence or in a specific environment that promotes nitration.

1.3.3 Proximity to the site of generation of nitrating agents

Proteins located proximally to the site of generation of a nitrating agent encounter the nitrating agents first and therefore have a higher probability of being nitrated. In a variety of human and experimental models of the disease, nitrated proteins have been detected only at the site of injury and only within specific cell types [26, 27], suggesting that proximity to the sites of nitrating agent generation may determine the targets modified by nitration. Recent data also indicated that hydrophobicity might also play a role in directing the site of nitration in model peptides by different nitrating species [34]. However, these simple observations have not been confirmed *in vivo*.

Overall, the data suggest that proteins can be targeted for nitration if they are in close proximity to the sites of nitrating species generation and within the diffusion distance of these species.

1.3.4 Abundance of the protein

The intracellular concentration of proteins makes them reasonably good targets for modification by reactive nitrogen species. Therefore, based simply on the abundance of protein, it is expected that different proteins will be targeted for nitration in various cell types. However, published data [35] indicate that the pattern of nitrated proteins observed by Western blotting with anti-nitrotyrosine antibodies does not always correspond to major bands on Coomassie-stained gels. There appear to be a limited number of protein targets for nitration and the susceptibility to nitrative modification is not solely a function of size or abundance of a particular protein.

1.3.5 Abundance of tyrosine residues

The frequency of tyrosine occurrence in proteins is approximately 3-4 mol% which is similar to that of phenylalanine but substantially higher than that of tryptophan. Compared to the other two aromatic amino acids, tyrosine also does not pack well in the

interior of proteins. Thus, there is a relatively good probability that tyrosine residues in some proteins will be exposed to the surface of the protein. The surface accessibility of the two equivalent carbons CE1 and CE2 in the ortho position of tyrosine residues may be critical for allowing these residues to be modified by nitration. However, surface exposure of the CE1 and CE2 carbons of the aromatic ring does not appear to be the sole requirement for nitration. Since not all surface exposed tyrosine residues were susceptible to nitration [36], therefore it can be concluded that nitration occurs predominantly on surface exposed tyrosine residues but, the degree of surface accessibility of the two carbon atoms CE1 and CE2 of the aromatic ring did not always predict the tyrosine residue that is modified by nitration [35].

1.3.6 Primary sequence and local environment

Analogous to other modifications of tyrosine residues in proteins such as phosphorylation and sulfation, nitration may also follow similar sequence and structural requirements. Specific amino acid sequences serve as mechanisms for specificity in these other tyrosine-mediated signaling systems. It is possible that tyrosine could be a target of nitration if located within an analogous specific peptide sequence. However, to date there is little evidence supporting a unique sequence required for tyrosine residue nitration.

A more likely mechanism for specificity of tyrosine nitration appears to be a consequence of local environment of tyrosine residues within the secondary and tertiary structure of the protein. The secondary structure of the protein and the local environment of the tyrosine residue may be important in determining the site of nitration. Nearly all tyrosine residues that can be nitrated are found in loop structures. More importantly, the presence of a neighbouring negative charge within a few angstroms from the tyrosine residue may be critical in determining the site of nitration. Peptides with a glutamate at position -1 relative to tyrosine showed the highest efficiency for nitration. An alternative suggestion for the role of negative charge in directing nitration to a specific tyrosine residue is the increase in the local concentration of the nitrating agent near the tyrosine residue.

Known sites of tyrosine nitration appear to contain turn inducing residues, but not cysteine or methionine residues since cysteine and methionine residues represent alternative targets for the reaction with nitrating agents that may limit the reactivity with tyrosine residues [37]. The absence of cysteine residues also indicates that the tyrosine residues are not located near disulfide bridge(s), which can prevent sulfation and apparently nitration by sterically hindering access to the tyrosine.

In conclusion, a single factor does not satisfactory explain the selectivity of tyrosine nitration.

1.3.7 The pathological and physiological significance of tyrosine nitration

The significance of NO_2Tyr *in vivo* is highlighted by observations that protein-linked NO_2Tyr is markedly elevated in a broad range of human diseases and clinical disorders [18, 38].

The presence of tyrosine residues in proteins nitrated was detected in human fluids and pathological tissues such as atherosclerotic plaques of coronary vessels, amyotrophic lateral sclerosis, and Alzheimer's lesions, among many others [reviewed in 18]. Such observations associated the presence of 3-nitrotyrosine to peroxynitrite-induced oxidative stress in human pathological conditions.

Although the accumulation of nitrated proteins correlates well with many disease states and is considered a marker of oxidative stress under pathological conditions [12, 39, 40], substantial evidence has accrued that protein tyrosine nitration is a post-translational modification playing a role in physiological processes, including signal transduction [26], neuronal differentiation [41, 72], and embryonic development [40].

The biological implications of protein tyrosine nitration in the transduction of NO effects in cells have been suggested by the identification of *in vivo* substrates for nitration in neurones, astrocytes, brain spinal cord and in other cell types during apparently normal physiological condition. The diverse biological effects of protein nitration, including enzyme activation or inactivation and altered cell receptor function, differentiation and

proliferation, raise the issue of whether protein nitration is a signaling mechanism or simply a pathway of protein damage that indiscriminately induces downstream events.

An important challenge is to demonstrate a direct relationship between protein nitration and functional changes, because conditions that favour protein nitration can readily induce the concomitant oxidation of other amino acids that might play crucial roles in modulating protein function. Site-directed mutagenesis of specific protein Tyr residues might not always clarify this dilemma because nitration-sensitive Tyr residues could play essential structural or functional roles in their own right.

In summary, nitration of proteins appears to be a selective post-translational modification with potentially important biological functions, still not completely understood up to now.

1.4 MODELS FOR EXPLORING TYROSINE NITRATION IN PHYSIOLOGICAL PROCESSES

As previously discussed, many evidences suggest that there is a significant increase in tyrosine nitration in many neurological disorders such as Alzheimer or Parkinson. On the other hand, basal levels of Tyr nitration have been observed in protein from various species under physiological conditions [26]. On this regard, two different experimental models (cells and organism) have been used in the present study to investigate the biological significance of protein nitration in physiological processes:

a) a cellular model (PC12 cells) to discuss the effects of micro- and nanoscale topography on neuronal proliferation and differentiation. Since it has been proved that cells sense and react to nanotopography *in vitro* as well *in vivo*, we characterized the behavior of PC12 cells on nanostructured TiO_2 films of different roughness (20 and 29 rms) in the presence and in the absence of the classical inducer of differentiation NGF. In a previous study carried out in our lab, it has been demonstrated that NGF induces NO production by nitric oxide synthases (NOS) and that differentiation in PC12 cells grown on PLL-glass in the presence of NGF is associated to an increase in protein nitration. Therefore we detected

whether increased protein nitration is also observed during PC12 differentiation triggered by nanostructured TiO_2 films in the absence of NGF. The observed neuritogenesis triggered by the topography of ns-TiO_2 in the absence of NGF was studied with particular focus on the expression of NOS and the pERK1/2-NOS signaling pathway;

b) an animal model (*Ciona intestinalis*) useful for studying chordate evolution and development. In line with several reports demonstrating the occurrence of oxidative stress during developmental processes in some invertebrates, we investigated the role of oxidative stress and NO-derived reactive nitrogen species (RNS) during *Ciona* development and metamorphosis-related events.

In this study we aimed at demonstrating that tyrosine nitration occur under normal physiological conditions associated with differentiation and developmental processes. Our finding intends to reinforce the emerging notion of protein nitration as a direct way to NO-signaling transduction.

1° Experimental model (PC12 cells)

1.5 NITRIC OXIDE PATHWAYS IN THE BRAIN

Nitric oxide (NO) is a signaling molecule that acts as an unconventional neurotransmitter/neuromodulator in the brain.

The formation of NO in the brain follows similar pathways to its generation in other tissues. The brain express all three identified nitric oxide synthase (NOS) isoforms and the generated NO can act upon a number of both physiological and pathological targets [42]. It is significant that NOS activity in the brain is higher than in any other tissue.

The constitutive isoform nNOS in neurons requires calmodulin binding in order to generate NO [43]. As the action potential travels down the axon, upon reaching the terminal bouton the wave of depolarisation causes opening of voltage-dependant calcium channels in the membrane. The rapid influx of Ca^{2+} allows calmodulin to binds nNOS, facilitating the generation of NO. As free Ca^{2+} levels drop, calmodulin no longer binds nNOS, thus allowing short, tightly controlled bursts to NO to be produced. The inducible iNOS is a cytoplasmatic enzyme expressed following *de novo* enzyme synthesis [42, 44]. Many brain cells have the ability to express iNOS but do not express the enzyme in great amounts under normal condition. Control of iNOS expression, and therefore NO generation, is believed to be mainly at the level of transcription but post-transcriptional regulation also occurs. Although the mechanism of induction is still not completely understood, nuclear transcription factor kB (NF-kB) is implicated in iNOS induction [45].

NO also functions in the brain as a vasodilator for fine, local control of cerebral blood flow. eNOS isoform is involved in the process. eNOS, targeted to small invaginations in the cell membrane called “caveolae”, is believed to help preserving cerebral blood flow [43]. This third isoform is also dependent upon elevated intracellular levels of Ca^{2+} binding calmodulin and increasing NO biosynthesis. NO synthesised by eNOS and acting on the soluble guanylate cyclase in smooth muscle represents an endogenous factors regulating local and global blood flow in the brain. As the high metabolic demand of the brain and especially the neuron will not tolerate a reduced blood flow, the action of NO upon the vasculature in the brain is of utmost importance in ensuring sufficient cerebral perfusion.

Although metabolism of NO within the brain appears vital for normal cerebral functions, an even larger number of studies have, on the other hand, evidenced that neurodegenerative conditions such as Alzheimer's disease Parkinson's disease and multiple sclerosis, involve NO in their pathogenesis [46, 47]. Its implication in several types of neuronal damage occurs when its production and release escape the control mechanisms and contribute to neurodegenerative processes. In fact, NO is a reactive free radical that can give rise to both nitrosative and oxidative stress through nitrosation, nitration or nitrosylation of various organic molecules, lipid peroxidation, DNA damage, impairment of mitochondrial function and eventually neuronal death [48, 49]. Dysregulation of NO production and release has been therefore proposed as an important primary or aggravating factor in several neurodegenerative pathologies, both acute and chronic, as well as in aging [50-52].

During the last few years, however, a growing amount of data has experimentally substantiated the early notion of a primary cell-protective and neuroprotective action physiologically mediated by NO [53, 54, and 49]. The concept that a physiological amount of NO is necessary to keep neurons alive and healthy and that, conversely, its absence or inhibition may exacerbate neuropathology, has gained substantial support by several recent researches.

In summary, nitric oxide is a signaling molecule mediating a variety of actions in the nervous system as well as in the cardiovascular and the immune system. Besides playing a role as a modulator of neuronal function in neurotransmitter release, synaptic plasticity, excitability, and learning, NO is also implicated in different stages of neuronal differentiation and development. NO is involved in the development of the visual system of *Drosophila* [55], controls neurogenesis in the vertebrate brain and mediates transition of a neural precursor cell from proliferation to differentiation.

1.5.1 Nitric oxide in neuronal differentiation

Several interesting new results have been accumulated during the last years on earlier stages of neurogenesis, in particular on control of precursor proliferation and initial

differentiation. To study neuronal differentiation and specific growth factor signaling mechanisms, the rat pheochromocytoma (PC12) cell line has been widely used as a neuronal model system. When exposed to physiological levels of neurotrophin nerve grow factor (NGF), these cells assume many of the features of sympathetic neurons including cell cycle arrest, survival in serum-free medium, and elaboration of long neuritis [56-61]. Besides NGF, which is the classical inducer of differentiation, cAMP-elevating agents, such as PACAP (Pituitary Adenylate Cyclase Activating Polypeptide), dorsomorphin and forskolin, promote growth arrest and neuritogenesis [62, 63]. In NGF-free media, it has been reported that proteins in the extracellular matrix (ECM) [64, 65], electric stimulation [66], and electroactive surfaces promote neuritis outgrowth [67].

In 1995, Peunova and Enikolopov demonstrated that the growth arrest and differentiative effect of NGF on PC12 cells is mediated by NO [68]. They showed that NO acts as a cytostatic agent, that NGF induces NOS expression in parallel with the proceeding of differentiation and, that NOS inhibition leads to reversal of NGF-induced cytostatis and thereby prevents full differentiation of cells towards neuronal phenotype.

However, in the absence of NGF, NO itself has the ability to produce neurite outgrowth by ERK activation through NO-cGMP-PKG pathway [69].

They also demonstrated that the most visible consequence of NGF action on PC12 is neurite outgrowth (Figure 2) and this is also affected by NOS inhibition. Under normal conditions, almost every cell gradually extended neuritis in response to NGF but, when PC12 are treated with a combination of NGF and NOS inhibitor, the number of cells with neuritis decreases dramatically. Their results suggest a model for NGF in PC12 cells in which at least three stages can be outlined. In the first proliferative stage, NGF activates a cascade of genes, eventually leading to the induction of the NOS gene. In the second stage, the accumulated NOS enzyme produces enough NO to inhibit DNA synthesis and, probably, to alert further checkpoint, thereby blocking further progression of the cell cycle, completing the proliferative phase of NGF action, and switching the cells to the cytostatic phase; probably, NO also directly induces some of the later differentiation markers by promoting gene activity. Finally, as soon as the cell perceives and processes

the cytostatic signal, it starts to implement the remaining program of differentiation traits (such as neurite outgrowth), which can only occur after cell division has ceased [68].
Overall, these data suggested that NO plays a role as a negative regulator of cells proliferation and an inducer of their differentiative pathways.

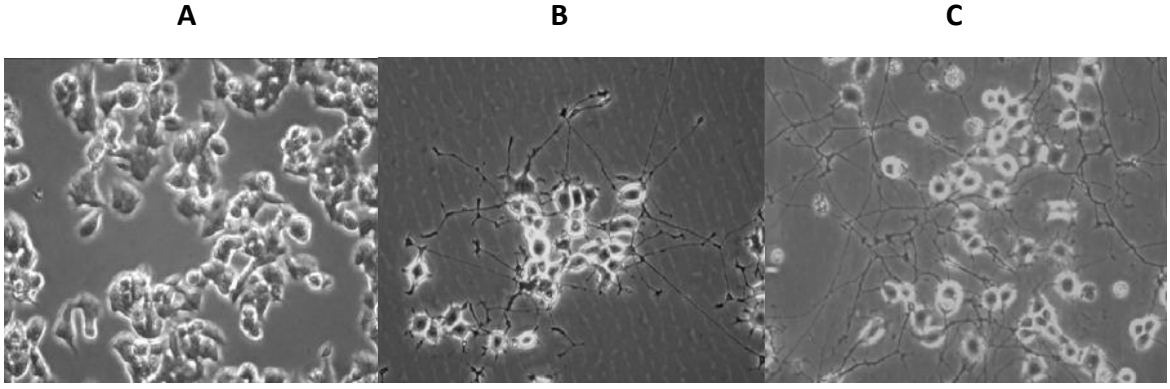

Figure 2. Phenotype of PC12 cells treated with NGF. **A)** PC12 cells at 0 day of differentiation; **B)** PC12 cells after 2 days of differentiation; **C**) PC12 cells after 5 days of differentiation.

1.5.1.1 Cytoskeletal proteins as target of nitration in PC12 cells

The neuronal cytoskeleton is composed of three interconnected filaments: microtubules, the actin microfilaments and intermediate filaments (IFs).

Microtubules serve as structural components within cells and are involved in many cellular processes including mitosis, cytokinesis, and vesicular transport. Microtubules are polymers of α- and β-tubulin dimers. The tubulin dimers polymerize end to end in protofilaments. Typically, the protofilaments arrange themselves in an imperfect helix with one turn of the helix containing 13 tubulin dimers each from a different protofilament.

Another important feature of microtubule structure is polarity. Tubulin polymerizes end to end with the α subunit of one tubulin dimer contacting the β subunit of the next. Therefore, in a protofilament, one end will have the α subunit exposed while the other end will have the β subunit exposed. These ends are designated (-) and (+) respectively.

Microtubule dynamics can also be altered by drugs: nocodazole and colchicines block the polymerization of tubulin into microtubules.

Microfilaments are solid rods made of a globular protein called actin. It polymerizes in a helical fashion to form an actin filament. Actin filaments provide mechanical support for the cell, determine the cell shape, enable cell movements and participate in certain cell junctions, in cytoplastic streaming and in contraction of the cell during cytokinesis. In muscle cells they play an essential role, along with myosis, in muscle contraction. Actin is one of the most abundant proteins and it is highly conserved.

The microfilaments are the thinnest component of the cytoskeleton. Much like the microtubules, actin filaments are polar, with a fast growing plus (+) or barbed end and a slow growing minus (-) or pointed end. These filaments have the appearance of a double-stranded helix.

Whereas microtubules and actin filaments are dynamic structures known to play key roles in neuronal development and function, such as establishment of neuronal cell shape, migratory processes, axonal outgrowth, synaptic plasticity, and intracellular transport, the functions of **Intermediate filaments** (IF) proteins in neurons have remained, until recently, more elusive. They differ from actin microfilaments and tubulin microtubules in their distribution in the cytoplasm and nucleus, their diverse primary structure, their nonpolar architecture, and their relative insolubility. Intermediate filament proteins are regulated by several post-translational modifications, including phosphorylation. These modifications and protein associations contribute in key ways to the function and dynamics of intermediate filaments.

IF proteins confer intracellular scaffold and mechanical stability to eukaryotic cells. Five major types of IF proteins are expressed in adult neurons: the three neurofilament proteins (NFTPs) (neurofilament light chain (NF-L), medium chain (NF-M) and heavy chain (NF-H)), peripherin, and α-internexin.

The abnormal accumulations of IFs are a pathological hallmark of many human neurodegenerative disorders including amyotrophic lateral sclerosis (ALS), dementia with Lewis bodies, Parkinson disease, and neuropathies. Studies with transgenic mice over

expressing IF proteins provide evidence that disorganization of the neuronal IF network can sometimes provoke neurodegeneration.

All IF proteins share a homologous central rod domain of approximately 310 amino acid residues that forms a highly conserved α-helical region. This rod domain is responsible for the formation of coiled-coil structures. The central rod domains are flanked by amino-and carboxy-terminal regions, also called the head and tail domains. The two end domains are less conserved and they confer functional specificities to the different types of IF proteins. The IF assembly involves the formation of two coiled-coil dimmers of protein subunits, which line up in a half-staggered fashion to form an antiparallel tetramer. The lateral and longitudinal association of tetramers makes up the final filament.

Neurofilament proteins constitute the major IF type in adult neurons. They are made up by the copolymerization of NF-L (61 kDa), NF-M (90 kDa) and NF-H (115 kDa) proteins. Neurofilaments are obligate heteropolymers requiring NF-L with either NF-M or NF-H for proper polymer formation. In contrast, peripherin and α-internexin can self-assemble into homopolymers and also co-assemble with neurofilament proteins.

Peripherin is a 57 kDa type III intermediate filament (IF) protein that was first identified in neuroblastoma and pheochromocytoma cells [70]. Peripherin may play an important role in neurite elongation during development [71]. In the adults, peripherin is almost exclusively expressed in the neurons of peripheral nervous system (PNS), and in the CNS only in neurons directly projecting to the periphery, and normally, it is undetectable in most brain neurons. Like others IFs, peripherin is heavily phosphorylated.

At the present, the biological functions of peripherin, especially in the brain, are still poorly understood.

Recently, there are evidences that some of the cytoskeletal proteins discussed above may be target of nitration. In our laboratory, we have concentrated on the presence, localization and subcellular distribution of nitrated proteins during NGF-induced neuronal differentiation in PC12 cells. In particular, our experiments suggested that tyrosine nitration of proteins is implicated in the pathway triggered by NO during NGF-induced neuronal differentiation.

Basal levels of nitrated proteins have been identified in neurones before [33], but no direct and positive correlation was known, between the appearance of nitrated proteins and the progression of neuronal differentiation.

By immunoblot analysis we identified basal levels of nitrated proteins in PC12 cells grown in the absence of NGF. In the presence of the neurotrophin, we found a significant increase starting from 2 days showing that nitrated proteins accumulate in PC12 cells in response to NGF. The presence of moderate levels of nitrated proteins in unstimulated PC12 cells is not surprising if we consider that these cells endogenously generate NO from constitutive nNOS and that nitrated proteins have been found, at basal level, in certain cell types suggesting a role of such post-translational modification in physiological processes. We also demonstrated that this event is coupled to activation of nitric oxide synthase (NOS) [72].

Looking for the molecular event triggered by NO in nerve growth factor (NGF)-induced neuronal differentiation, we reported that the nitration of PC12 proteins is not uniform across all proteins. Specific proteins appear to be targeted for nitration during neuronal differentiation and we observed that this modification occurred mainly among the cytoskeletal proteins. Many of them were identified by MALDI-TOF analysis: tau, peripherin, β-tubulin, neurofilaments triplet-L, β-actin and α-tubulin [41, 73]. We confirmed the presence of nitrated peripherin, tau and α-tubulin also in rat brain [73, 74]. This is consistent with a recent paper on endogenously nitrated proteins in mouse brain showing that there is an approximate 2- and 3-fold preference for nitration of mitochondrial and cytoskeletal proteins [75]. Our finding of α-tubulin being subjected to tyrosine nitration during the progression of neuronal differentiation is of particular interest since very little is known regarding the occurrence of this modification on α-tubulin *in vivo* and its possible functions. It has been reported that cultured cells incubated in the presence of free 3-nitrotyrosine selectively incorporated this modified amino acid into the extreme carboxyl terminus of α-tubulin resulting in microtubule dysfunction and alteration in cell morphology [38] or microtubule destabilization and prevention of complete myogenic differentiation [76]. These studies suggest that nitration of α-tubulin in the C-terminus could be deleterious for cell function. However,

using a proteomic approach to identify proteins nitrated *in vivo* during inflammatory challenge, a recent paper shows that α-tubulin is one of the few nitrated proteins in unstimulated cells and that its levels do not increase following a proinflammatory stimulus, suggesting that it is not a specific target during this pathological process [77].

Moreover, nitrated α-tubulin has been identified in a specific region of the nervous system in invertebrates [78] and in chorioallantoic membrane during chick embryo development [40]. Consistent with these papers, we found that nitration of α-tubulin may indeed occur in cells under physiological conditions.

As reported for other known post-translational modifications of tubulin, it is therefore possible that tubulin nitration could play a role in regulating microtubule behavior during neuronal morphogenesis.

Interestingly, Palumbo et al. [78] proposed that α-tubulin nitration could be a natural mechanism of cytoskeletal protein turnover. In accordance with this hypothesis, many papers showed that certain proteins after nitration are targeted for degradation by the proteasome [79, 80].

In our laboratory, we also demonstrated that, in differentiating PC12 cells, the change in the subcellular distribution of tyrosine-nitrated proteins could depend or be related to microtubule stabilization. In fact, nitrated tubulin may be incorporated in microtubules that are labile and depolymerize during the extraction procedure in the first days, but that become more stable in the progression of differentiation. Alternatively, nitration could be itself a signal conferring stability to microtubules. A further interesting hypothesis is that nitration of proteins in physiological processes might mimic or interfere with other post-translational modifications occurring on tyrosine residues such as phosphorylation [81]. α-tubulin is an *in vivo* tyrosine kinase substrate, which is phosphorylated in the neuronal differentiation pathway of PC12 cells in response to NGF [82], and the degree of tyrosine phosphorylation of α-tubulin has been suggested to be an important factor in determining the state of assembly of microtubules [83, 84].

So, we can hypothesize that, during neuronal differentiation of PC12 cells, nitration of tyrosine residues in α-tubulin could interfere with its phosphorylation state and,

consequently, regulate microtubule dynamics during induction of neurite extention. A second major result of our research regards the finding of nitrated TAU.

Tau is a member of the microtubule-associated protein that modulates microtubule structure and dynamics. It is an abundant microtubule-associated protein in neuronal cells and it has been implicated in axonal growth and development of neuronal polarity [85]. A key role of Tau in neurite outgrowth has been reported in cultured cells including PC12 cells induced to differentiate with NGF [86].

We found that nitration of TAU protein occurs in differentiating PC12 cells and that the modified protein is associated with the cytoskeletal fraction. Until now, there was only a single report that TAU protein could be nitrated and, it was linked to a pathological event as the formation of filaments TAU inclusions in neurodegenerative pathologies [87]. Our data suggested that nitration of TAU may be a physiological process, in agreement with recent papers, suggesting the physiological nitration of cytoskeletal proteins in different model systems from invertebrates to mammalian cultured cells [40, 72, 88].

Overall, our studies indicate that nitration could be a novel post-translational modification that regulates TAU function in neuritogenesis and differentiation. In addition, we also hypothesize that nitration of TAU in physiological conditions might mimic or interfere with other post-translational modifications occurring on tyrosine residues such as phosphorylation, as emerging for other cytosolic and cytoskeletal proteins [81, 88]. Therefore, nitration of TAU might have a crucial role in the signal transduction pathway triggered by NO during neuronal differentiation.

In conclusion, our findings indicate that tyrosine nitration of proteins could be a novel molecular mechanism involved in the signaling pathway by which NO regulates NGF-induced differentiation in PC12 cells. Tyrosine nitration affects mainly the cytoskeletal fraction within cells and the major cytoskeletal protein that is targeted by nitration is α-tubulin. Since the microtubule cytoskeleton plays an important role in controlling different spatial organizations in differently differentiated cells, we also suggest that tyrosine nitration might be an important event in the complex and dynamic organization of the cytoskeleton underlying neuritogenesis and differentiation. However many other experiments both *in vivo* and *in vitro* need to be carry out to sustain such hypothesis.

1.6 NANOSTRUCTURED MATERIAL: EFFECT ON ns-TiO_2 TOPOGRAPHY ON PC12 DIFFERENTIATION

1.6.1. The native extracellular matrix (ECM)

Culturing cells out of their natural niches requires a comprehensive insight into the biochemical and biophysical rules that dictate cell biology.

All cells reside in a complex microenvironment that is tailored to guide their physiological functions. As shown in Figure 3, the complex 3D cellular environment provides mechanical and biochemical signals that are important in guiding cell growth and function. Composition of the ECM dictates matrix stiffness, nutrient diffusion to tissues, and cell-matrix interaction, including cell adhesion and migration. Nonstructural factors, such as cell density, cell-cell interactions, and bound or secreted signaling proteins, are also important in guiding cell differentiation and function.

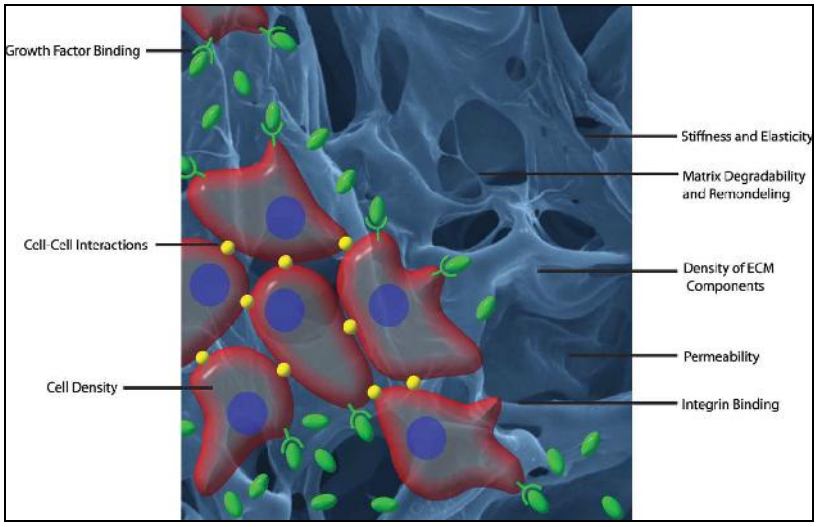

Figure 3. The complex 3D cellular environment provides mechanical and biochemical signals that guide cell function.

Structural elements of the ECM include a hydrated meshwork of polysaccharides, natural polymers (collagens, elastin, and fibrinogen) and adhesion proteins, as well as growth

factors, chemokines and cytokines. The more fibrous components (e.g., collagen and elastin) provide architectural rigidity and tension for the cells, while the non-fibrous components (predominantly glycosaminoglycans) regulate turgor pressure, form intimate intracellular connections, and modulate the binding and activity of growth factors. Additional events, such as alternative splicing, proteolytic processing and glycosylation, increase the number of unique structures and expand the functions of these large, multifunctional molecules [89]. The cellular environment is paramount: during embryogenesis and differentiation into the three primary germ cell layers; in complex tissue and organ formation; throughout adulthood in maintaining homeostasis; and in response to insult. During early development highly organized chemical gradients in the ECM guide cell migration to form the gastrula. Cell differentiation is further directed through morphogenesis and organogenesis by both cell-matrix and cell-cell interactions [90]. Most cells in the body are maintained in a quiescent state following embryogenesis; however, proliferation and differentiation of some specialized cells (such as hematopoietic progenitor cells) are continually regulated by ECM interactions. In addition, the ECM has been shown to be instrumental in physiological response to wounding and infection [91, 92]. The vital instructive cues in the cellular microenvironment include cell binding interactions, mechanical and structural support, and the presentation of regulatory molecules.

1.6.1.1 Cellular adhesion to the ECM

The matrix environment in which cells are grown influences the type and extent of cellular adhesion, which in turn affects cell proliferation [93]. Integrins are the primary cell surface receptors that are responsible for cell-matrix adhesion. They are composed of two transmembrane units: a large α subunit and a smaller β subunit that form non-covalent heterodimers in the presence of extracellular Ca^{2+} [94]. Various combinations of α- and β-subunits allow for the formation of 24 different heterodimers, which determine ligand specificity. Although some redundancy exists between integrin pairs and their respective ligands, the loss of almost any integrin has deleterious effects. Most

importantly, integrins not only act as anchors to the ECM but also transduce mechanochemical signals to the cell via intracellular transduction. Initial binding of integrins often leads to the clustering of additional specialized adhesive proteins and local remodeling of cytoskeletal and cytoplasmic proteins. The resulting focal adhesions sensitize cells to mechanical stimuli, including the rigidity and elasticity of the ECM.

Integrins bind a number of “insoluble” components of the ECM including laminin, elastin, and hyaluronan, among others The types and concentrations of these insoluble factors provide signals that are disseminated by the integrin family, promoting activation of diverse cytoplasmic proteins to control a number of cellular processes: differentiation, survival/apoptosis, cell polarity, gene regulation, actin organization, proliferation, and cell migration [94-96]. For example, the polarity of epithelial cells is essential in tissue organization for structural formation, and the directionality of product secretion. It has been shown that epithelial cell integrins must interact with a laminin-rich basement membrane to form the proper architecture and achieve normal cell function. Cells cultured in a 2D environment lack basal and apical membrane differentiation, while cells cultured in a 3D matrix may present appropriate integrins to maintain polarity.

Progress in elucidating the role of each integrin and its downstream regulation of cell behavior will aid in the design of more specialized ECM surrogates that are specific to a desired cellular outcome. The use of defined ECM scaffolds will provide greater insight into the impact of integrin-matrix interactions.

1.6.1.2 Density and stiffness of the ECM

Cells are not only sensitive to ECM adhesion but also to its density and stiffness. For example, cultured fibroblasts exhibited significantly different migration patterns when the density of the matrices was changed [97]. When ECM density was increased, by increasing concentrations of collagen, the migration of fibroblasts was reduced. Thus, an inverse correlation between matrix density and cell migration was observed while matrix ligand and integrin receptor concentrations were held constant.

An important work by Discher and colleagues demonstrated the importance of matrix elasticity on stem cell fate [98]. Mesenchymal stem cells (MSCs) were cultured on collagen-coated gels that mimicked the elasticity of various tissues. The MSCs responded to gel elasticity by differentiating into lineages that corresponded to the stiffness of the native environment (Figure 4 A). For example, MSCs cultured on soft gels, to mimic brain elasticity, developed a neuronal morphology with filopodia branching and spreading. Interestingly, medium stiffness gels, which mimic striated muscle elasticity promoted differentiation to myogenic cells, and the gels with the highest stiffness to mimic bone elasticity enhanced osteogenic differentiation.

Increasing matrix stiffness disrupts cell morphology, and leads to increased proliferation. As shown in Figure 4 B, increasing ECM rigidity elevates the activity of the Ras homolog gene family member A (RhoA), which subsequently induces cytoskeletal tension, decreases cell-cell contact, disrupts cell polarity, and increases growth rate.

A **B**

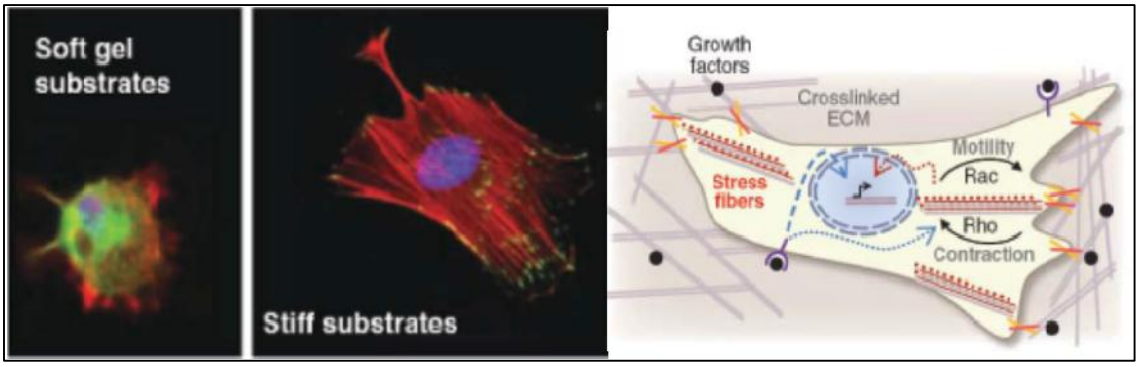

Figure 4. **(A)** Cells cultured on gels that mimic a soft tissue environment anchor less strongly to the substrate than cells cultured on gels that mimic a stiff tissue environment; **(B)** Signals from growth factors bound to the ECM affect cell function by mediating gene expression through various kinases such as Rho and Rac.

1.6.1.3 Permeability of the ECM

In addition to rigidity and elasticity, other architectural features of the ECM are also important in dictating cell behavior.

Metabolic activity requires access to nutrients and the removal of waste, both of which are primarily a function of diffusion. The porosity and permeability of the ECM directly affect the extent and nature of diffusion, and therefore influence cell processes.

To grow properly, cells require an ECM that permits the diffusion of nutrients and waste. The diffusion of other nutrients (proteins or steroid hormones) is dependent on the tortuosity and elimination pathways of the tissue. High cell density and dense ECM composition reduces the supply of nutrients to the interior of multilayered tissues, and prevents the removal of deleterious waste compounds. For instance, this phenomenon is very common in solid tumors that develop necrotic cores as a result of poor diffusion. As such, the overall permeability of the ECM affects the diffusion of nutrients and, consequently, affects cell differentiation and function.

1.6.1.4 Degradation and remodeling of the matrix

Following binding to the ECM, cells respond to the environment by releasing different proteases. The type of concentration of protease released depends on the composition of the ECM and its sensitivity to enzymatic degradation. In this manner, cells are defined by their environment, but also simultaneously remodel it. Most cells reside in a state of homeostasis, reaching full development at the end of embryogenesis. Some cells, however, go through significant physiologic changes at much later stages of development, requiring remodeling of the cell environment. Among these are cells of the mammary gland, which branch into ducts and terminal lobular units during puberty, and again change during pregnancy, finally reaching a fully developed state only after parturition. Epithelial mammary cells initially respond to hormone secretion and the elasticity of their environment by growing small projections. This is followed by remodeling of their environment through secretion of proteases, such as matrix metalloproteinase (MMP),

and enzymes, such as hyaluronidases. Degradation of the ECM changes the local modulus, decreases the number of cell-matrix adhesions, and also results in the release of ECM fragments that may possess biological activity. The cues that result from degradation are relayed back to the cell, guiding subsequent behavior and function. Thus, the ability of cells to remodel their environment, in concert with hormonal cues and reciprocal signaling, allows for proper functional development.

1.6.1.5 Cell-cell interactions

The cellular microenvironment includes cell-cell interactions where cell density alone can influence cell function. Moreover, different cell types invariably influence cell function. Cell-cell interactions are instrumental in recapitulating the native environment and promoting the morphogenesis of functional tissue. For example, mammary epithelial cells in situ maintain physical contact with neighboring myoepithelial cells via a combination of connections, including adherens and gap junctions. Adherens junctions generate the polarization of epithelial cells, leading to the development of basal and apical membranes that are required for proper secretory function. Cell-cell interactions are also required for appropriate phenotypic growth. Bhatia et al. have shown that hepatocytes co-cultured with fibroblasts restore the appropriate hepatocellular phenotype [99].

Overall, the cellular environment is paramount in guiding cell growth and function. The combination of the structural characteristics of the matrix, the types of cell-matrix adhesions, as well as other factors such as cell-cell interactions, and bound or secreted signaling proteins are all important aspects of the cellular environment that must be regulated for proper cell function.

1.6.2 Model ECMs

In the last few years cell and matrix biologist have long realized that understanding cell behavior within complex multicellular tissues requires systematically studying cells within the context of specific model microenvironment. Considering the impact of the ECM on

cellular behavior, tissue engineering has emerged as an excellent approach to create ECM models that mimic the regulatory characteristics of natural extracellular matrices (ECMs) and ECM-bound growth factors, both for therapeutic applications and basic biological studies.

Many of the physiological processes that occur *in vivo* can be reconstructed and recreated by simple 2D models which represent a versatile and accurate way to screen the effects of isolated compounds of the ECM on cells. However, recent findings suggest that 3D matrices provide better model systems for physiologic situations. Indeed, many physiological (examples exist in morphogenesis and organogenesis) and pathological (e.g., in tumor growth) cellular processes have been demonstrated to occur exclusively when cells are organized in a 3D fashion. Only to mention some examples, breast epithelial cells exhibited a tumoral trend when assayed in 2D, while regressed to normal state upon transferal to 3D models resembling their natural niche [100, 101]. Therefore, while 2D models embody a preliminary screening assays, three-dimensional matrices permit us to reconstruct the complexity that entails the native ECM and elucidate how physical and chemical variables affect cellular function.

The differences in cell behavior observed between 2D and 3D cultures come from perturbations in gene expression that stem from how the cell experiences its microenvironment differently in two dimensions as compared to the natural 3D surroundings (Figure 5).

For instance, cells plated onto 2D substrates are polarized, maintaining only part of their surface anchored and exposing remaining parts to the culture media. Moreover, the contact with neighboring cells is also limited to the flat edges that share each-others. This leads to unnatural, polarized integrin binding and mechanotransduction, which both affect intracellular signaling and phenotypic fate [102]. This is in sharp contrast with the natural environment of the tissues, where each cell closely interacts with the nearby cells and the ECM.

The inherent polarity also leads to unnatural interactions with soluble factors. In 2D culture, cells experience the homogenous concentration of nutrients, growth factors, and cytokines present in the bulk media with the section of the membrane that contacts the

surrounding media. In contrast, the concentrations of soluble factors that influence cell migration, cell-cell communication, and differentiation possess dynamic spatial gradients *in vivo* [103].

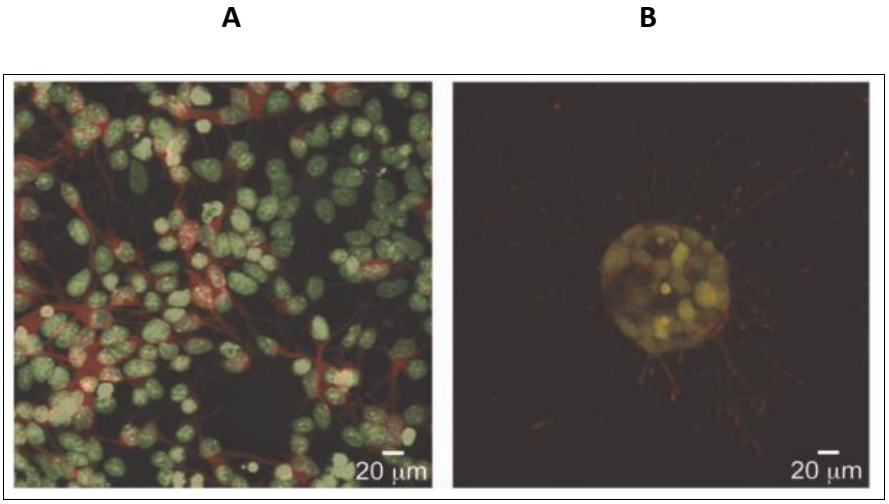

Figure 5. Cells experience a drastically different environment between 2D and 3D culture. For instance, neural cells cultured in monolayer (**A**) are constrained to extend processes in the plane. Cell bodies are stained green and β-tubulin in axonal extensions is stained red. When cultured within hydrolytically degradable poly (ethylene glycol) based hydrogels (**B**) the same cells form neurospheres and extend processes isotropically in three dimensions [104].

Morphology alone has been shown to influence subtle cellular processes such as global histone acetylation [105] as well as proliferation, apoptosis [106], differentiation, and gene expression. 2D culture confines cells to a planar environment and restricts the more complex morphologies observed *in vivo*. Furthermore, differences in migration exist between a 2D surface and a 3D environment. Not only is a cell confined to a plane in 2D, but also encounters little to no resistance to migration from a surrounding ECM. This applies to other phenomena that occur over longer length scales, such as cancer metastasis and tissue organization, where the behavior is regulated by mechanical interactions with the surrounding cellular microenvironment. Thus, to properly study cell physiology, mechanotransduction, and tissue morphogenesis *in vitro*, cells should be

cultured in 3D model microenvironments that recapitulate critical mechanical and biochemical cues present in the native ECM while facilitating hierarchical processes such as migration and tissue organization. Nonetheless, mimicking the ECM by our own means is not simple, especially because there is much we do not know yet about the cell-ECM cross-talk that occurs *in vivo*.

1.6.2.1 3D culture models

Tissue engineers and cell biologists have begun to develop material systems to culture mammalian cells within 3D ECM mimics to circumvent the limitations posed by traditional 2D cell culture. To this end, cells have been encapsulated within microporous, nanofibrous, and hydrogel scaffolds. However, in the last decade, nanostructured materials have received enormous interest due to their ability to promote the correct tissues growth *in vitro* and *in vivo*.

Microporous scaffolds allow for convenient encapsulation of cells but they contain porosities (~100 μm) greater than the average cell diameter (~10 μm); thus, they effectively serve as 2D scaffolds with curvature.

Nanofibrous scaffolds provide a 3D topology that better mimics the architecture formed by fibrillar ECM proteins; however, many are too weak to handle the stress needed for proper mechanotransduction. These limitations are not found in hydrogels, which capture numerous characteristics of the architecture and mechanics of the native cellular microenvironment [107].

Due to their ability to simulate the nature of most soft tissues, **hydrogels** are a highly attractive material for developing synthetic ECM analogs. These reticulated structures of cross linked polymer chains possess high water contents, facile transport of oxygen, nutrients and waste, as well as realistic transport of soluble factors. Furthermore, many hydrogels can be formed under mild, cytocompatible conditions and are easily modified to possess cell adhesion ligands, desired viscoelasticity, and degradability.

Hydrogels used for cell culture can be formed from a vast array of natural and synthetic materials, offering a broad spectrum of mechanical and chemical properties. The most

frequently used natural models for cells culture are typically formed of proteins and ECM components such as collagen, fibrin, hyaluronic acid, or matrigel, as well as materials derived from other biological sources such as chitosan, alginate or silk fibrils. Since they are derived from natural sources, these gels are inherently biocompatible and bioactive. They also promote many cellular functions due to the myriad of endogenous factors present, which can be advantageous for the viability, proliferation, and development of many cell types. On the other hand, hydrogels can be formed of synthetic molecules such as poly (ethylene glycol) (PEG), poly (vinyl alcohol) (PVA), and poly (2-hydroxy ethyl methacrylate). PEG hydrogels have been shown to maintain the viability of encapsulated cells and allow for ECM deposition as they degrade, demonstrating that synthetic gels can function as 3D cell culture platforms even without integrin-binding ligands. Such inert gels are highly reproducible, allow for facile tuning of mechanical properties, and are simply processed and manufactured.

However, among the scaffold currently in use, the majority are either complex or often ill-defined, making it difficult to determine exactly which signals are promoting cellular function. Even if these biosystems have provided seminal understanding for cell biology field in the past few decades, they are far from being ideal. Among the main limitations we can find a reduced flexibility to modulate their biophysical and biochemical properties, immunogenity, and batch-to-batch variability.

Assuming some of these limitations, in the last years **nanostructured materials** have received much attention because of their ability to mimic the extracellular matrix (ECM) nanotopography and physical, chemical and mechanical properties. The strong interest is motivated by growing evidences that the modulation of topographical and chemical cues at the nanoscale plays a relevant role in determining the cell interaction with the environment.

Some nanomaterials occur naturally, but of particular interest are engineered nanomaterials (EN), which are designed at the molecular (nanometre) level to take advantage of their small size and novel properties that are generally not seen in their conventional, bulk counterparts. The two main reasons why materials at the nano scale can have different properties are: **(1)** increased relative surface area and **(2)** new

quantum effects. Nanomaterials have a much greater surface area to volume ratio than their conventional forms, which can lead to greater chemical reactivity and affect their strength. Also at the nano scale, quantum effects can become much more important in determining the materials properties and characteristics, leading to novel optical, electrical and magnetic behaviors.

Common types of nanomaterials include nanoparticles, nanostructured surfaces, carbon nanotubes and quantum dots which are already being used in many commercial products and medical technologies for instance drug and gene delivery systems, cell therapies, organ printing, cell patterning, diagnostic systems and tissue engineering scaffolds.

1.6.3 The effect of surface topography

Cellular behavior *in vivo* and *in vitro* is influenced by mechanical, biochemical and topographical properties of the extracellular microenvironment where cells grow [89, 108, and 109].

The topography of the ECMs is characterized by features over different length scales ranging from the nano to the mesoscale and it regulates the cellular behavior in a way that it is still far from a complete understanding. The coexistence of ECM features at different length scales is probably one of the key factors, however it is not clear if there is a hierarchical organization of different structures and to what extent the various length scales can influence cellular response.

According to the most recent studies on biomaterials, cells can actively 'sense' and adapt to the surface of adhesion and activate specific intracellular signals that influence cell survival and behavior. *In vivo*, as described above, cell attachment is the consequence of the binding with specific cell adhesion proteins in the ECM, and it is intrinsically influenced, besides by receptor-ligand specific interactions, by the physical and mechanical signals arising from the topography of the external environment. *In vitro*, on the other hand, cells set up a complex network of interactions both with the artificial surface and with the secreted and serum ECM proteins.

Currently, nanostructured surfaces have attracted attention motivated by the existence of many functional nanoscale structures within tissue. For example, a study using the atomic force microscope (AFM) has quantified the fine structure of the basement membrane (basal lamina) underlying the corneal epithelium [110]. The results from that study, among the others, justify the interest for nanostructured substrates by revealing a very complex topographical structure composed of pores and networks of fibers with diameters around 70 nm as well as larger structures.

In this sense, in order to elucidate the role of substrate topography, a large number of studies have been devoted to the investigation of cell interactions with artificially produced nanostructures such as pits, pillars, grooves, dots or random structures obtained by chemically or physically etching metallic, semiconducting and polymeric surfaces [111, 112, 63]. The fabrication strategies employed to create synthetic substrates with tailored topography at the nano and microscale are essentially based on hard and soft lithography for the fabrication of ordered structures. These approaches top-down, despite the great improvements in miniaturization and accuracy, when not based on natural matrix-related proteins are not able to reproduce the morphology and the hierarchical organization typical of the ECMs [113]. Up to now, very few studies have been devoted to the elucidation of the interaction of cells with nanostructured materials obtained by the bottom-up approach of nanoparticle assembling. This is quite surprising since nanoparticle-assembled materials have an increasing role in the fabrication of biocompatible devices as well as diagnostic and therapeutic platforms; moreover, a bottom- up approach can offer more possibilities to organize the structure on a multi-length scale similar to that observed in ECM.

In the last years, several studies have been performed to investigate how topographical features can influence neuronal growth, orientation, and differentiation. Particular attention has been concentrated on the effect of micro- and nanoscale topography on axonal guidance and neuronal regeneration [63, 114, and 115]. It was observed that, in addition to serve as contact guidance, topography often works synergistically with the appropriate biochemical cues to regulate differentiation as well as proliferation [112]. Experimental results suggest that a combination of spatial, chemical and mechanical

inputs, together with the genetic properties and proteins expression in the cell, control the shape and functions of neuronal cells during neuron growth and differentiation [116, 117]. Ferrari and colleagues [reviewed in 63, 114, and 115] also suggested that nanotopographic guidance cues act cooperatively with NGF to regulate both the generation and the orientation of neurite even under conditions of sub-optimal NGF concentration in PC12 cells. Using nanostructured substrates, they showed that, in PC12 cells stimulated by various factors including NGF, neuronal polarization and contact guidance are based on a geometrical constraint of focal adhesions and that the maintenance of the established polarity is independent from NFG stimulation while strictly dependent on the topography of the substrate. Their results suggested that different neurotrophic molecules can modulate contact guidance and the underlying establishment of cellular adhesions with the substrate by the selective activation of specific molecular pathways. Therefore, the reading of the topographical guidance cues can be considered a function of the molecular differentiation pathway active in the cell [63].

Recently, Lamour et al. proposed that the physical properties of the substrates can be considered as a new kind of stimulus by observing that surface free-energy gradients at the nanoscale trigger neuritogenesis of PC12 cells in the absence of NGF or other inducers [118, 119]. They hypothesized that PC12 cells would respond to surface properties by secreting an unknown factor that may favor neuritogenesis, however they did not provide elements to clarify the mechanisms and the proteins involved in the physical signaling.

To address how the nanoscale stimuli distribution on a substrate is transduced into a signaling cascade, we studied the differentiation of PC12 cells on nanostructured titania substrates fabricated by nanoparticle assembling. We used nanostructured titania (ns-TiOx) as reference material since it is amongst the most studied and well-characterized biomaterials in biomedicine applications.

1.6.4 Nanostructured titanium

Nanostructured Titanium have been synthesized using Supersonic Cluster Beam Deposition (SCBD) [120] which offers the possibility to organize the structure of a surface on a multi-length scale similar to that observed in ECM. These films, resulting from a random stacking of nanoparticles, possess, at the nanoscale, a granularity and porosity mimicking those of typical extracellular matrix structures and adsorption properties that could allow surface functionalization with different macromolecules such as DNA, proteins, and peptides [121-125].

Recent works have characterized the biocompatibility of nanostructured TiOx films produced by the deposition of a supersonic beam of TiOx clusters [121, 123]. Interestingly, Carbone et al. explored the biocompatibility of this novel nanostructured surface with a wide range of cell lines (cancer and primary cells) in comparison with a surface which is commonly employed for culturing cells [121]. They observed that, in terms of morphological appearance and growth properties, cells adhere and grow on cluster assembled TiO_2 with similar modalities as on the reference biocompatible surface (i.e. gelatin-coated coverslips). They found the same cytoskeletal parameters (tubulin, actin and focal adhesion) both for cells grown on cluster assembled TiO_2 and on gelatin. So, their results strongly suggest that cluster-assembled TiO_2 is a biocompatible support that allows normal growth and adhesion of primary and cancer cells with no need for coating with Extracellular Matrix (ECM) proteins.

Therefore ns-TiOx films are universally considered highly biocompatible materials usable as optimal substrate for different applications in cell-based assays, biosensors, clinical implants or microfabricated medical devices.

The size of the clusters composing the ns-TiOx film, as well the size of many ECM proteins, are of the order of a few tenths of nanometers; as an immediate implication, on a sufficiently small scale (i.e. few hundreds of nanometers) the surface morphology of cluster-assembled ns-TiOx can mimic a generic ECM environment. Given that the topographic features of the substrate play an essential role, the morphology of cluster assembled ns-TiOx may favor the interaction of cells with its surface. So, it is of extreme

interest to quantitatively characterize the interaction of this new material with proteins, as this is the basis for controlling cell-surface interactions. Moreover, cluster-assembled titania thin films are optically transparent and free of defects causing visible light scattering. Hence they are also particularly suited for high-resolution and confocal microscopy characterizations.

Overall, their excellent mechanical strength, chemical stability, biocompatibility and their large nanoscale porosity, along with the abundance of adsorption sites and defects, make Ns-TiOx films an ideal tool for investigating the role of nanoscale roughness in cell-substrate interaction. By exploiting these properties, we used ns-TiO_2 with tailored nanoscale roughness to grow PC12 in the presence and in the absence of NGF in order to characterize the role of nanotopography on cell differentiation. We believe that understanding neuronal cell responses to nanostructured topographies is essential for the design of biomaterials that interface with the neuronal tissue.

2° Experimental model (*Ciona intestinalis*)

1.7 NITRIC OXIDE IN MARINE INVERTEBRATES

Since the discovery of the biological effects of nitric oxide (NO) more than two decades ago, NO has been identified as an important physiological modulator and a messenger molecule in mammals. Parallel to these studies, evidence accumulated in recent years has revealed that the NO signaling pathway is spread throughout the entire phylogenetic scale, being increasingly found in lower organisms, ranging from Chordata to Mollusca.

It has been shown that in marine invertebrates NO is involved in multiple processes that are related to feeding, defence, environmental stress, learning, metamorphosis, swimming, symbiosis, haemocyte aggregation and regulation of blood pressure. Some of the most interesting examples are reported below.

In the sponges *A. polypoides* and *P. ficiformis* NO is a cellular signal of environmental stress [126]. Exposure of sponges to heat stress increased NO production. Considering that sponges are the most primitive metazoan group whose evolution dates back 600 million years, the presence of NOS in particular dendritic cells coordinated in a sort of network in the sponge parenchyma may represent the most primitive NO-based sensorial network in the animal kingdom.

In *Octopus vulgaris* NO is reported to be involved in visual and tactile learning [127, 128]. Intramuscular injections of the NOS inhibitor NG-nitro-l-arginine methyl ester (l-NAME) block both types of learning.

In *Sepia officinalis* NO was found to be involved in the ink defence system, a characteristic behavior adopted by the animal to confuse predators and alert conspecifics to danger while retreating [129]. Ink defence depends on the activity of a highly specialized organ, the ink gland, which is responsible for the continuous production of the black insoluble melanin pigment that the animal accumulates in the ink sac and ejects on demand [130]. It has been reported that NO plays a role in the ink defence system both at ink gland and nervous system level.

Considerable attention has been also focused to the study of the possible role of NO in fertilization using marine invertebrates which represents good systems for developmental studies. The first evidence that NO could be a universal trigger for egg activation [131]

was disproved by subsequent studies. Simultaneous measurements of intracellular NO and free calcium levels at fertilization of the sea urchins *L. pictus* and *Psammechinus miliaris* [132] indicate that NO is not the primary egg activator but its levels rise after, not before, the calcium wave is initiated and is calcium dependent. So NO acts late during the fertilization response in the eggs and its function is to enhance and sustain calcium signal.

In the chordate *Ascidiella aspersa* NO has no role at fertilization [133] suggesting that chordates may have evolved a separate method of egg activation different from sea urchins.

In the chordate *C. intestinalis* NO activates ion channels in the oocytes. Treatment of *Ciona* unfertilized oocytes with a nitric oxide donor results in the generation of an inward current similar to the current induced by the fertilizing spermatozoon [134].

NO acts also at later stages of development: it is an endogenous inhibitor of metamorphosis in the marine snail *Ilyanassa obsoleta* [135], in the ascidians *Boltenia villosa* and *Cnemidocarpa finmarkiensis* [136] and in the sea urchin *L. pictus* [137].

The relative simplicity of the marine invertebrate systems with respect to mammals provides a valuable basis for further insights into the role of NO signaling pathways especially for what concerns those peculiar situations that may nonetheless reveal hitherto overlooked aspects of the physiology of this messenger molecule.

1.8 AN EMERGING MODEL ORGANISM: *CIONA INTESTINALIS*

Ciona intestinalis is currently recognized as the major model chordate in developmental and evolutionary biology. The tunicate (or urochordate) *C. intestinalis* is a solitary ascidian species that lives in shallow waters in the inter- to subtidal zones of most temperate coasts around the world. These sessile animals are usually found in groups attached to a variety of natural and artificial immersed material in harbours or in association with aquaculture equipment. The body is cylindrical with two siphons and a gelatinous translucent outer tunic, containing cellulose, which varies in colour from pale greenish/yellow to orange (Figure 6). In older individuals, the outer tunic becomes progressively more leathery and often takes on a brownish hue as a result of algal or

bacterial fouling. Inside the tough outer tunic is a thin sac-like membrane composed of an external epithelium, connective tissue, muscles and blood vessels which encloses the internal organs. Contraction of the longitudinal muscle bands and circular muscle fibres embedded in this membrane allow the organism to retract rapidly when disturbed. The body is divided into a large atrial cavity which contains the branchial sac and a smaller visceral cavity containing the digestive and reproductive organs [138].

Figure 6. Photograph of live *Ciona intestinalis.*

C. intestinalis is classified as a hermaphrodite in which the production of eggs and sperm is concurrent. However, in the very early stages of maturity, it shows a tendency towards protandric hermaphroditism: sperm production precedes egg production. Once individuals reach maturity gametes are produced continually as long as temperatures are suitable. Eggs and sperm are expelled through the exhalent siphon and fertilization occurs externally. After 18 hr of the embryonic development (Figure 7) a tadpole-larva is formed. The ascidian tadpole is composed of only 2600 cells, which constitute a small set of larval organs including the epidermis, central nervous system, notochord and tail muscle along with the rudiments of the adult gut, mesodermal organs and gonads. This configuration of

the tadpole, with the dorsal nervous system overlying a notochord, represents the basic chordate body plan.

Figure 7. The sea squirt *Ciona intestinalis*. (a) Adults are filter feeders with in-current and out-current siphons. The white duct is the sperm duct, while the adjacent orange duct contains eggs. (b–l) Embryogenesis. (b) Fertilized egg, (c) two-cell embryo, (d) four-cell embryo, (e) 16-cell embryo, (f) 32-cell embryo, (g) gastrula (,150 cells), (h) neurula, (i to k) tailbud embryos, and (l) tadpole larva. Embryos were dechorionated to show their outer morphology clearly. (m) A juvenile a few days after metamorphosis showing the internal structure. ds, digestive system; en, endostyle; ht, heart; OS, neural complex; and pg, pharyngeal gill. Scale bars: 1 cm (a), 50 mm (b, l) and 0.5mm (m).

Once fully formed, *Ciona* larva develops passing through different larval stages: early, middle and late according to Chiba et al. [139].

The first stage is of just hatched larvae, which have a rounded trunk and do not have a well-developed adhesive papilla. The second stage starts at about 2-4 hr after hatching.

These larvae have three adhesive papillae and a preoral lobe in the elongated trunk. Then, the last stage starts at about 4-9 hr after hatching. These larvae become competent acquiring the ability to sense, discriminate and respond to environmental cues that induces settlement and/or metamorphosis (Figure 8). Metamorphosis begins when larva sticks to a suitable substrate by the adhesive papillae, next the tail is retracted and resorbed. Then the larva rotates the body axis and begins tissue remodelling. The process involves numerous coordinated morphogenetic movements and physiological changes by which the larval tissues are destroyed or remodelled and eventually replaced by adult tissues and organs. A detailed description of the development of tissues and organs in larvae and juveniles has been recently carried out [139]. A wide variety of environmental stimuli and endogenous signals have been reported to induce metamorphosis.

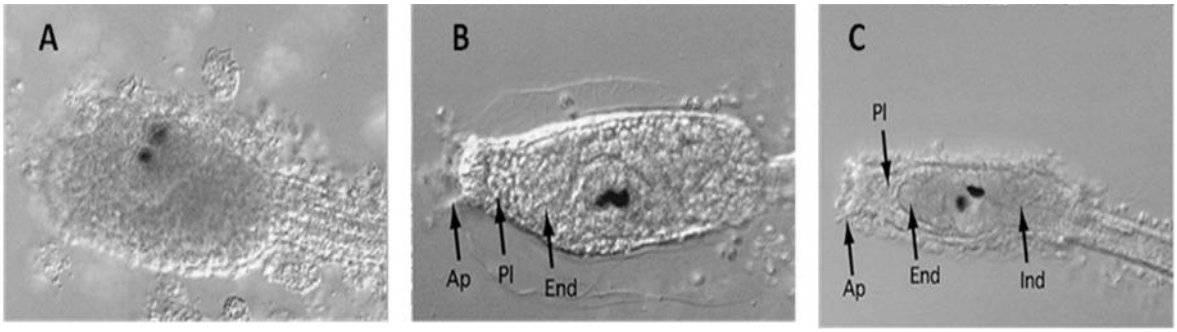

Figure 8. Early developmental stages of *Ciona intestinalis* larvae. (**A**) The early-swimming larva stage (0–2 hr after hatching). (**B**) The mid-swimming larva stage (2–4 hr after hatching). (**C**) The late-swimming larva stage (4–9 hr after hatching). Ap, adhesive papillae; Pl, preoral lobe; End, endostyle disc; Ind, intestine disc. Scale bars, 100 µm.

Recently, considerable interest has been focused to the isolation and characterization of the genes that are expressed during ascidian metamorphosis. In *H. curvata* a novel epidermal growth factor-like protein, Hemps, has been found to play a key role in the regulation of metamorphosis [140, 141]. Interestingly, no Hemps homologues can be found in *Ciona* genome [142], thus suggesting significant differences in the genetic networks operating at metamorphosis in different ascidians. In *Ciona* some genes have

been shown to be involved in the initiation of metamorphosis. Among these, six genes *Ci-meta1-Cimeta6* have been reported, but none of these is expressed in the tail before and during its resorption [143, 144]. Moreover, two other genes have been recently identified, *Ci-Sccpb* and *Ci-sushi*, which are expressed at the tip of the tail and in tail epithelia, respectively [145].

Apoptotic processes play an important role during the sequential events leading from hatching to metamorphosis of *Ciona* larvae [146, 147]. In particular, two apoptotic waves occur, at first in the central nervous system and soon after in the tail. The second wave originates at the tail extremity, propagates through cell to cell up to the tail base, promoting caspase-3-dependent apoptosis of tunic, epidermis, striated muscle and notochord cells [146]. It has been recently reported that the MAP kinases ERK and JNK are both required for the wave of apoptosis and metamorphosis in *Ciona* [145]. ERK is activated in the initial stages of larval development, in the papillae of swimming larvae, and later at metamorphosis in tail cells before the wave of apoptosis occurs. The JNK cascade is activated at the time of competence in the tadpole central nervous system, in the pharyngeal rudiment, sensory vesicle, neck, visceral ganglion and nerve cord. A model of metamorphosis has been proposed in which JNK activity in the CNS induces apoptosis in several adjacent tail tissues by expression of genes such as *Ci-sushi* [145].

1.8.1 Regulatory roles of NO during larval development and metamorphosis in C. intestinalis

The current interest in the physiological functions of NO in invertebrates has prompted many authors to examine the spatial and temporal expression of NOS as well as the localization and the possible role of NO during larval development and metamorphosis-related events.

Notably, the NO/cGMP signaling pathway, together with the stress-inducible protein HSP90, have been shown to be involved in the metamorphosis of the ascidians *Boltenia villosa* and *Cnemidocarpa finmarkiensis* [137]. Treatment of ascidian hatched larvae with NOS and guanylyl cyclase inhibitors, as well as with drugs that inhibit the function of

HSP90, increased the frequency of tail resorption [137]. NOS is expressed in the tail muscle cells of the ascidian larvae and it has been suggested that the NO/cGMP signaling regulates metamorphosis possibly in combination with HSP90 acting on NOS activity [148, 149].

Recently, it has been reported that NO is involved in larval development and metamorphosis of *Ciona intestinalis* [150]. This study provides evidence that nitric oxide (NO) regulates tail regression in a dose-dependent manner, acting on caspase-dependent apoptosis. An increase or decrease of NO levels resulted in a delay or acceleration of tail resorption, without affecting subsequent juvenile development. A similar hastening effect was induced by suppression of cGMP-dependent NO signaling. Inhibition of NO production resulted in an increase in caspase-3-like activity with respect to untreated larvae. Detection of endogenously activated caspase-3 and NO revealed the existence of a spatial correlation between the diminution of the NO signal and caspase-3 activation during the last phases of tail regression. Real-time PCR during development, from early larva to early juveniles, showed also that during all stages examined, NO synthase (NOS) is always more expressed than arginase and it reaches the maximum value at late larva, the stage immediately preceding tail resorption. The spatial expression pattern of NOS is very dynamic, moving rapidly along the body in very few hours, from the anterior part of the trunk to central nervous system (CNS), tail and new forming juvenile digestive organs. NO detection revealed free diffusion from the production sites to other cellular districts. Overall, the results of this study suggest a new important link between NO signaling and apoptosis during metamorphosis in *C. intestinalis* and hint at novel roles for the NO signaling system in other developmental and metamorphosis-related events preceding and following tail resorption.

In continuing the investigation of NO signaling during *Ciona* metamorphosis and molecular targets, we have chosen to investigate the role of oxidative stress and NO-derived reactive nitrogen species (RNS) in the process. We disclose an alternate signaling pathway of NO in *Ciona* metamorphosis which is mediated by protein tyrosine nitration targeted to ERK and snail.

Part 2- Materials and Methods

1° Model (PC12 cells)

Experimental procedures

2.1 SUBSTRATES

The substrates were prepared in the laboratory of Prof. Milani at The Interdisciplinary Centre for Nanostructured Materials and Interfaces (CIMaINa), University of Milan.

Poly-L-Lysine-coated glass cover slips (Colaver, 64MU4113) and microcrystalline TiO_2 films were used as reference samples for cell culture. Flat TiO_2 films were grown on glass slides by electron beam evaporation of a titanium target. The evaporated metal was partially oxidized during the deposition and almost fully oxidized in subsequent air exposure. To complete the oxidation and remove contaminants, these substrates were subjected to the same annealing process applied to nanostructured films, as described below.

Cluster-assembled ns-TiO_2 substrates were grown on clean glass slides by Supersonic Cluster Beam Deposition (SCBD) using a Pulsed Microplasma Cluster Source (PMCS), as described in detail in [120]. Figure 9 shows a schematic representation of the deposition apparatus. The source (PMCS) is composed by a ceramic hollow body inside of which is obtained a cylindrical cavity at whose end there is a solenoid valve which regulates the inlet of a high pressure gas. The opposite end is connected to the expansion chamber through a low conductance nozzle and it represents the cluster beam exit nozzle. The cavity of the source is crossed by a cylindrical rod that works as a cathode. The system anode consists in an earthing copper drilled disc located in front of the valve.

Briefly, the PMCS operation principle is based on the ablation of a titanium rod by argon plasma, ignited by a pulsed electric discharge [151]. The ablated species thermalize with the argon and condense to form clusters. The mixture of clusters and inert gas is then extracted in vacuum through an aerodynamical focusing assembly to form a seeded supersonic beam [152], the clusters are then collected on a substrate located in the beam trajectory. Since the clusters kinetic energy is low enough to avoid fragmentation, the nanoparticles impinging on the substrates maintain their original structure and, via random stacking, a nanostructured film is grown [153]. The deposition process takes place under high vacuum thus allowing the partial oxidation of the Ti clusters, further oxidation is obtained upon air exposure to atmospheric conditions and it is completed with a mild annealing for 2 hr at the temperature of 250 °C under a continuous flux of dry

air. The annealing procedure has the further purpose of removing adsorbed species on the sample surfaces.

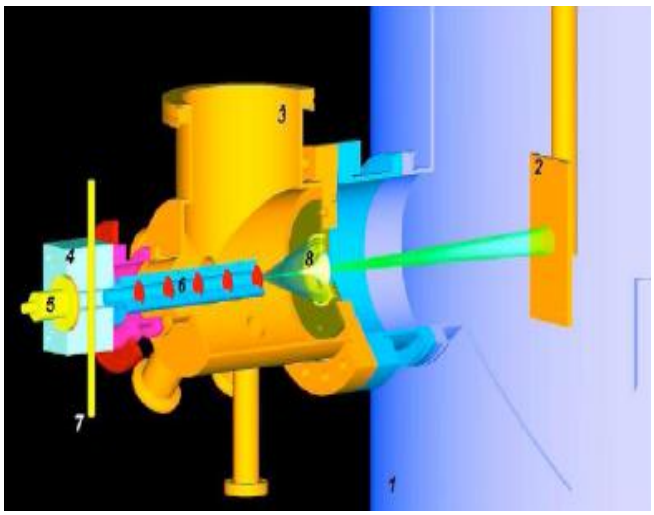

Figure 9. Schematic representation of the deposition apparatus. The deposition chamber (1) hosts the sample holder (2). The PMCS is placed in an expansion chamber (3). The source consists of a ceramic cavity (4) closed by a pulsed valve (5) and a nozzle (6) (in this case an aerodynamic lens assembly). The cathode (7) is a rod of the material to be sputtered; it provides atoms for cluster growth. The anode is embedded into the ceramic body. The supersonic beam produced enters the deposition chamber passing through a skimmer (8).

Film roughness was measured by Contact Stylus Profilometry (Dektak Veeco), the surface morphology was characterized by atomic force microscopy (AFM-Digital Instruments Nanoscope multimode IV). The AFM is equipped with rigid cantilevers with single-crystal silicon tips (nominal radius 5-10 nm) and operated in Tapping Mode. Typically, several (4-6) 2 μm × 1 μm images (2048 × 1024 points) were acquired on each sample, and flattened by line-by-line subtraction of first and second-order polynomials in order to get rid of the tilt of the sample and of the scanner bow. From flattened AFM images, the average nanoscale root-mean-square roughness and specific area parameters were calculated.

The electronic structure of as-deposited and annealed ns-TiO_2 was characterized in a UHV ($1 \cdot 10^{-9}$ mbar) apparatus Leybold LHS 10/12 equipped with a hemispherical electron analyzer and conventional X-ray source (Al Kα = 1486.7 eV). The high-resolution spectra were acquired in constant pass-energy mode Epass= 30 eV with an overall energy resolution of 1.0 eV. All spectra are referenced to the Fermi level and the binding energy scale is calibrated via the Au $4f_{5/2}$ core level line (located at 88.5 eV) of a clean polycrystalline Au sample. No charging effects on the samples under investigation were observed during all the measurements. The line shapes were fitted with mixed singlets obtained by a linear combination of a Gaussian and a Lorentzian profiles sited on a Shirley background.

2.2 CELL CULTURE AND ANALYSIS

2.2.1 Cell culture

Rat PC12 cells (PC-12 Adh ATCC Catalog no.CRL-1721.1TM) were used as a model to test nanostructured surface effect on cell differentiation because of their faculty to assume neuronal phenotype (i.e. extension of neurites) responding to some stimuli, as the Nerve Growth Factor (NGF).

After annealing the glass cover slips coated with ns-TiO_2 or flat TiO_2 were sterilized by exposure to UV light (15 W UV lamp) for 30 min. Sterilized glass pre-coated with Poly-L-Lysine 0.01% solutions (Sigma-Aldrich) were used as positive controls.

PC12 were maintained in RPMI-1640 Medium (Sigma-Aldrich) supplemented with 10% horse serum (HS; Sigma-Aldrich), 5% fetal bovine serum (FBS; Sigma-Aldrich), 2 mM l-glutamine, 100 units/ml penicillin, 100 µg/mL streptomycin, 1 mM pyruvic acid (sodium salt) and 10 mM Hepes in 5% CO_2, 98% air-humidified incubator (Galaxy S, RS Biotech, Irvine, California, USA) at 37 °C. Cells were detached from culture dishes using a solution 1 mM EDTA in HBSS (Sigma-Aldrich), centrifuged at 1000 x g for 5 min, and resuspended in culture medium. Subcultures or culture medium exchanges were routinely established every 2nd to 3rd day into Petri dishes (Ø 10 cm). During the experiment the PC12 were

suspended in low serum medium (1% HS) added with 50 ng/mL NGF, 2 mM SMT (selective inducible NOS inhibitor) (Sigma-Aldrich) and control solvent where specified, and seeded at a cell density of 5-20 x $10^4/cm^2$ for nitration, proliferation, neurite and NOS inhibitor analysis. Following seeding, cells were maintained in 5% CO_2, 98% air-humidified incubator at 37 °C, and the medium was exchanged every 24 and 48 hr after PBS wash. For nitration analysis, cells were seeded on rectangular glass slides (25 x 75 mm, Thermo Fisher Scientific, Milano, Italy) and cultured into 4-wells rectangular dishes (Thermo Fisher Scientific). For all other analyses, cells were seeded on round cover glass (13 mm diameter, TAAB) and cultured into 24 multiwells testplates (TPP).

2.2.2 Measurements and analysis

Cells were imaged using an inverted phase contrast microscope (Axiovert 40 CFL; Zeiss), digital images were acquired with an AxioCam ICm1 (Zeiss) at different magnifications (Objective: LD A-Plan 20x/0.30 Ph1 and LD A-Plan 40x/0.50 Ph2) and measurements were made by ImageJ 1.44p software.

The neurite length and differentiation rate were evaluated according to the following definition: the length was the straight-line distance from the tip of the neurite to the junction between the cell body and neurite base. In the case of branched neurites, the length of the longest branch was measured. For each cover glass, 20 and 40X images were acquired randomly by scanning the wells, measuring in each image: N, as total number of cells; n, as number of cells with the neurite longer than 20 µm (cells considered positive for neurite extension); l, as neurite length in µm; R, as differentiation rate determined by the equation R = 100 * n / N. The actual distributions of neurite lengths were presented for each condition, along with the population median, as frequency over all cells considered (at least 100). Cell spreading assay: for each cover glass, 10 and 20X images were acquired randomly by scanning the wells and the cell density for cm^2 was measured. Each substrate type was tested 3 times. All data are expressed as sample arithmetic mean ± S.E.M. Significance of differences was determined using Student's t-test (* p<=0.05; ** p<=0.01; *** p<=0.001).

2.3 LYSATE PREPARATION

2.3.1 Whole-cell extracts

For preparation of whole-cell extracts, cells from cultures exposed to NGF from zero to 2 days were washed with phosphate-buffered saline (PBS) and extracted for 10 min at room temperature with sodium dodecyl sulfate polyacrylamide gel electrophoresis (SDS-PAGE) sample buffer (2% w/v SDS, 10% v/v glycerol, 5% v/v β-mercaptoethanol, 0.001% w/v bromophenol blue, and 62.5 mM Tris, pH 6.8), then the fraction was collected.

2.3.2 Soluble and insoluble fractions

To separate cytosolic and cytoskeletal-associated proteins, cells were washed with phosphate-buffered saline (PBS) and extracted for 10 min at room temperature with PEM buffer (85 mM Pipes, pH 6.94, 10 mM EGTA, 1 mM $MgCl_2$, 2 M glycerol, 1 mM PMSF, 0.1 mM leupeptin, 1 µM pepstatin, 2 µg/mL aprotinin) containing 0.1% v/v Triton X-100. After extraction, the obtained Triton X-100-soluble fractions were diluted 3:1 with 4X SDS-PAGE sample buffer. The insoluble material remaining attached to the dish was scraped into SDS-PAGE sample buffer. Equal proportions of each fraction, representing proteins from the same number of cells, was measured by the Bradford method and separated by SDS-PAGE as described below.

2.4 PROTEIN ASSAY

The concentration of cell extracts was determined using the Bradford method. The Bradford assay is based on Coomassie Brilliant Blue G-250 (CBBG) that specifically binds to protein at arginine, tryptophan, tyrosine, histidine and phenylalanine residues. CBBG binds to these residues in the anionic form, which has an absorbance maximum at 595 nm. The assay is monitored at 595 nm in a Hewlett Packard 8452 spectrophotometer, and

determines the CBBG-protein complex. Bovine plasma immunoglobulin was used as standard protein.

2.5 SDS-PAGE

Cell lysates were prepared, for SDS-PAGE, adding a solution of acetone:methanol (8:1) and maintained overnight at -20 °C to ensure complete protein precipitation. The solution was centrifuged at 13000 rpm for 15 min at 4 °C and the supernatant was discarded. The pellet obtained from the centrifugation was dissolved in the sample buffer and the protein samples were boiled at 100 °C for 5 min and centrifuged at 10000 rpm for 3 min allowing protein denaturation.

Electrophoresis was performed in a Mini Protean II apparatus (Bio-Rad) at 20mA/gel constant current until the dye front reached the end of the running gel. After the running, the protein samples were transferred from gels to nitrocellulose or Immobilon™-P membranes and immunostained with specific antibodies as detailed below.

2.6 WESTERN BLOT ANALYSIS

2.6.1 Blotting proteins from gel to nitrocellulose or Immobilon™-P membrane

Western blotting was performed using a mini trans-blot apparatus (Biorad) according to standard procedures. The transfer membrane (nitrocellulose or Immobilon™-P filter) was cut to the dimensions of the gel and labelled to identify the gel and the orientation of the membrane. The Immobilon™-P Polyvinylidene Difluoride filter (Sigma-Aldrich) was activated in 100% methanol for 15 seconds, placed in distilled water for 2 min and then soaked in CAPS buffer (10 mM CAPS pH 11 + 10% methanol) under shaking for at least 15 min. The nitrocellulose membrane (GE Healthcare) was wet in distilled water for 2 min and then soaked in TRIS-GLYCINE buffer (25 mM Tris/192 mM Glycine + 10% methanol) for 15 min. The gel was soaked in transfer buffer and allowed to equilibrate for 15 min. Then, the membranes were laid onto the gel, taking care to remove any bubble between

them. Gel and filter were placed between sheets pre-soaked in CAPS or TRIS-GLYCINE buffer, and two rigid plastic supports ("sandwichs") that were then placed into the electrophoretic chamber with the filter facing the anode. The proteins, negatively charged because of the high pH, migrate towards the anode, and are absorbed by the filter. Proteins on the gel were electrophoretically transferred onto Immobilon™-P filter or nitrocellulose membrane, for 1 h at 180mA and for 2 hr at 100mA respectively.

2.6.2 Immunostaining

Insoluble fraction of PC12 cells were probed with specific antibodies followed by horseradish peroxidise-conjugated secondary antibodies and detected by Chemiluminescence method, as described below in detail.

Anti-nitro Tyr

i. Blocking: Immobilon™-P membrane was incubated in 6% w/v nonfat dry milk in 50 mM Tris, pH 7, 150 mM NaCl (TBS2) with 0.05% v/v Tween 20 for 1 h at room temperature.
ii. Washing: membrane was washed 1 X 15 min and 2 X 5 min in TBS2 0.05% Tween.
iii. Primary antibody- Anti-Nitrotyrosine (Invitrogen, Camarillo, California, USA): the primary antibody was incubated diluted 1:750 in a solution of 1% Bovine serum albumin in TBS2 0.05% Tween overnight at 4 °C.
iv. Washing: membrane was washed 1 X 15 min and 2 X 5 min in TBS2 0.05% Tween.
v. Secondary antibody-Anti-IgG mouse conjugated with peroxidase (Calbiochem Darmstadt Germany): the secondary antibody was incubated diluted 1:20000 in a solution of 1% Bovine serum albumin in TBS2 0.05% Tween for 1 h at room temperature.
vi. Washing: membrane was washed 1 X 15 min and 2 X 5 min in TBS2 0.05% Tween.

Anti-Actin

i. Blocking: Immobilon™-P membrane was incubated in 10% w/v nonfat dry milk in 50 mM Tris, pH 7.6, 150 mM NaCl (TBS) with 0.1% v/v Tween 20 overnight at 4 °C.
ii. Washing: membrane was washed 3 X 7 min in TBS 0.1% Tween.
iii. Primary antibody- Anti-Actin (Sigma-Aldrich, Saint Louis, Missouri, USA): the primary antibody was incubated diluted 1:4000 in 5% w/v nonfat dry milk in TBS 0.1% Tween for 2 hr at room temperature.
iv. Washing: membrane was washed 3 X 7 min in TBS 0.1% Tween.
v. Secondary antibody-Anti-IgG mouse conjugated with peroxidase (Calbiochem Darmstadt Germany): the secondary antibody was incubated diluted 1:2000 in 5% w/v nonfat dry milk in TBS 0.1% Tween for 1 h at room temperature.
vi. Washing: membrane was washed 3 X 7 min in TBS 0.1% Tween.

Anti-MaP1b

i. Blocking: nitrocellulose membrane was incubated in 10% w/v nonfat dry milk in 50 mM Tris, pH 7.6, 150 mM NaCl (TBS) with 0.05% v/v Tween 20 for 1 h at room temperature.
ii. Washing: membrane was washed 1 X 15 min and 4 X 5 min in TBS 0.05% Tween.
iii. Primary antibody- Anti-MAP1b (Sigma-Aldrich, Saint Louis, Missouri, USA): the primary antibody was incubated diluted 1:500 in a solution of 1% Bovine serum albumin in TBS 0.05% Tween overnight at 4 °C.
iv. Washing: membrane was washed 1 X 15 min and 4 X 5 min in TBS 0.05% Tween.
v. Secondary antibody-Anti-IgG mouse conjugated with peroxidase: the secondary antibody was incubated diluted 1:15000 in a solution of 1% Bovine serum albumin in TBS 0.05% Tween for 1 h at room temperature.
vi. Washing: membrane was washed 1 X 15 min and 4 X 5 min in TBS 0.05% Tween.

Anti-Human Tau

i. Blocking: Immobilon™-P membrane was incubated in 10% w/v nonfat dry milk in 50 mM Tris, pH 7.6, 150 mM NaCl (TBS) with 0.05% v/v Tween 20 for 1 h at room temperature.
ii. Washing: membrane was washed 1 X 15 min and 4 X 5 min in TBS 0.05% Tween.
iii. Primary antibody- Anti-Human Tau (Upsate, New York, USA): the primary antibody was incubated diluted 1:500 in a solution of 1% Bovine serum albumin in TBS 0.05% Tween overnight at 4 °C.
iv. Washing: membrane was washed 1 X 15 min and 4 X 5 min in TBS 0.05% Tween.
v. Secondary antibody-Anti-IgG mouse conjugated with peroxidase: the secondary antibody was incubated diluted 1:20000 in a solution of 1% Bovine serum albumin in TBS 0.05% Tween for 1 h at room temperature.
vi. Washing: membrane was washed 1 X 15 min and 4 X 5 min in TBS 0.05% Tween.

Anti-NOS

i. Blocking: Immobilon™-P membrane was incubated in 5% w/v nonfat dry milk in PBS (Phosphate-buffered saline) for 2 hr at room temperature.
ii. Primary antibody- Anti-NOS (Abcam, Cambridge, UK): the primary antibody was incubated diluted 1:500 in 5% w/v nonfat dry milk in PBS overnight at 4 °C.
iii. Washing: membrane was washed 3 X 10 min in PBS 0.3% Tween.
iv. Secondary antibody-Anti-IgG rabbit conjugated with peroxidase: the secondary antibody was incubated diluted 1:5000 in 5% w/v nonfat dry milk in PBS for 1 h at room temperature.
v. Washing: membrane was washed 3 X 10 min in PBS 0.3% Tween.

Anti-iNOS

i. Blocking: Immobilon™-P membrane was incubated in 5% w/v nonfat dry milk in PBS (Phosphate-buffered saline) for 2 hr at room temperature.
ii. Primary antibody- Anti-iNOS (Abcam, Cambridge, UK): the primary antibody was incubated diluted 1:500 in 5% w/v nonfat dry milk in PBS overnight at 4 °C.
iii. Washing: membrane was washed 3 X 10 min in PBS 0.3% Tween.
iv. Secondary antibody-Anti-IgG rabbit conjugated with peroxidase: the secondary antibody was incubated diluted 1:5000 in 5% w/v nonfat dry milk in PBS for 1 h at room temperature.
v. Washing: membrane was washed 3 X 10 min in PBS 0.3% Tween.

Anti-Tubulin

i. Blocking: Immobilon™-P membrane was incubated in 5% w/v nonfat dry milk in TBS 0.05% Tween for 1 h at room temperature.
ii. Washing: membrane was washed 1 X 15 min and 2 X 5 in TBS 0.05% Tween.
iii. Primary antibody- Anti-Tubulin (Abcam, Cambridge, UK): the primary antibody was incubated diluted 1:1000 in a solution of 1% Bovine serum albumin in TBS 0.05% Tween overnight at 4 °C.
iv. Washing: membrane was washed 1 X 15 min and 2 X 5 in TBS 0.05% Tween.
v. Secondary antibody-Anti-IgG mouse conjugated with peroxidase: the secondary antibody was incubated diluted 1:20000 in a solution of 1% Bovine serum albumin in TBS 0.05% Tween for 1 h at room temperature.
vi. Washing: membrane was washed 1 X 15 min and 2 X 5 in TBS 0.05% Tween.

Anti-ERK

i. Blocking: nitrocellulose membrane was incubated in 5% w/v nonfat dry milk in PBS 0.1% Tween for 1 h at room temperature.

ii. Primary antibody- Anti-ERK (Cell Signaling, Danvers, Massachusetts): the primary antibody was incubated diluted 1:2500 in 5% w/v nonfat dry milk in PBS 0.1% Tween overnight at 4 °C.
iii. Washing: membrane was washed 3 X 10 min in PBS 0.1% Tween.
iv. Secondary antibody-Anti-IgG rabbit conjugated with peroxidase: the secondary antibody was incubated diluted 1:5000 in 5% w/v nonfat dry milk in PBS 0.1% Tween for 1 h at room temperature.
v. Washing: membrane was washed 3 X 10 min in PBS 0.1% Tween.

Anti-pERK

i. Blocking: nitrocellulose membrane was incubated in 5% w/v nonfat dry milk in PBS 0.1% Tween for 1 h at room temperature.
ii. Primary antibody- Anti-pERK (Cell Signaling, Danvers, Massachusetts): the primary antibody was incubated diluted 1:250 in 5% w/v nonfat dry milk in PBS 0.1% Tween overnight at 4 °C.
iii. Washing: membrane was washed 3 X 10 min in PBS 0.1% Tween.
iv. Secondary antibody-Anti-IgG mouse conjugated with peroxidase: the secondary antibody was incubated diluted 1:5000 in 5% w/v nonfat dry milk in PBS 0.1% Tween for 1 h at room temperature.
v. Washing: membrane was washed 3 X 10 min in PBS 0.1% Tween.

2.6.3 Stripping and Reprobing

Tyr nitration of the proteins (actin, MAP1b, tubulin, NOS, iNOS, tau, ERK and p-ERK) was checked by stripping the western blot membrane and reprobing it with anti-nitroTyr antibodies as previously described. The membrane was submerged in stripping buffer (100 mM 2-Mercaptoethanol, 2% SDS, 62.5 mM Tris-HCl, pH 6.7) and incubated at 50 °C for 30 min, with occasional agitation, to remove primary and secondary antibodies. Later,

the membrane was washed in PBS-T or TBS-T at room temperature using large volumes of wash buffer and immunostained with Anti-Nitrotyrosine antibodies.

2.6.4 Immunodetection system (ECL)

Immunolabeled proteins were detected, according to the GE Healthcare Life Sciences protocol, using ECL Plus™ Western Blotting Detection Reagents (Buckinghamshire, UK) which provide an improved non-radioactive method for the detection of immobilized specific antigens conjugated to Horseradish Peroxidase (HRP) labelled antibodies.
The membranes were incubated in a mixed detection reagent (A and B solutions in a ratio of 40:1) for 5 min in a dark room and then placed in an x-ray film cassette with a sheet of autoradiography film on top of them. This step was repeated several times at different exposure times. Once, it was established the correct exposure time, the films were immersed in a developer and then in fixative solutions.
Solution A and Solution B: ECL Plus substrate solution containing Tris buffer, Stock Acridan solution in Dioxane and Ethanol.
The density of each band was estimated using a documentation system (GS-800) and an analysis program (Quantity-OneTM) from BioRad Laboratories (Hercules, California, USA).

2.7 PROTEIN IDENTIFICATION BY MASS SPECTROMETRY

2.7.1 In situ digestion

For mass spectrometry analysis, PC12 cells homogenates were separated by SDS-PAGE and digested *in situ* by trypsin as described by Cappelletti G. et al. [72]. Upon SDS-PAGE, the gel was stained with colloidal CBB G-250 (Sigma) and each lane was excised, cut in 2 mm bands and destained in 0.1% trifluoroacetic acid:acetonitrile 1:1 before drying in a Speed Vac. Dried gels were rehydratated in 10 mM dithiothreitol in ammonium bicarbonate 0.1 M and incubated at 56 °C for 1 h. Following cysteine derivatization by iodoacetamide at 25 °C, the gels pieces were dried, rehydratated with trypsin (sequence

grade, Sigma-Aldrich) solution (0.2 µg trypsin/band in 100 µl 50 mM ammonium bicarbonate, 9% acetonitrile), and incubated overnight at 37 °C.

2.7.2 Peptide extraction

Digestion was stopped by adding 1 µl of 50% trifluoroacetic acid. The in-gel tryptic digest solution was collected in a new test tube and the peptides were extracted from the gel using 0.1% trifluoroacetic acid:acetonitrile 1:1. The material was centrifuged at 9000 rpm for 3 min, sonicated for 3-5 min and the supernatant was added to the peptide mixture collected previously. The extract was dried, resuspended in 10 µl 0.3% v/v formic acid and desalted using Zip-Tip C18 (Millipore) before mass spectrometric (MS) analysis.

2.7.3 Zip-Tip C18

The following protocol was applied:

- Equilibrate the ZipTip for Sample Binding: **1)** pre-wet the tips with 100% CH_3CN 3 times (3 x 10 µl); **2)** wash the tips with TFA 0.1% 3 times (3 x 10 µl).
- Bind and Wash the Peptides: **1)** bind the sample to ZipTip pipette tip. Aspirate and dispense the material 7-10 cycles for maximum binding of complex mixtures; **2)** wash the tips with TFA 0.1% at least once.
- Elute the Peptides: elute the sample with 50% CH_3CN in TFA 0.1%, 3 times (3 x 10 µl), into a clean vial, for mass spectrometry analysis.

2.8 MASS SPECTROMETRY

Mass spectrometry is an analytical tool useful for measuring the mass-to-charge ratio (*m/z*) of one or more molecules present in a sample. These measurements can often be used to calculate the exact molecular weight of the sample components. Typically, mass spectrometers can be exploited to identify unknown compounds via molecular weight

determination, to quantify known compounds, and to determine structure and chemical properties of molecules**.** Basically, a mass spectrometer is composed of an ion source, of a system to separate the ions according to their *m/z*, and of an ion detector. The sample has to be introduced into the ionization source of the instrument. Once inside the ionization source, the sample molecules are ionized, because ions are easier to manipulate than neutral molecules. These ions are extracted into the analyzer region of the mass spectrometer where they are separated according to their mass (m) to-charge (z) ratios (*m/z*). The separated ions are detected and this signal sent to a data system where the *m/z* ratios are stored together with their relative abundance for presentation in the format of a *m/z* spectrum. The analyzer and detector of the mass spectrometer, and often the ionization source too, are maintained under high vacuum to give the ions a reasonable chance of travelling from one end of the instrument to the other without any hindrance from air molecules. The entire operation of the mass spectrometer, and often the sample introduction process also, is under complete data system control on modern mass spectrometers.

2.8.1 Ionization techniques

Ionization techniques are also known as interfaces because they allow the passage of the analytes from samples to the mass analyzer. These techniques are crucial to determine what types of samples can be analyzed by MS (liquid, solid, etc.) and to know which kind of ionizing charged will have the molecules measured. Two techniques often used with liquid and solid biological samples: matrix-assisted laser desorption/ionization (MALDI) [154, 155] and electrospray ionization (ESI) [156].

2.8.1.1 Electrospray ionization

Electrospray ionization (ESI) produces gaseous ionized molecules directly from a liquid solution creating a fine spray of highly charged droplets in the presence of an electric field.

The sample solution is sprayed from a region of the strong electric field at the tip of a metal nozzle maintained at a potential of anywhere from 700 V to 5000 V. The needle to which the potential is applied serves to disperse the solution into a fine spray of charged droplets. Either dry gas, heat, or both are applied to the droplets at atmospheric pressure thus causing the solvent to evaporate from each droplet. As the size of the charged droplet decreases, the charge density on its surface increases. The mutual Coulombic repulsion between like charges on this surface becomes so great that it exceeds the forces of surface tension, and ions are ejected from the droplet through a "Taylor cone". Another possibility is that the droplet explodes releasing the ions. In either case the emerging ions are directed into an orifice through electrostatic lenses leading to the vacuum of the mass analyzer. These charged analyte molecules can be singly or multiply charged. This is a very soft method of ionization as very little residual energy is retained by the analyte upon ionization.

Several variations on the electrospray process have been developed such as nanospray ionization. Nanospray is a form of ESI that employs low flow rate from 10 to 1000 nL/min. As the flow rate is lowered, a lower volume of mobile phase passes through the emitter producing smaller aerosol droplets. This makes nanospray ionization more effective than conventional ESI at concentrating the analyte at the emitter tip, producing significant increases in sensitivity demonstrated by the signal response of the mass spectrometer.

2.8.2 LC-ESI-MS/MS

An important enhancement to the mass resolving and mass determining capabilities of MS is obtained by coupling it with chromatographic separation techniques. Common combinations are gas chromatography-mass spectrometry (GC/MS) or liquid chromatography-mass spectrometry (LC/MS).

In this work, digested samples were separated by liquid chromatography using an UltiMate 3000 HPLC (Dionex, now Thermo Fisher Scientific).

Buffer A was 0.1% v/v formic acid, 2% acetonitrile; buffer B was 0.1% formic acid in acetonitrile.

Chromatography was performed using a PepMap C18 column (15 cm, 180 µm ID, 3 µm resin, Dionex). The gradient was as follows: 5% buffer B (10 min), 5%-40% B (60 min), 40%-50% B (10 min) and 95% B (5 min) at a flow rate of 1.2 µL/min.
Mass spectrometry was performed using a LTQ-Orbitrap Velos (Thermo Fisher Scientific) equipped with a nanospray source (Proxeon Biosystems, now Thermo Fisher Scientific). Eluted peptides were directly electrosprayed into the mass spectrometer through a standard non-coated silica tip (New Objective, Woburn, MA, USA) using a spray voltage of 2.8 kV.

2.8.2.1 LTQ ORBITRAP

LTQ Orbitrap Velos is a hybrid mass spectrometer incorporating the LTQ Velos™ dual cell linear trap and the Orbitrap™ analyzer [157, 158]. The ion storage and the injection into the Orbitrap allows high resolving power, mass accuracy, and transmission over a wide dynamic range and forms the basis for a hybrid mass spectrometer combining these analytical parameters with the MS^n capability of the linear ion trap mass spectrometer.
Briefly, the LTQ Orbitrap Velos (Figure 10) consists of four main components: **1)** a dual cell linear ion trap for sample ionization, selection, fragmentation, and AGC™; **2)** an intermediate storage device (curved linear trap) that is required for short pulse injection; **3)** an Orbitrap analyzer for Fourier transformation based analysis and **4)** a collision cell for performing higher energy CID experiments.
The LTQ Orbitrap Velos ETD has also an additional reagent ion source for enabling post-translational modification analyses of peptides by Electron Transfer Dissociation (ETD).
As its name suggests, Orbitrap is a device that is able to store and trap ions [159]. It is not conventional ion trap as a linear ion trap [160], because there is neither RF nor a magnet to hold ions inside, but an electrostatic field that trap ions [161]. The electrostatic attraction towards the central electrode is compensated by a centrifugal force that arises from the initial velocity of ions, which makes ion moving like a satellite on orbit. The electrostatic field forces the ions to move in complex spiral patterns. The axial component of these oscillations can be detected as an image current on the two halves of an

electrode encapsulating the Orbitrap. A Fourier transform is employed to obtain oscillation frequencies for ions with different *m/z* values, which can be determined from these values. Since ions can be trapped for long times, the frequency of their image current can be registered with high accuracy, allowing to obtain high resolution mass spectrum.

The combination of this mass analyzer with linear ion traps is perfect, because the first allows high resolution measurements, whilst the second allows to perform MS^n experiments. Thus, also product ions of these experiments can be registered with high resolution and high mass accuracy, opening new perspectives in a wide range of applications.

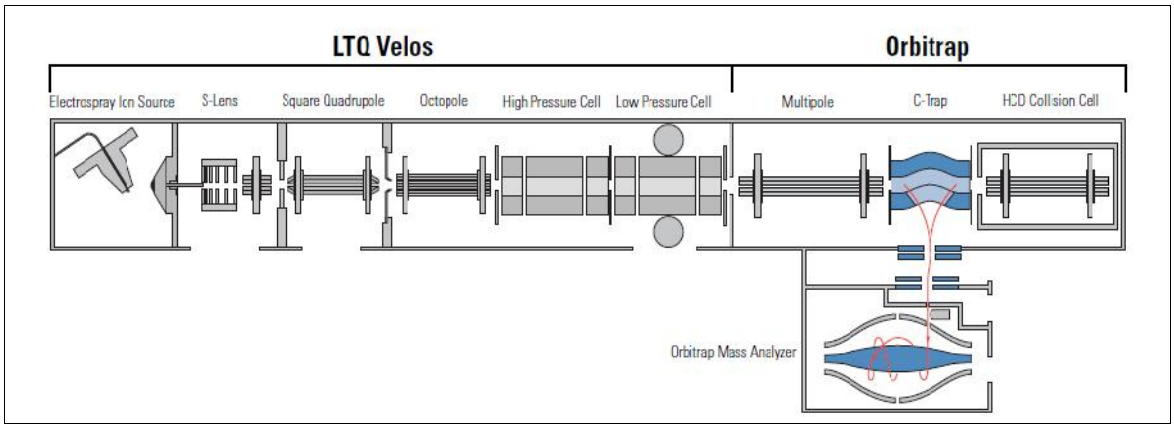

Figure 10. Schematic view of the LTQ Orbitrap Velos ETD.

2.8.2.2 Tandem mass spectrometry

An important application of mass spectrometry is the possibility to fragment molecules to study the different fragments and to better understand the structure and possible mutations of the molecules.

These fragmentation studies can be done by Tandem Mass Spectrometry technique or MS/MS analysis. This technique involves the activation of a known precursor ion, formed

in the ion source, and the mass analysis of its fragmentation products. MS/MS analysis can be done using different ion activation techniques: CID (Collision-induced dissociation), HCD (Higher energy collision dissociation), and ETD (Electron-transfer dissociation).
In this work, the LTQ-Orbitrap was operated in positive mode in data-dependent acquisition mode to automatically alternate between a full scan (m/z 350-2000) in the Orbitrap and subsequent CID MS/MS in the linear ion trap of the 20 most intense peaks from full scan. Two replicate analysis of each sample were performed. Data acquisition was controlled by Xcalibur 2.0 and Tune 2.4 software (Thermo Fisher Scientific).

2.8.3 Database analysis

Searching for nitrated proteins against the rat NCBInr database (release February 15, 2012) was performed using the Sequest search engine contained in the Proteome Discoverer 1.1 software (Thermo Fisher Scientific). The following parameters were used: 10 ppm for MS and 0.5 Da for MS/MS tolerance, carbamidomethylation of Cys as fixed modification, Met oxidation, Tyr nitration, Trp nitration and Ser/Thr/Tyr phosphorylation as variable modifications, trypsin (2 misses) as protease, False Discovery Rate for peptides 1% (against decoy).

2° Model (*Ciona intestinalis*)

Experimental procedures

2.9 ANIMALS, EMBRYOS AND INCUBATION EXPERIMENTS

This study was conducted in collaboration with Dr. Anna Palumbo at the "Stazione Zoologica Anton Dohrn" in Naples who collected all the samples and carried out the experiment *in vivo*. Specimens of *C. intestinalis* were collected in the Bay of Naples and maintained in tanks with circulating sea water until use. Eggs and sperms were collected separately from the gonoducts. Eggs from a single animal were fertilized with a mixture of sperms obtained from different individuals. Embryos were cultured at 18 °C in 0.2 µm filtered sea water. Under these conditions, just hatched larvae (early larvae) were obtained about 18-20 hr after fertilization. Development was followed with an Olympus stereomicroscope. Samples at appropriate stages were identified using the morphological criteria reported by Chiba et al. [139] and were selected on the basis of at least 95% homogeneity. The samples were collected by low speed centrifugation and the pellets were frozen for protein extraction. When necessary, early larvae were treated in sea water at 18 °C with the following modifiers of NO signaling, at the final concentrations indicated in the text: [1-(2-trifluoromethylphenyl) imidazole] (TRIM), (Z)-1-{N-[3-Aminopropyl]-N-[4-(3-aminopropylammonio)butyl]-amino}-diazen-1-ium-1,2-diolate] (spermine NONOate, SPER/NO), peroxynitrite, spermine, [manganese (III) tetrakis (4-benzoic acid) porphyrin chloride] (MnTBAP), urate. TRIM, SPER/NO and MnTBAP were purchased from Alexis Biochemicals (Vinci-Biochem, Vinci, Italy). Spermine and urate were from Sigma, Milan, Italy.

Peroxynitrite was synthesized by the reaction of nitrite with acidified H_2O_2, as previously described [162].

2.10 PROTEIN EXTRACTION

Larva and embryo pellets were homogenized in two volumes of RIPA lysis buffer (150 mM NaCl, 50 mM Tris-HCl pH 7.6, 5 Mm EDTA, 0.5% NP-40, 0.5% sodium deoxycholate, 0.1% SDS) supplemented with protease inhibitors (1 mM PMSF and Complete Protease Inhibitor Cocktail Tablets, Roche, Monza, Italy) and phosphatase inhibitors (PhosSTOP

Cocktail Tables, Roche). Lysates were clarified by centrifugation and total protein concentration was determined using the Bio-Rad Protein Assay Reagent (Bio-Rad, Milan, Italy) as described in the above section 2.4.

2.11 ELECTROPHORESIS

Before electrophoresis, protein samples used for anti-ERK, anti- p-ERK, anti-snail and anti-actin immunoblotting were incubated at 85 °C for 5 min whereas samples examined for nitrated proteins were not.

2.11.1 SDS-PAGE

Ten percent SDS-PAGE was carried out as previously reported in Tedeschi G. et al. [163]. Following mono-D electrophoresis, gels were stained with Blue Coomassie or blotted onto nitrocellulose (Hybond, GE Healthcare) or polyvinylidenfluoride (PVDF, Immobilon-P, Millipore, commercialized by Sigma) membranes.

2.11.2 Two dimensional electrophoresis

Analytical or preparative two dimensional electrophoresis (2-DE) was carried out on protein extract by performing the reduction and the alkylation prior the first dimension. Briefly, the sample was diluted in 7 M urea, 2 M thiourea, 2% NP-40, 40 mM Tris-HCl and incubated at room temperature for 90 min with 5 mM tributylphosphine (TBP). After this step, the sample was incubated with 20 mM iodoacetamide (IAA) at room temperature for 90 min in the dark. Following precipitation with in an anhydrous solution of acetone and methanol (8:1, v/v) at -20 °C, the precipitate was suspended in the 2-D PAGE sample buffer (7 M urea, 2 M thiourea, 2% NP-40, 0,5% Resolyte 3.5-10 NL, bromophenol blue) and sonicated for 1 min. For the first dimension, 800 µg (preparative 2-DE) or 30 µg (analytical 2-DE) of protein were applied to rehydrated IPG strip (immobiline dry strip pH 3-10 NL, 70 mm; Amersham Pharmacia, Cologno Monzese, Italy). The dry IPG strips were

rehydratated overnight in 350 µl of rehydratation buffer containing 7 M urea, 2 M thiourea, 2% NP-40, 0,5% Resolyte 3.5-10 NL, bromophenol blue. Samples were loaded by sample cups. IEF was carried out at 14 °C, 19,600 V total voltage, for 6 hr. The first dimension IEF was performed with the Multiphor II system (Amersham Pharmacia, Milano, Italy). Before the second dimension, the strips were rinsed with buffer (6 M urea in 0.375 M Tris-HCl pH 8.8, 2% SDS, 20% glycerol, bromophenol blue). The second dimension was performed on 10% polyacrylamide gels (Mini-Protean, Biorad), at 40mA/gel constant current until the bromophenol band had reached the end of the gel. Following SDS-PAGE, 2-DE gels were either stained with ammoniacal silver (analytical 2-DE), or with colloidal blue CBB G (Sigma) (preparative 2-DE to be used for mass spectrometry based protein identification) or blotted onto nitrocellulose or PVDF membranes.

2.12 WESTERN BLOT AND IMMUNOSTAINING

Western blotting was performed according the protocol described in the above section 2.6. Blotted membranes were immunodetected as follows:

Snail detection: the PVDF membrane was dehydrated with methanol and equilibrated in Phosphate buffered saline (PBS) pH 7.5. A monoclonal antibody generated against the purified human snail protein was kindly provided by Dr. Becker of the Institut für Pathologie, Technical University of München. Incubation was performed for 1 h at room temperature in a solution of 1% BSA in PBS at the dilution 1:100. After washing with PBS the membrane was incubated with horseradish peroxidase-linked anti mouse IgG (whole molecule) (Sigma) diluted 1:10000 in 1% BSA in PBS. After 1 h the membrane was washed with PBS.

ERK, pERK, actin and nitrotyrosine detection was performed as described previously (section 2.6.2).

As a control to rule out false immunopositive spots the nitrotyrosine groups were converted to aminotyrosine by treating the membrane with freshly made 10 mM sodium dithionite in 50 mM pyridine acetate buffer, pH 5.0 for 1 h at room temperature, under stirring, in the dark [163].
Labelled proteins were detected using enhanced chemiluminescence system (ECL PLUS, GE Healthcare o) or Supersignal West Pico Chemiluminescent Substrate (Pierce, EuroClone). Proteins were visualized on an autoradiography film (BiomaxKodak).

2.13 IMMUNOPRECIPITATION

Samples of extracted proteins from treated and untreated larvae were preincubated with a 1:1 suspension of Protein A-Sepharose in PBS for 1 h at 4 °C with vigorous shaking. Then, the samples were centrifuged at 14000 rpm for 10 min at 4 °C and the supernatants were incubated with anti-p-ERK (1:25) with gentle shaking. After overnight incubation at 4 °C, a 1:1 suspension of Protein A-Sepharose in PBS was added and the mixture was further incubated for 3 hr at 4 °C with vigorous shaking. The samples were centrifuged and the immunoprecipitates, washed twice with PBS, were dissolved in Laemmli's buffer without β-mercaptoethanol, boiled at 90 °C for 10 min and analyzed by electrophoresis. The p-ERK-free supernatant was then incubated with anti-ERK (1:50) and treated as reported above.

2.14 GEL STAINING

Two different procedures were used:

COOMASSIE BLUE G250 (used with preparative gels). The gels were placed first in a fixing solution containing 40% methanol, 7% acetic acid for 1 h, then in a stain solution containing 16% Coomassie Brilliant Blue G250, 20% methanol, for at least 2 hr up to 2 days. The gels were destained in a solution containing 25% methanol, 10% acetic acid to remove background.

AMMONIACAL SILVER STAIN (used with analytical gels). Ammoniacal silver staining was performed according to [164]. The gels were placed first in a strong fixing solution containing 40% ethanol, 10% acetic acid for 1 h, then in a bland fixing solution containing 5% ethanol, 5% acetic acid for at least 3 hr up to 3 days. Then gels were incubated in a sensitizing solution containing 1% glutaraldehyde, 0.5 M sodium acetate for 30 min. The gels were washed 3 X 10 min in double distilled water and then incubated 2 X 30 min in 0.5% 2,7 naftalendisulfonic acid. The gels were washed 4 X 15 min in double distilled water and incubated in the silver solution containing 0.8 g/l NaOH, 15 ml ammonium hydroxide and 5 g/l silver nitrate for 30 min. After 3 X 5 min washes in double distilled water, the development was obtained with a solution containing 0.1 g/l citric acid and 1 ml/l formaldehyde. Staining was stopped by rinsing the gels with 5% acetic acid.

2.15 GEL IMAGING

Stained gel and film images were digitized using an EPSON 1660 densitometer (Bruker Daltonics, Milano, Italy). Computer aided 2-DE image analysis to match signals from immunoblots and protein spots were carried out using Melanie 5 software (Bruker Daltonics, Milano, Italy).

2.16 PROTEIN IDENTIFICATION

2.16.1 N-Terminal sequence analysis

Proteins were separated by SDS-PAGE, electrotransferred to PVDF membranes (Immobilon-P, Sigma) and stained with Coomassie Blue. The amino acid sequence was determined by automated Edman degradation using a pulsed-liquid sequencer (Procise model 491 Applied Biosystems, Foster City, CA, USA). Similarities with the entries in the SwissProt, TrEMBL, and NCBI sequence databases were searched using the BLAST program.

2.16.2 MALDI-TOF analysis

Peptide mass finger printing and automated protein database searching are commonly used for the high-throughput identification and characterization of proteins excised from 2-DE gels.

In this work we used matrix-assisted laser desorption ionization (MALDI) [154] which has become a widespread analytical tool to analyze peptides, proteins and most other biomolecules.

In MALDI analysis, a large excess of matrix material is coprecipitated with analyte molecules (that is, the molecules to be analyzed) by pipetting a submicroliter volume of the mixture onto a metal substrate and allowing it to dry. The resulting solid is then irradiated by nanosecond laser pulses, usually from small nitrogen laser with a wavelength of 337 nm (Figure 11).

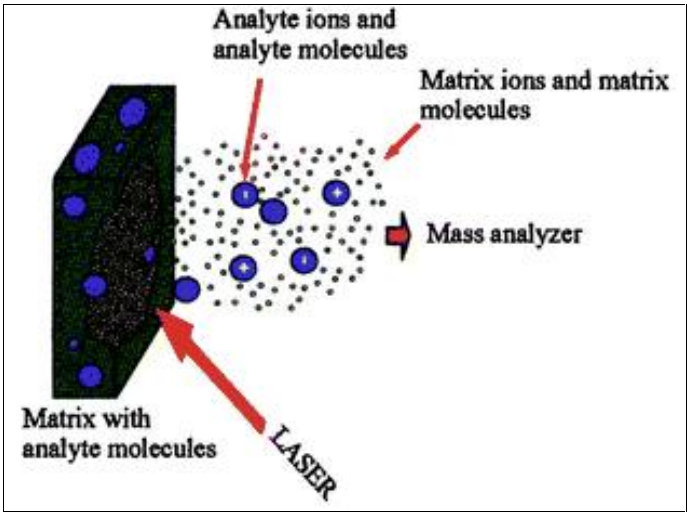

Figure 11. Schematic of MALDI process. A sample cocrystallized with the matrix is irradiated by a laser beam, leading to sublimation and ionization of peptides.

The matrix is typically a small organic molecule which adsorbs at the wavelength of the laser employed. The most common matrices used for peptide analysis are α-cyano-4-

hydroxycinnamic acid and dihydrobenzoic acid (DHB). Matrices differ in the amount of energy they impart to the biomolecules during desorption and ionization and hence the degree of fragmentation (unimolecular decay) that they cause. The mass range below 500 Daltons (Da) is often obscured by matrix-related ions in MALDI. Proteins generally undergo fragmentation to some extent during MALDI, resulting in broad peaks and loss in sensitivity; therefore MALDI is mostly applied to the analysis of peptides.

There are three types of mass analyzers typically used with the MALDI ionization source: a linear time-of-flight (TOF), a TOF reflectron, and a Fourier transform mass analyzer (Figure 12).

In a TOF mass spectrometer the mass determination in the high vacuum area is performed by a very precise measurement of the period of time after acceleration process of the ions in the source and impact on the detector.

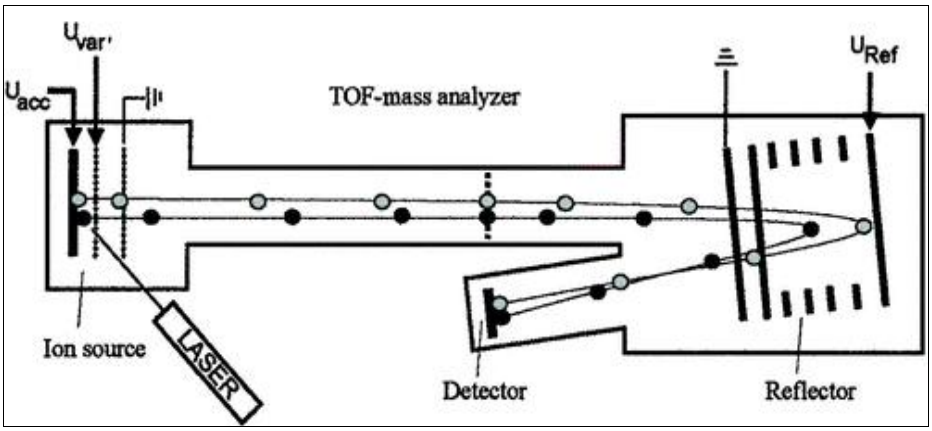

Figure 12. Schematic of MALDI TOF instrument. About 100-500 ns after the laser pulse, a strong acceleration field is switched on (delayed extraction), which imparts a fixed kinetic energy to the ions produced by the MALDI process. These ions travel down a flight tube and are turned around in an ion mirror, or reflector, to correct for initial energy differences. The mass-to-charge ratio is related to the time it takes an ion to reach the detector; the lighter ions arrive first. The ions are detected by a channeltron electron multiplier.

An electro-static field accelerates ions formed during a short laser pulse inside the source to a kinetic energy of some keV. After leaving the source the ions passes a field-free drift region in which they are separated due to their *m/z* ratio. This takes place because at a fixed kinetic energy ions with a different *m/z* values are accelerated in the ion source to different velocities. Knowing the acceleration voltage and the length of the drift region the *m/z* ratio can be determined by measuring the flight time.

Figure 13 illustrates the principle how a TOF mass spectrometer works in linear and reflector mode. Ions formed by the laser pulse being of the same charge, but different *m/z* values are accelerated to different velocities. Large ions with high *m/z* values strike the detector at a later moment than small ions. Ions of the same mass start with a certain energy spread. This affects the achievable peak width to a certain amount. Applying a reflector, the influence of the energy distribution upon the flight time can be compensated at the location of the reflector detector.

After acceleration by means of a certain voltage U the kinetic energy of the ions is defined as:

$$E_{kin} = ½ mv^2 = z e U$$

Where: m= ion mass; v= velocity of the ion after acceleration; z= charge number; e= elementary charge.

The velocity v results from the ion flight time t through the field-free region L of the flight tube:

$$v = L/t$$

Replacing v by the formula given above results in:

$$½ m (L/t)^2 = z e U$$

Arranging to m/z delivers:

$$m/z = (2eU/L^2)t^2$$

Associated with a TOF instrument the relation of molecule mass and charge number (*m/z*) is proportional to the square of the flight time t. Thus the related mass can be determined from the measured flight time. Calibration is performed with well-known reference masses. The range of typical MALDI flight times is between few μs and some 100 μs. The drift regions are typically 1m-4m long.

An important feature of a mass analyzer is the resolving power, i.e. to distinguish between ions of only little mass differences. Therefore, the resolution is defined as the ratio of the mass m and mass difference Δm (full with at half maximum, i.e. at 50% height):

$$R = m/\Delta m$$

The resolution of the in the instrument used for this study (Reflex IV, Bruker Daltonik) is > 25000 for m/z ~ 3000, when operated in reflectron mode.

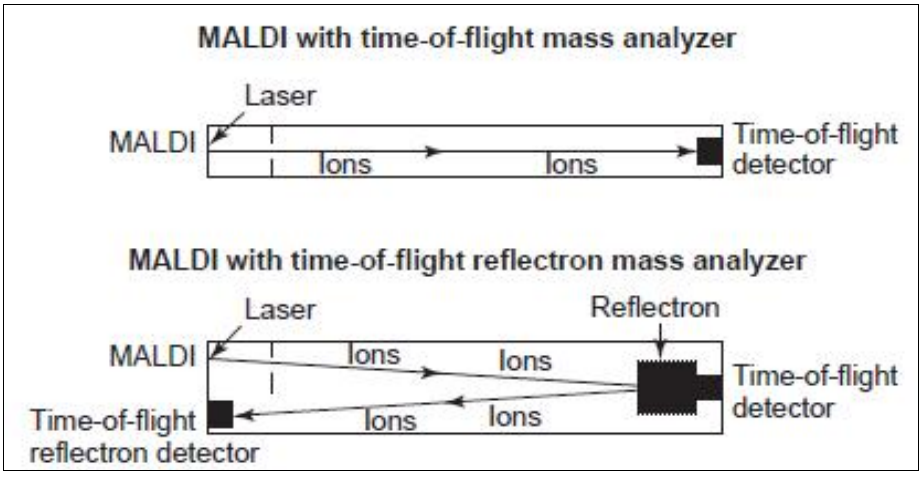

Figure 13. MALDI with TOF and TOF reflectron.

In MALDI-TOF each spectrum has to be calibrated by external calibrants. The external calibration is based on a different (external) spectrum. This calibration spectrum comes from the same plate which is used for the measurement of the spectra to be analysed. Since inhomogenieties in the geometry of the plate surface have a huge impact on the reproducibility it is advisable to prepare the calibrant as close to the sample to be analysed as possible. If the spot of the calibration spectrum is next to the spectrum of interest it is called a “nearest neighbourhood calibration”. If the maximal possible mass accuracy is desired, a nearest neighbourhood calibration is mandatory. Even if a nearest neighbourhood calibration is performed, there may still be a mass error occurring due to small changes in the target geometry and also due to different geometries of the sample preparation itself. The mass error that can be attributed to the plate geometry from one sample position to an adjacent sample position is below 50 ppm for Bruker MALDI-Ion sources. An additional error may come from variations in the sample preparation.

In this work, matrix assisted laser desorption ionization-time of flight (MALDI-TOF) analysis was carried out on the spot to be identified following 2-DE, in gel digestion and peptide extraction as described in the above section 2.7.

Following a desalting/concentration step on a ZipTipC18 using 40% acetonitrile in 0.1% trifluoroacetic acid as eluent, the peptide mixtures were loaded on an Anchor chip target (Bruker Daltonics, Bremen, Germany) using the thin layer technique and α-cyano-4-hydroxy-cinnamic acid as matrix and analyzed with a nitrogen laser (337nm) operated in reflector mode. External standards were used for calibration (Bruker peptide calibration standard). Each spectrum was accumulated for at least 600 laser shots. Measured peptide masses were used to search the Swiss-Prot, MSDB, TrEMBL, and NCBI sequence databases for protein identification by the Mascot program.

Putative nitrated peaks were identified by an increase in mass of 45 units, due to the nitro group, and/or an increase of 16 and 32 units lower than the one representing nitration [165, 166], which correspond to products from prompt fragmentation caused by the immediate loss of an oxygen molecule to form a nitroso species, followed by loss of a second oxygen molecule possibly to form nitrene or dehydroazepine species, as outlined by Sarver et al. [165]. These authors report that such characteristic addition to the

molecular ion of the modified peptide containing the nitro-substituted tyrosine group provides the unequivocal evidence for the presence of this modification.

Part 3- Results and Discussion

1° Experimental model (PC12 cells)

3.1 SUBSTRATE CHARACTERIZATION

The surface morphology of Supersonic Cluster Beam Deposition (SCBD) deposited TiOx films produced at different nanoscale roughness was investigated by Atomic Force Microscopy (AFM) and Scanning Electron Microscope (SEM).

Figure 14 display the AFM characterization of the control substrates and nanostructured samples: figs. (a) and (b) show the morphology of the glass cover slips before and after the coating with of Poly-L-Lysine with a calculated rms roughness of 0.343 ± 0.004 nm and 0.271 ± 0.020 nm, respectively; fig. (c) presents the AFM map (2 x 1 μm^2) of flat TiO_2 film with rms roughness of 0.229 ± 0.004 nm and figs. (d)-(g) report SEM and AFM images of cluster-assembled ns-TiO_2 films with roughness of 20.2 ± 0.5 nm and 29.1 ± 1 nm respectively (corresponding to 50 nm and 200 nm film thickness).

As previously described, the random stacking of nanoparticles on substrates resulting from SCBD, produces films with a homogeneous nanoscale porosity and roughness: the nanoparticles landing on the substrate stick on the surface of the growing film without any relevant diffusion or re-arrangement as it is typical of a ballistic deposition regime [123, 167]. AFM images of all ns-TiOx samples clearly appear to have a fine raster of nanometer-sized grains with porosity at the subnanometer scale and with the thicker film showing larger height fluctuations.

Recently, ns-TiO_2 substrates have been also evaluated in terms of the reproducibility and control of their structural (morphology) and physico-chemical properties by accurate statistical intraslide/interslide data, showing an extremely good reproducibility among different production batches [124].

In Figure 15, it is shown the core level photoelectron spectra at O 1s and Ti 2p edges before and after the moderate annealing. The spectra acquired after thermal treatment appear more noised, attesting a slightly increment of the insulation, however in both cases the peak positions of Ti $2p_{1/2}$ and Ti $2p_{3/2}$ fall at 464.9 eV and 459.1 eV respectively, corresponding to Ti (IV) bound to oxygen. Both peaks are symmetric, and the FWHM of $Ti2p_{3/2}$ is 1.6 eV, that is slightly larger than “defect-free” titanium dioxide single crystal (FWHM =1.25) as expected for ns-TiO_2 samples having a not negligible amorphous

fraction. In the O 1s binding energy region, the peak at 530.7 eV (FWHM = 1.6 eV) corresponds to O 1s core-level of oxygen atoms bound to Ti(IV), whereas the small broad shoulder at higher binding energies, 532.6 eV, is mainly due to the usual oxygen sources of contaminants such as physisorbed water and carbon bounded to oxygen. The stoichiometry evaluation assesses the fully oxidation of the nanostructure film which changes from TiO_{2-x} with x=0.16 (as deposited sample) to TiO_2 (after annealing).

On the basis of results obtained, we believe that nanostructured TiOx is an optimal substrate suitable for different applications in cell culture.

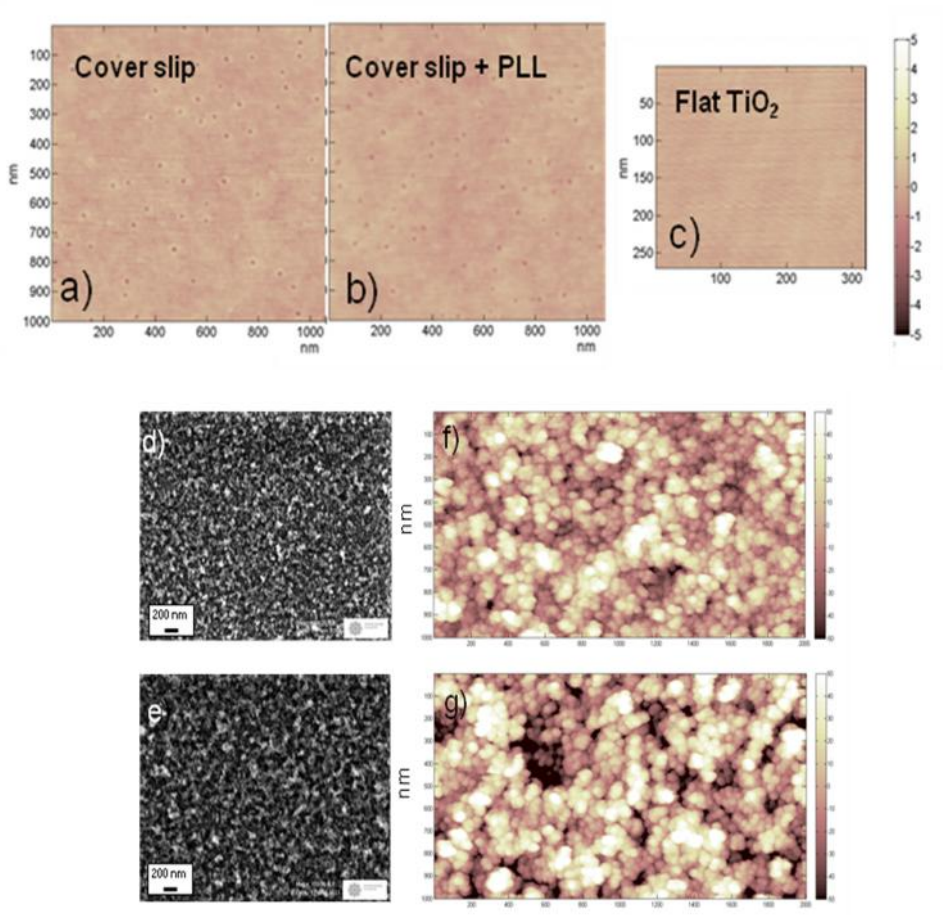

Figure 14. AFM images of reference samples: **a)** coverslip (1x1 μm^2); **b)** Poly-L-Lysine coated coverslip (1x1 μm^2); **c)** flat TiO_2 (2x1 μm^2). The vertical color scales range between 0 and 10 nm. Nanostructured samples: **d)** and **e)** high resolution SEM images and **f)** and **g)** AFM topographies (2x1 μm^2) of 50 nm and 200 nm thick nanostructured TiO_2, respectively.

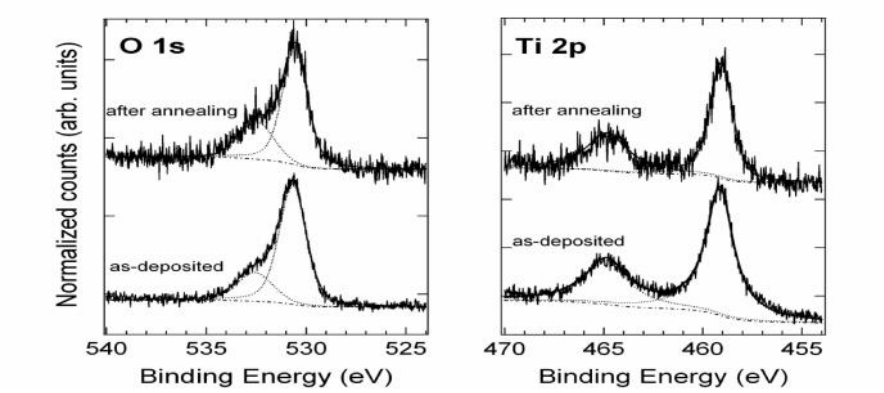

Figure 15. O 1s and Ti 2p photoemission spectra before and after thermal annealing at 200 °C of ns-TiO_2 films. Ti $2p_{1/2}$ and Ti $2p_{3/2}$ peaks fall at 464.9 eV and 459.1 eV respectively and O 1s peak shows two components one at 530.7 eV and the other at 532.6 eV.

3.2 TIO_2 NANOTOPOGRAPHY TRIGGERS NEURITOGENESIS IN THE ABSENCE OF NGF

To test the role of the nanoscale morphology of ns-TiO_2 in promoting neurite formation, PC12 cells were cultured on flat TiO_2 and cluster-assembled ns-TiO_2 substrates (20 nm and 29 nm rms roughness) either in NGF-free medium or in the presence of 50 ng/ml NGF and neurite formation was scored after 2 days. PLL-glass and flat microcrystalline TiO_2 were used as control. Figure 16 shows phase contrast optical images of PC12 cells cultured for 48 hr on PLL-Glass (A) and (B), flat TiO_2 (C) and (D), ns-TiO_2 20 rms (E) and (F) and ns-TiO_2 29 rms (G) and (H) with the following conditions: low serum medium (1% horse serum) only (A, C, E and G) or with 50 ng/ml NGF (B, D, F and H). As shown in Figure 16 (E) and (G), PC12 cells cultured on ns-TiO_2 undergo neurite expansion in NGF-free medium. After 2 days of culture neurites extend up to 103.74 µm or 154.68 µm on 20 rms and 29 rms roughness, respectively. The presence of NGF in the culture medium does not alter significantly the cell behavior: the length and number of the neurite observed are comparable as shown in Figure 17 (A) and (B) where the neurite length distributions and the cell differentiation rate are reported.

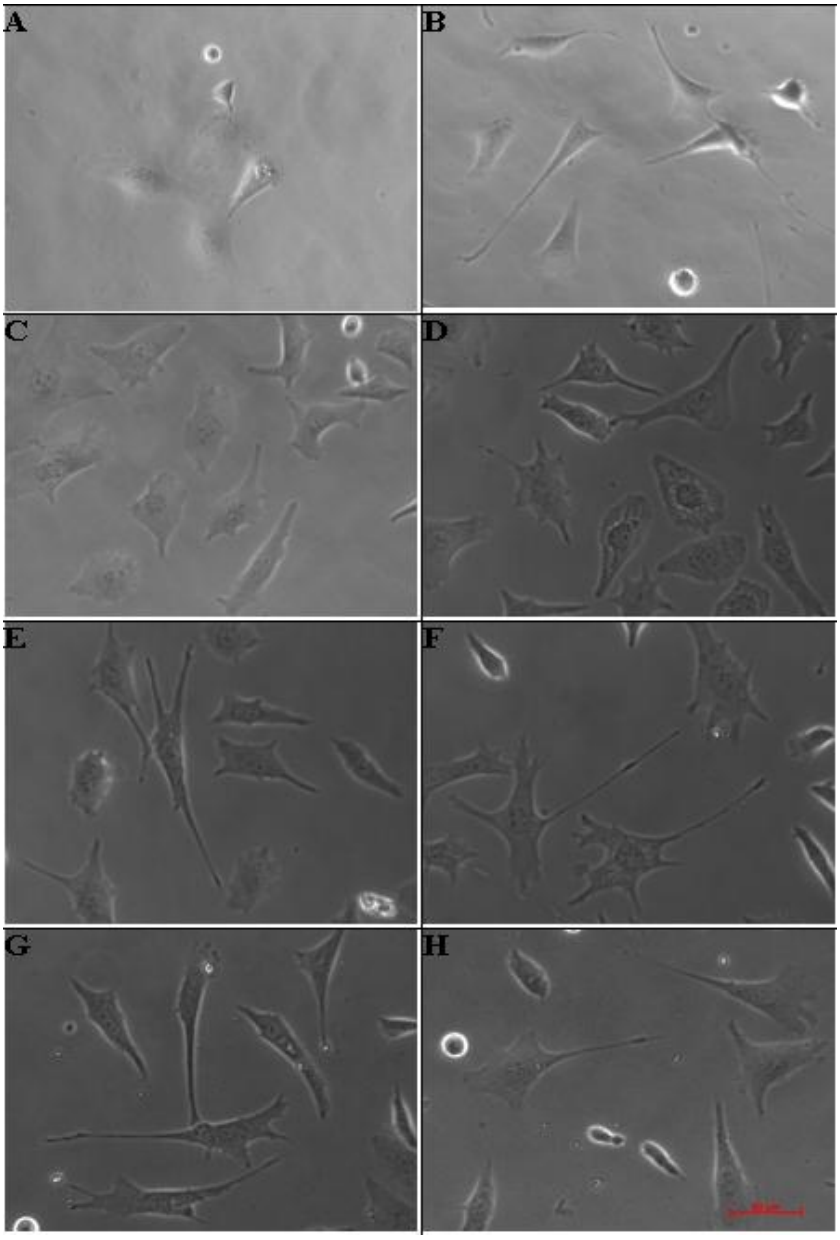

Figure 16. Effect of nanostructured TiO_2 surface on neurite formation in PC12 cells. Phase contrast photographs 40X magnification, Bar = 50 µm. PC12 cells were cultured for 48 hr in low serum medium (1% horse serum) only (A, C, E and G) or with 50 ng/mL NGF (B, D, F and H) on four kinds of substrates: PLL-Glass (A, B), flat TiO_2 (C, D), ns-TiO_2 20 nm rms (E, F) and ns-TiO_2 29 nm rms (G, H).

No significant differences in cells behavior were observed between 20 or 29 rms roughness ns-TiO_2 surfaces. At odd with nanostructured Titania substrates, PC12 cells

extended neurites on a PLL substrate only when medium was supplemented with NGF. Interestingly, neurite formation on PLL-glass upon NGF was equivalent to that detected on ns-TiO_2 films in terms of number and length. As far as cell division is concerned, Figure 17 shows that the nanostructure hampers cell growth as does NGF, when PC12 cells are seeded on PLL-glass in the presence of NFG. On the other hand, the behavior of PC12 cells on flat microcrystalline TiO_2 was very similar to the one observed for cells grown on PLL-glass and neuritogenesis was induced only by NGF addition (Figure 17).

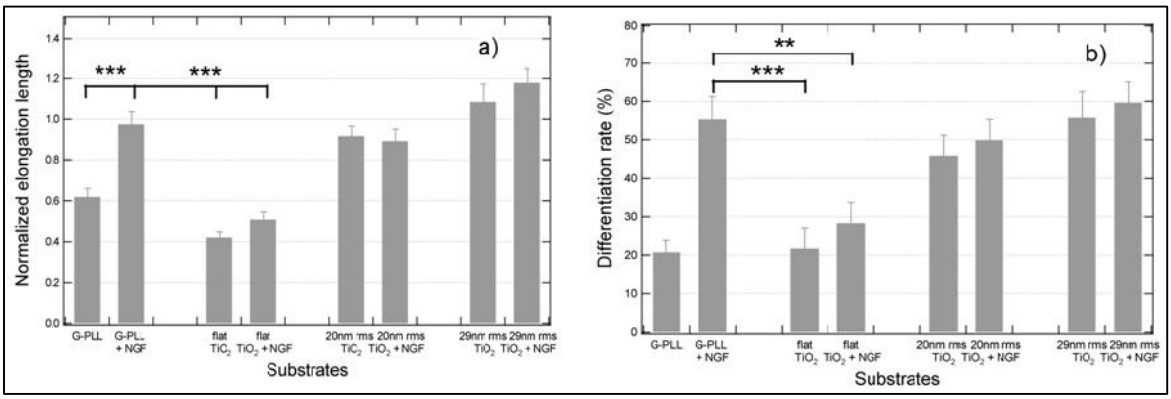

Figure 17. Histograms of the neurite length mean **(a)** and differentiation percentage **(b)** for each condition shown in Figure 16. ** $p<0.01$, *** $p<0.001$, unpaired Student t Test. G-PLL+NGF elongation length mean and differentiation values are not statistically significantly different from ns-TiO_2 20 nm rms and ns-TiO_2 29 nm rms.

Beside neurite extension, we checked also the expression of the neuronal marker MAP1B, a cytoskeletal protein involved in microtubule assembly whose expression increases upon PC12 cell differentiation induced by NGF. As expected, Western blot analysis carried out by specific antibodies shows that nanotopography leads to an increase in MAP1B expression regardless the roughness of the surface or the presence/absence of NGF (data not shown).

PC12 cells have been reported to require continuous NGF treatment for differentiation, survival and the phenotypic maintenance of the differentiated state; following cell growth

longer that 2 days on ns-TiO_2 substrates we observed that cells can survive up to 7 days on these surfaces as on glass in the presence of NGF.

Overall, these results strongly suggest that: **a)** nanostructure can impede cell proliferation and triggers neuritogenesis in the absence of other inducers; **b)** the phenomenon is related to the nanoscale topography of the surface; **c)** once triggered by surface roughness, neuritogenesis was unaffected by the addition of NGF. This implies that, in our model, topography may vicariate NGF but does not act cooperatively with the chemical stimulus to promote neuritogenesis upon differentiation. Our results are in remarkably good agreement with the observations reported by Lamour et al. using chemically modified glass surfaces as substrate for cell growth in the absence of NGF and with previous reports showing that NGF is not absolutely necessary to initiate PC12 cells differentiation [118, 119].

3.3 TIO_2 NANOTOPOGRAPHY PROMOTES THE EXPRESSION OF NITRIC OXIDE SYNTHASE (NOS) AND CYTOSKELETAL PROTEINS NITRATION

As described previously, nitric oxide (NO) is a signaling molecule involved in NGF-induced differentiation of PC12 cells [168]. NO triggers a switch to growth arrest and neuronal differentiation [68] and it modulates neuritogenesis by regulating signaling pathways through several mechanisms [169] such as binding to heme or iron sulphur sites in regulatory proteins [170] or by modifying tyrosines in cytoskeletal proteins [124, 41, 73, 74]. This biological messenger is produced by a group of enzymes called nitric oxide synthases (NOS) through the catalytic conversion of L-arginine to L-citrulline. In PC12 cells there are two forms constitutively expressed, the endothelial (eNOS) and the neuronal (nNOS), which are regulated by the cytosolic concentration of Ca^{2+} [171], and an inducible isoform (iNOS) which is predominantly involved in the production of NO preceding the development of the differentiated phenotype induced by NGF [68]. The three isoforms co-localize directly or indirectly with the cytoskeleton, including actin microfilaments, microtubules and intermediate filaments [172].

To uncover the molecular mechanism through which nanotopography leads neuritogenesis in PC12 cells grown on n-TiO_2, we tested the hypothesis that NO may be involved in the process through the increase of NOS expression. This was checked by Western blot analysis using either general NOS antibodies as well as iNOS specific antibodies. The results, summarized in Figure 18 (A) and (B), respectively, clearly show that the expression of the enzyme is increased in cells grown on nanostructured TiO_2 similarly to the level observed on PLL-glass following NGF addition.

On the contrary, cells grown on a flat TiO_2 surface show a behavior almost overlapping the one of cells grown on PLL-glass and do not present any increase in NOS expression in the absence of NGF (Figure 18 A). These finding suggest that the morphology of the substrate modulates NOS expression which is induced by nanoscale roughness and that iNOS is involved in cell differentiation as previously reported in PC12 cells grown on PLL-glass [68].

A

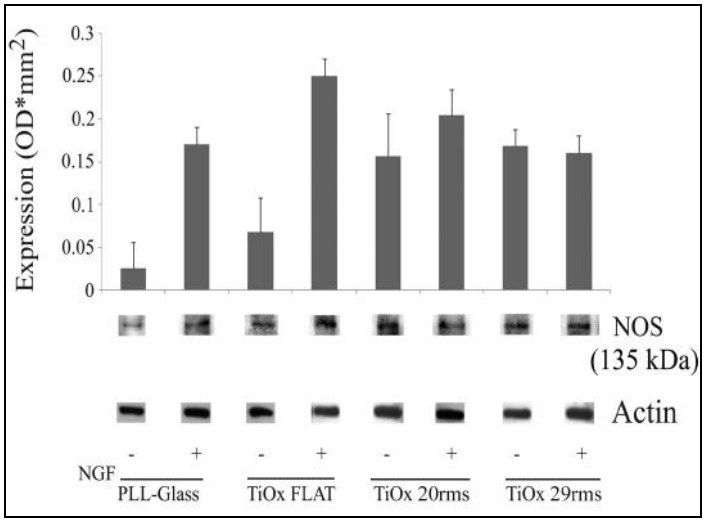

B

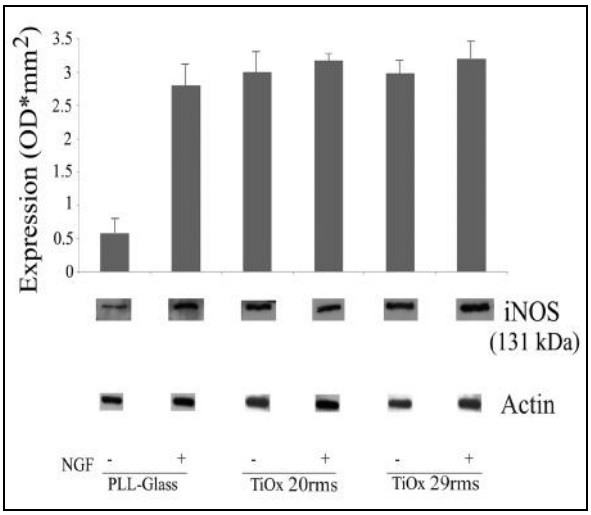

Figure 18. Topography of TiO_2 promotes the expression of nitric oxide synthase (NOS). NOS **(A)** and iNOS **(B)** expression were evaluated by Western blot analysis using anti-NOS and anti-iNOS antibodies in PC12 cells grown on PLL-coated glass (PLL-Glass), flat Titania (TiO_2-flat) and nanostructured Titania of different roughness (20 nm and 29 nm rms) in the presence and in the absence of 50 ng/mL NGF. Equal amounts of lysates (70 μg) were loaded on SDS-PAGE and probed with antibodies as indicated in the "Materials and Methods" section.

To further confirm the involvement of NOS in the differentiation process induced by nanotopography, we checked the nitration of proteins on PC12 cells grown on n-TiO_2

since, in previous studies on cells grown on PLL-glass, we reported that NGF triggers protein nitration during neuronal differentiation and that cytoskeleton becomes the main cellular fraction containing nitrated proteins [72]. The protein nitration was evaluated by means of anti-nitroTyr antibodies (Figure 19) as well as by tandem mass spectrometry (Table 1) on the Triton insoluble fraction of PC12 cells that is enriched in cytoskeletal components.

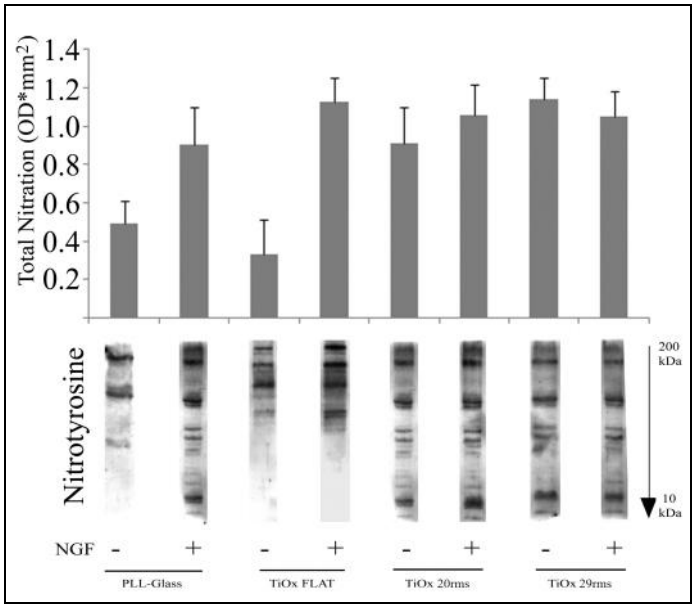

Figure 19. Topography of TiO_2 promotes cytoskeletal proteins nitration. Western blot analysis using anti-nitroTyr antibodies allows to detect nitrated proteins in the Triton insoluble fraction of PC12 cells grown on PLL-coated glass (PLL-Glass), flat Titania (TiO_2-flat) and nanostructured Titania of different roughness (20 nm and 29 nm rms) in the presence and in the absence of 50 ng/mL NGF.

Figure 19 shows that, in keeping with the results previously reported, PC12 cells grown on PLL-glass present a basal level of protein nitration which increases upon NGF induced differentiation at a level similar to the one evaluated for PC12 cells grown on ns-TiO_2 independently from the presence of the inducer NGF. The behavior of PC12 cells grown on flat TiO_2, on the contrary, is identical to the behavior of cells grown on PLL-glass where

the increase in protein nitration is induced by NGF, thus suggesting that the nano-roughness is involved in the nitration process.

The identification of the proteins found nitrated in PC12 cells grown on different TiO_2 substrates in NGF free media was carried out by tandem mass spectrometry looking for peptides containing at least one nitration at Tyr and/or Trp residues. In keeping with the previous findings [72], many of them are components of the cytoskeleton as shown in Table 1, which reports the list of the cytoskeletal proteins found nitrated in such conditions.

Accession	Uniprot	MW [kDa]	calc. pI	Description
	Accession			
gi4501885	P60711	41,7	5,48	actin, cytoplasmic 1
gi4501889	P63267	41,8	5,48	actin, gamma-enteric smooth muscle isoform 1 precursor
gi157823033	D3ZRN3	41,9	5,49	beta-actin-like protein 2 [*Rattus norvegicus*]
gi67078528	Q4V884	71,3	5,71	cell division cycle protein 16 homolog
gi114145461	Q0V8T4	145,6	6,24	contactin-associated protein like 5-3 precursor
gi256773236	Q63164	485,8	5,63	dynein heavy chain 1, axonemal
gi2642598	P16884	115,3	5,95	high molecular-weight neurofilament
gi57012436	Q6IFW6	56,5	5,15	keratin, type I cytoskeletal 10
gi6981182	Q64715	198,4	4,84	microtubule-associated protein 2
gi57164139	Q5M844	36,5	5,76	nesprin-4
gi293348155	D3ZGY7	149,2	5,40	PREDICTED: pleckstrin homology domain containing, family G, member 3-like isoform 1
gi293355776	F1LSL8	285,8	5,95	PREDICTED: spectrin, beta, non-erythrocytic 4
gi149025027	B1WBU8	58,8	6,20	similar to pleckstrin homology domain protein (5V327) (predicted)
gi54400730	Q5XIM9	57,4	6,46	T-complex protein 1 subunit beta
gi12963615	Q9ERD7	50,4	4,93	tubulin beta-3 chain
gi61557414	Q6PEC1	12,7	5,47	tubulin-specific chaperone A

Table 1. List of nitrated cytoskeletal-related proteins in PC12 cells grown on the TiO_2 surface (20 nm rms).

As reported in [73, 74, and 163] alpha-tubulin, actin and tau are among the major target of this post-translational modification which may confer increase stability to cytoskeleton

during neuronal differentiation [173]. Therefore, the expression of tubulin, actin and tau isoforms 50 and 70 kDa, were specifically evaluated using the corresponding antibodies while their Tyr nitration was checked following stripping of the membrane and reprobing with anti-nitroTyr antibodies. The results are summarized in Figure 20 where the ratio between nitration and expression is reported for each protein tested.

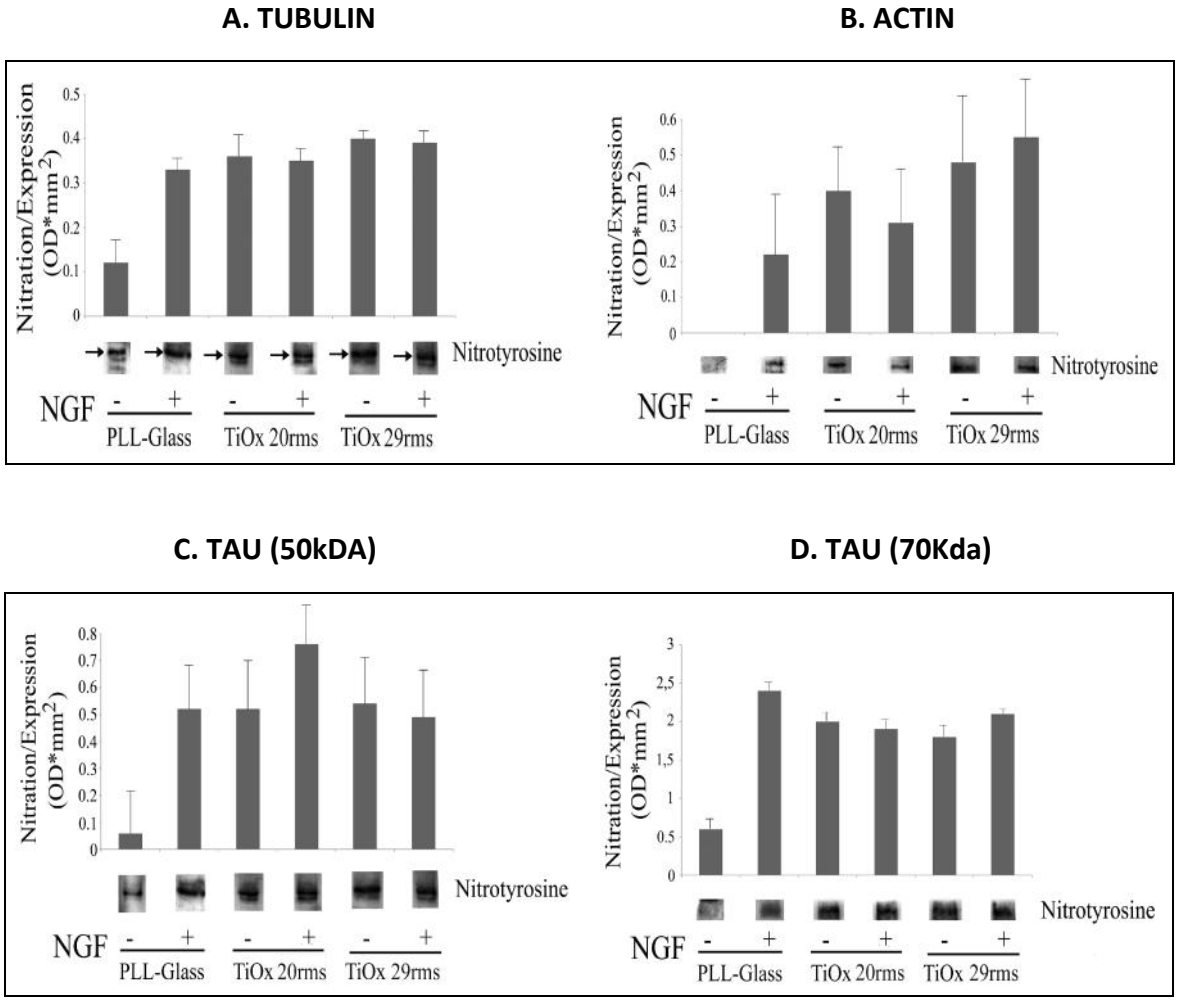

Figure 20. Nitration of tubulin, actin and tau isoforms. The expression of tubulin **(A)**, actin **(B)** and tau isoforms 50 **(C)** and 70 kDa **(D)** were evaluated using the corresponding specific antibodies in the Triton insoluble fraction of PC12 cells grown on PLL-coated glass (PLL-Glass) and nanostructured Titania of different roughness (20 nm and 29 nm rms) in the presence and in the absence of 50 ng/mL NGF. Tyr nitration of the same proteins was checked following stripping of the membrane and reprobing with anti-nitroTyr antibodies. The results are means of 2 different experiments.

The pattern of their nitration follows the same pattern reported above for protein nitration in general (Figure 19) confirming that the nanoscale roughness induces nitration in the absence of NGF.

3.4 EFFECT OF iNOS INHIBITOR ON PC12 CELLS GROWN ON NANOSTRUCTURED TIO_2

To ascertain that NOS is critical in PC12 cell differentiation triggered by the substrate nanostructure, cells were grown in the presence of iNOS inhibitor (S-methylisothiourea, SMT).

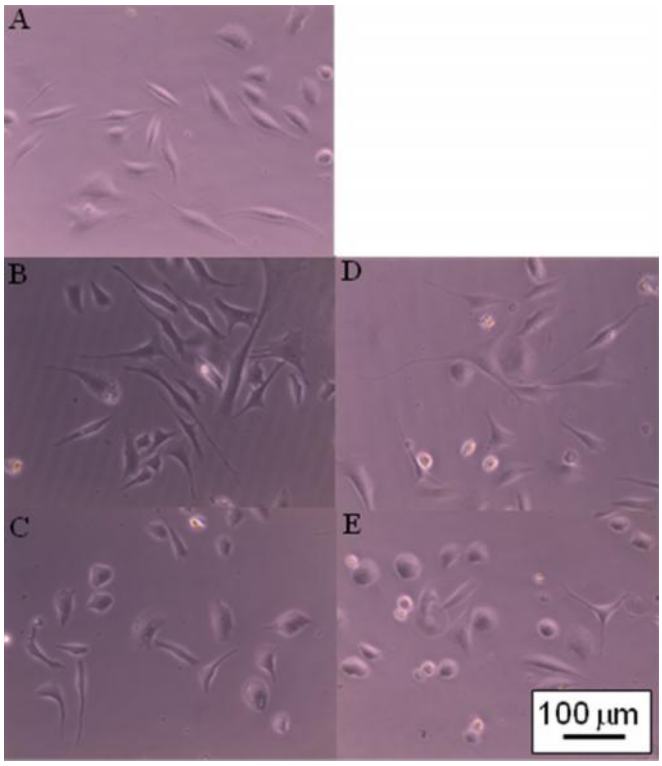

Figure 21. Effect of iNOS inhibitors on neurite formation in PC12 cells induced by nanostructured TiO_2 surface. Phase contrast photographs 40X magnification, Bar = 50 µm. PC12 cells were cultured on PLL-coated coverslips for 48 hr in low serum medium (1% horse serum) only **(A)**, with 50 ng/mL NGF **(B)** or with 50 ng/mL NGF and 2 mM SMT **(C)**. PC12 cells were cultured on ns-TiO_2 (20 nm rms) for 48 hr in low serum medium (1% horse serum) only **(D)** or with 2 mM SMT **(E)**.

As shown in Figure 21 (A)-(C) and Figure 22, PC12 cells cultured under control conditions on PLL-glass undergo neurites expansion and differentiation only in the presence of NGF and both processes are hampered by incubation with SMT.

The same effect was observed when PC12 cells were cultured on ns-TiO_2 of 20 rms roughness in NGF-free medium: Figure 21 (D) and (E) and Figure 22 clearly show that prevention of neurite growth and differentiation is induced by SMT also under this growing condition at an extent similar to the one observed on PLL-glass.

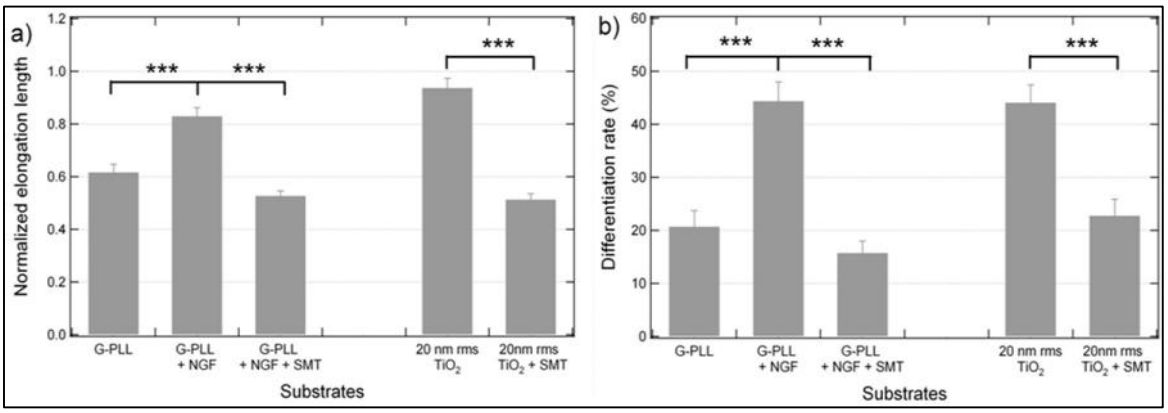

Figure 22. Histograms of the neurite length mean **(a)** and differentiation percentage **(b)** in the presence of selective inducible NOS inhibitor (2 mM SMT) for each condition shown in Figure 21. *** $p<0.001$, unpaired Student t Test.

Altogether, these results clearly suggest that iNOS is involved in cell differentiation observed in PC12 cell grown on ns-TiO_2 without NGF. Based on these finding we confirm our hypothesis that nanotopography mimics the effect of NGF, promoting NOS expression and cytoskeletal protein nitration.

3.5. EFFECT OF NANOSTRUCTURED TIO_2 ON THE HUMAN NEUROBLASTOMA SH-SY5Y CELL LINE

We aimed at defining whether the effects produced by nanostructured TiO_2 on neurite growth was specific for PC12 cells or was a generalized effect produced by the substrate on different neuronal cell types. To this aim, we maintained the human neuroblastoma SH-SY5Y cell line either on glass or ns-TiO_2 20 nm and 29 nm rms roughness. As shown in the case of PC12 cells, neuroblastoma cells grown on ns-TiO_2 displayed longer neurites, as revealed by bright field examination, as well as by the staining for the protein SNAP-25. The neurite length distributions analysis showed an evident shift of the normal distribution toward higher length values. No difference between different ns-TiO_2 roughness was observed. Western blot analysis by anti nitrotyrosine antibodies, shows that there is an increase in protein nitration triggered by the nanostructure TiO_2 as described above in PC12 cells suggesting that this behavior is common to different neuronal cell types (data not shown).

3.6. INVOLVEMENT OF ERK SIGNALING CASCADE IN NANOSTRUCTURED-INDUCED NEURITOGENESIS

The addition of NGF to PC12 cells causes neurite elongation through a sustained activation of ERK, a mitogen-activated protein kinase whose phosphorylation is essential to neuronal differentiation [174]. As reported by Yamazaki et al. [69], this activation occurs upon activation of NOS and can be obtained also by NO itself, in the absence of NGF, during NO-induced neuritogenesis. These observations prompted us to check if the ERK-signaling cascade may be also involved in the differentiation process triggered by nanotopography. We checked the phosphorylation of ERK, by Western blot analysis, using anti p-ERK antibodies (Figure 23).

The results clearly show that when cells are grown on ns-TiO_2 in NGF-free media ERK is phosphorylated to the same extent as in cell grown on glass or on flat TiO_2 upon stimulation by NGF. In the latter two substrates the activation of ERK is almost

undetectable in the absence of NGF. The data strongly suggest that the activation of ERK is indeed induced by either NGF or the nanotopography, when the chemical inducer is absent.

Our data are in extremely good agreement with previous findings by Foley et al. [115] who described the involvement of ERK in the differentiation of PC12 cells cultured on synthetic substrates whose topographical features act to modulate neuritogenesis under sub-optimal concentration of NGF.

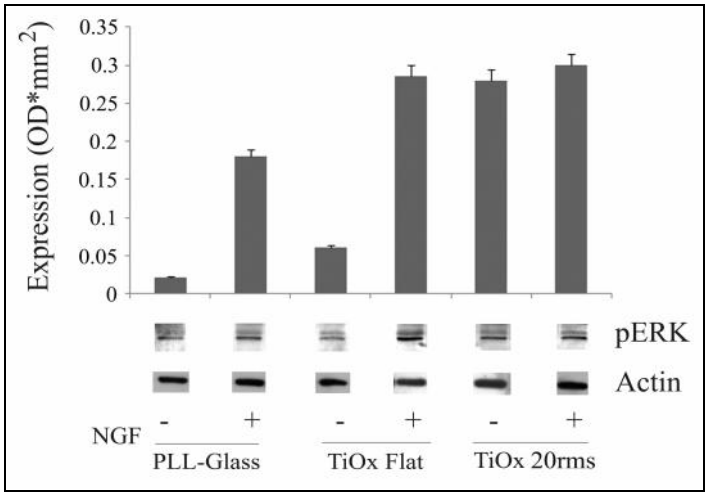

Figure 23. Involvement of ERK signaling cascade in nanostructured-induced neuritogenesis. The phosphorylation of ERK was evaluated by Western blot analysis, using anti p-ERK antibodies, on PC12 cells grown on PLL-coated glass (PLL-Glass), flat Titania (TiO_2-flat) and nanostructured Titania (TiO_2 20 nm rms) in the presence and in the absence of 50 ng/mL NGF. Equal amounts of lysates (70 μg) were loaded on SDS-PAGE and probed with anti p-ERK antibodies. The results are means of 3 different experiments.

Since NGF treatment has been shown to up-regulate $\alpha_1\beta_1$ integrin molecules in PC12 cells [175, 176] and integrin-mediated FAK activation augments EGF/ERK signaling [177], they suggested that the formation and organization of focal adhesions on nanoscale features may cooperate with NGF to promote neuritogenesis when the concentration of the

chemical inducer is low while it is ineffective at 50 ng/ml NGF when the signaling cascade is already at its maximum. This is in accordance with our finding that nanotopography mimics the effect of NGF but it does not act cooperatively with NGF to promote neuritogenesis. However how the topography may affect the ability of a cell to initiate the signaling pathway was not addressed by their research.

Based on our finding, we propose that the perturbation of the actin cytoskeleton caused by the surface nanoroughness increases NOS expression and the NO-signaling cascade activation therefore explaining the cell behavior observed on nanostructured TiO_2 (Scheme 1).

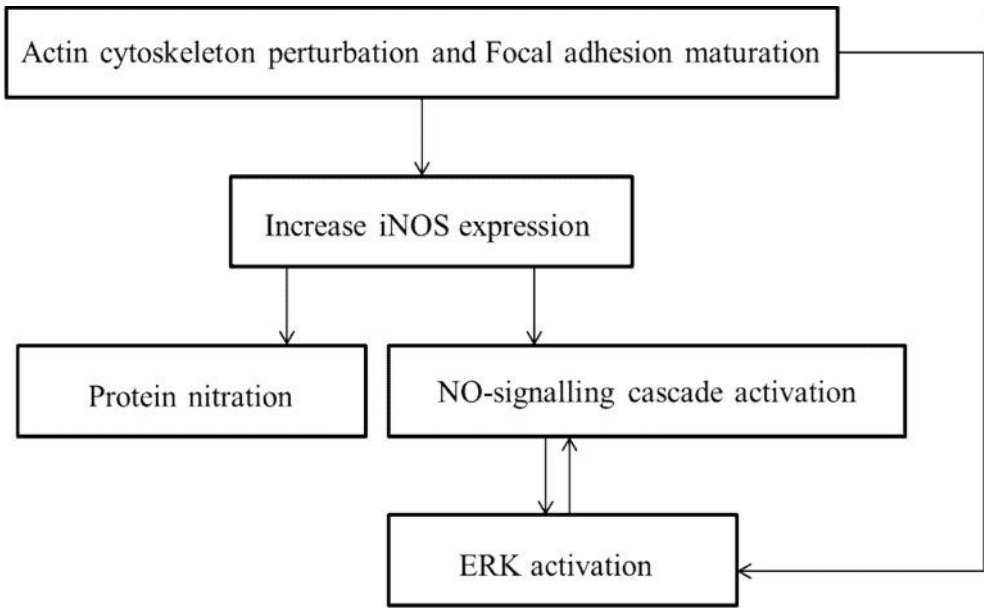

Scheme 1. Proposed mechanism for the differentiation of PC12 cells triggered by nano roughness. The perturbation of the actin cytoskeleton caused by the nano-roughness of the surface increases iNOS expression and the NO-signaling cascade activation through ERK phosphorylation.

One question arises from this picture: how nanotopography may increase NOS expression in order to produce NO. Many data suggest that NOS activity may be regulated by

cytoskeleton at transcriptional, post-transcriptional and post-translational level [172] and that the cytoskeletal reorganization induced by extracellular stimuli such a shear stress, hypoxia and drugs play an important role in regulating NOS expression and activity [172, 178]. On this regards, recent findings clearly demonstrated that β-actin association with eNOS modulates NO production shifting the enzymatic activity from superoxide formation toward NO production [179]. iNOS gene transcription is regulated by changes in the actin cytoskeleton in alveolar epithelial cells [180], glomerular mesangial cells [181] and vascular smooth muscle cells [182, 183]. In macrophages it is proposed that microtubule depolymerisation activates stress fibers formation through regulation of iNOS gene expression by actin microfilaments [184-186]. Moreover, in these cells the interaction of iNOS with actin binding protein α-actinin has been demonstrated [172]. Colocalization of nNOS with cytoskeleton in skeletal muscle cells optimizes NO production, improving metabolism, elasticity and mechanical properties of the cells [187, 188]. Recently, Gupta et al. [189] demonstrated a clear interaction between integrins and iNOS in modulation of cell migration. Their results clearly show that integrin $\alpha_9\beta_1$ enhances cell migration through production of NO by iNOS regulated by SRC tyrosine kinase. Moreover, the iNOS/Src/Fak axis was found to be critical in cell mobility processes in macrophages [190].

Based on these observations, we confirm the previous hypothesis that ns-TiO_2 surfaces nanotopography perturbs the actin cytoskeleton resulting in the increase in NOS expression and the activation of the NO-signaling cascade through ERK phosphorylation. Therefore, the results presented in this work suggest for the first time that NO signal cascade is involved in the differentiation process induced by nanotopography, adding new information on the mechanism and proteins involved in the neuritogenesis triggered by the surface properties. We suppose that NO could be the “secret factor” produced by PC12 cells in response to surface properties that Lamour very recently proposed in order to explain the influence of surface energy distribution on neuritogenesis [118].

2° Experimental model (*Ciona intestinalis*)

3.7 EFFECTS OF MODULATION OF NO LEVELS ON METAMORPHOSIS

The involvement of NO in metamorphosis in *Ciona intestinalis* was previously demonstrated by Dr. Anna Palumbo using two main approaches aimed at increasing or decreasing NO levels [150]. In the first case, bioavailability of arginine necessary for NO production was increased using the arginase inhibitor nor-NOHA and a delay of the process was observed. Conversely, endogenous NO was reduced by the NOS inhibitor (L-nitro-arginine L-NA) resulting in an acceleration of metamorphosis. In the present study, we report a re-examination of the effects of NO using alternative NOS inhibitors and donors and in particular the NOS inhibitor TRIM and the slow NO-releaser SPER/NO. TRIM is an imidazole derivative which inhibits NOS interfering with the binding of both L-arginine and the cofactor BH_4 [191]. Although a less potent inhibitor of NOS *in vitro* than L-nitro-arginine methyl ester, TRIM exhibits however a more potent antinociceptive activity, suggesting that other factors *in vivo* contribute to potentiate its action [192].

In the present work, we treated just hatched larvae (early larvae) with the NOS inhibitor TRIM to decrease NO levels (Figure 24 A). After 24 hr, TRIM at 250 μM concentration induced a significant slow down of metamorphosis, as revealed by the increase of late larvae or larvae during tail resorption and a concomitant decrease of juveniles at early rotation stage with respect to the control. Examination of the treated larvae at 48 hr did not show any difference from the control. At 500 μM concentration, TRIM proved to be toxic.

To investigate the effects of a slow-releasing NO donor, early larvae were treated with 250 μM SPER/NO. An acceleration of the metamorphosis process was observed (Figure 24 B), as apparent from the decrease of the percentage of late larvae or larvae during tail resorption to 27% with respect to 65% of the control performed in the presence of spermine, the product produced by exhausted SPER/NO. Lower concentration of SPER/NO (100 μM) had no effect, whereas higher concentrations e.g. 500 μM proved to be toxic.

As shown in Figure 24, the effects of TRIM and SPER/NO on metamorphosis seem to be in contrast with those previously reported following administration of L-NA and nor-NOHA

[150]. This apparent discrepancy may be related to our incomplete knowledge of how these substances act *in vivo* in *Ciona* larvae. It is possible that the selective NOS inhibitor TRIM affects metamorphosis in a different manner with respect to the non selective inhibitor L-NA. Moreover, the complexity of the metamorphosis process which includes apoptosis, ERK activation and NO production, makes it difficult to identify the specific pathway (s) affected.

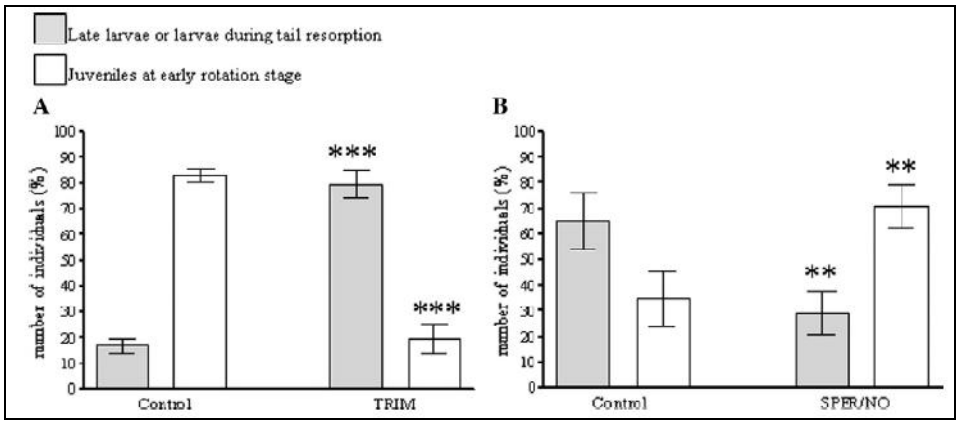

Figure 24. **Modulation of NO levels affects metamorphosis**. Early larvae were treated with NOS inhibitor 250 µM TRIM **(A)** and the NO donor 250 µM SPER/NO **(B)**. In the case of SPER/NO the control was performed in the presence of 250 µM spermine. After 24 hr the number of late larvae, larvae during tail regression and juveniles at early rotation stage were counted and reported as percent of the total. Data, expressed as means ± SEM, were assessed by variance analysis (one-way ANOVA after arcsine transformation). Asterisk represents the significance respect to the control (***P < 0.0001; **P < 0.001). Number of experiments = 10 (A) and 7 (B).

3.8 EFFECTS OF RNS MODULATION ON METAMORPHOSIS

Generation of reactive oxygen species (ROS), such as hydrogen peroxide (H_20_2) and superoxide is a common phenomenon resulting from diverse metabolic activity of the cells. ROS elicit oxidative stress and affect a wide variety of physiological and pathological processes including embryonic development, maturation and aging [193]. A define role of

the ROS and antioxidants is also well established in various cellular processes such as development, differentiation, regeneration and apoptosis. Recently, it has become evident that when tightly controlled, ROS such as oxygen and H_20_2 act as intracellular signaling molecules and perform critical function in the cell. These effects may be mediated by interaction with the NO signaling pathway and the resulting generation of peroxynitrite and NO_2, which can lead to protein tyrosine nitration.

On this regard, we investigated the role of nitrating agents, such as peroxynitrite, and free radical scavengers on the process of metamorphosis. Figure 25 A clearly shows that addition of the tyrosine nitrating agent peroxynitrite at 250 µM concentration resulted in an acceleration of the process, as revealed by the decrease of late larvae or larvae during tail resorption and a concomitant increase of juveniles at early rotation stage respect to the control.

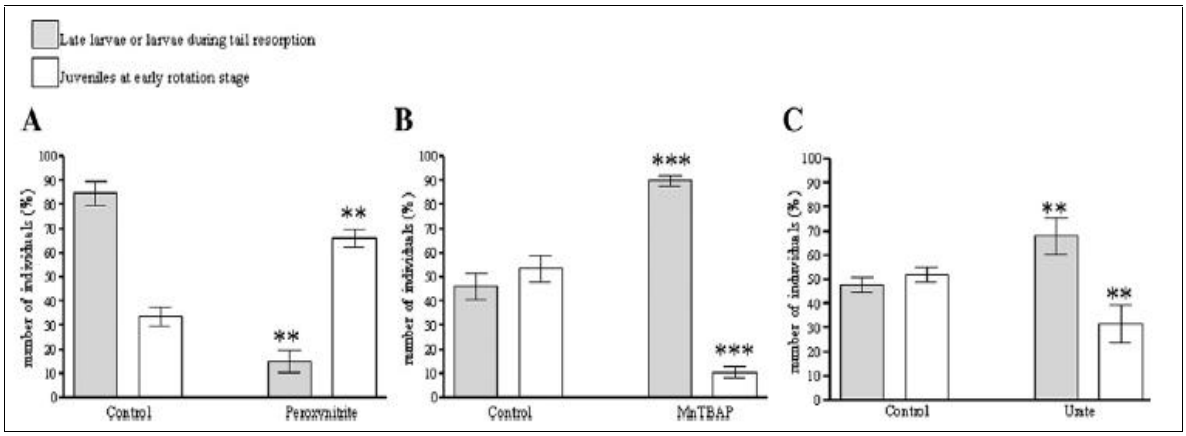

Figure 25. Modulation of RNS levels affects metamorphosis. Early larvae were treated with 250 µM peroxynitrite **(A)**, 50 µM peroxynitrite scavenger MnTBAP **(B)** and the antioxidant 600 µM urate **(C)**. After 24 hr the number of late larvae, larvae during tail regression and juveniles at early rotation stage were counted and reported as percent of the total. Data, expressed as means ± SEM, were assessed by variance analysis (one-way ANOVA after arcsine transformation). Asterisk represents the significance respect to the control (***P < 0.0001; **P < 0.001). Number of experiments = 7 (A), 9 (B), 5 (C).

The same acceleration of the process was apparent with 500 μM peroxynitrite whereas no effect was observed at 100 μM concentration.

Consistently, treatment of early larvae with the peroxynitrite scavenger MnTBAP led to a marked decrease in the rate of metamorphosis resulting in a lower proportion of juveniles compared to the control (Figure 25 B). Likewise, urate, an endogenous antioxidant that converts the nitrating radical NO_2 to NO_2^-, was found to inhibit the rate of the process (Figure 25 C).

In line with several reports demonstrating the occurrence of oxidative stress during developmental processes in some invertebrates [194-196], the present findings indicate that ROS production is associated with *Ciona* larval development, when the animals became in contact with oxidative environment and are no longer protected by corion membrane. Therefore NO-derived protein nitrating agents may be involved as promoters of metamorphosis in *Ciona*.

3.9 PROTEIN NITRATION DURING LARVAL DEVELOPMENT: PROTEOMIC AND IMMUNOCHEMICAL IDENTIFICATION OF MAIN TARGETS

Originally regarded as a post-translational protein modification serving as an indicator of NO-mediated oxidative inflammatory reactions, this pathway is increasingly appreciated as an authentic signaling pathway.

In this context, we examined protein nitration patterns during development by Western blot analysis of protein extracts at different stages using an antibody against nitrotyrosine (Figure 26).

In the embryonic stages, gastrula and late tailbud, few nitrated bands could be detected. However, a series of distinct immunopositive bands became visible after hatching in early and in late larvae. This observation suggested that protein nitration becomes more consistent with, and is implicated in, larval development. MnTBAP-treated larvae showed a suppression of immunopositivity. No effect was observed on nitrated bands in the presence of the NOS inhibitor TRIM (data not shown). All of the immunopositive bands disappeared after treatment with dithionite, which reduces nitrated tyrosines to amine

derivatives (data not shown) [197]. At late larva stage the band corresponding to the nitrated protein at 65 kDa was identified as snail homolog (Genbank accession number AF002987) by N-terminal sequence analysis carried out by automatic Edman degradation upon electroblotting on PVDF of the protein extract.

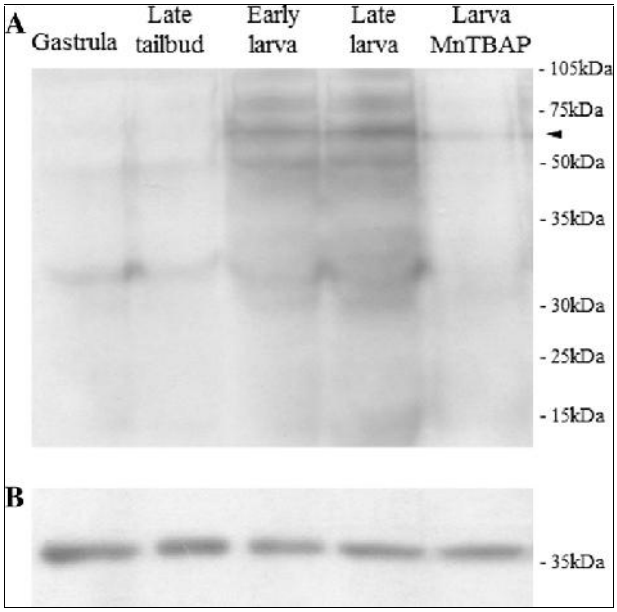

Figure 26. Protein nitration during *C. intestinalis* development. Protein extracts of stages were examined for anti-nitrotyrosine **(A)** and anti-actin immunopositivities **(B)**. Early larvae were treated with 50 µM MnTBAP and protein extract was examined after 8 hr. Arrow indicates 65 kDa.

In order to improve the protein separation and identify nitrated proteins by mass spectrometry the extract was separated by 2-DE (Figure 27) and nitrated proteins were detected by Western blot with anti-nitrotyrosine antibodies.

In accordance with the N-terminal sequence analysis, three nitrated spots were identified as snail homolog by anti-snail antibodies (Figure 27) and fingerprint mass analysis (Figure 28) suggesting the presence of three different snail isoforms.

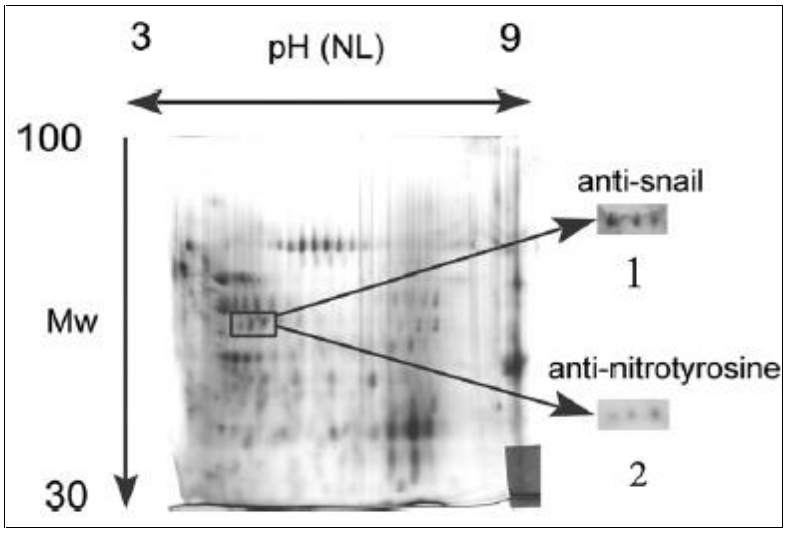

Figure 27. Identification of nitrated snail. The protein extract from late larvae was separated by 2-DE and stained by silver. Snail was detected by anti-snail antibodies. The same spots were also detected by anti-nitrotyrosine antibodies.

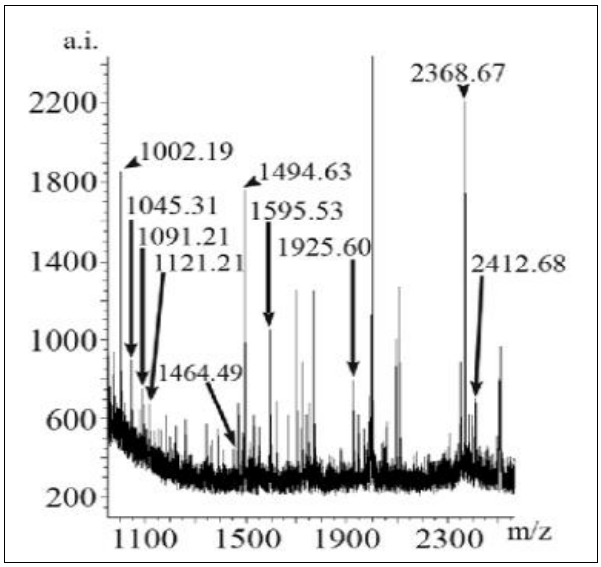

Figure 28. MALDI-TOF analysis of the nitrated spot. Molecular masses are reported as monoisotopic mass.

A very good sequence coverage (39%) (Figure 29) was obtained combining the results from mass spectrometry and N-terminal sequence analysis. 4 Tyrosines out of 10, namely Y139, Y370, Y445, Y549, were found nitrated searching for peaks that show an increase in mass corresponding to the addition of nitro (NO_2) (+45), nitroso (NO) (+29) and nitrene (N) (+13) species [13] (Table 2).

```
        10         20         30         40         50         60
MTSVEPMLYQ GKHAVQKNEG ESTRPCTLSG DDSFYCSGES TNSTSSPTSS ITSSRSCGPD

        70         80         90        100        110        120
SDEGFPRQDD LDLRDKASKN LQRSVELFCP IKSKSVDHDN DLMPMDLSCK KRTSPKQNCK

       130        140        150        160        170        180
TASMPKTSPT IKSEPIDDYP ASLTRNAPPS SMPSVSPPSS NITREFPPSM FPSWPYFSTP

       190        200        210        220        230        240
ITSSVGGFPS FPSSYIAGKY LHPALFLPPP ATSCQTVPTN SPLGLSVGNS MLPGLHQLAA

       250        260        270        280        290        300
SHFQPSMIKP VAQPQGVPQE QNSPNHDDQK FAQGSPQPRF SPTNLVQDPS LLAEFARVFS

       310        320        330        340        350        360
RQVEQFRPKP SFEENNMKNQ NSERRRKNAK PLKISADVSP PHPQLNDMRS ISFKDLPTMV

       370        380        390        400        410        420
SQTHDHTAFY GAQKNRQELK RKSSSEDNSE SPTGKKVCLD SKTTWRQIDA PTFQISDAIE

       430        440        450        460        470        480
EQNKAPQPVS FKPCRIPCTE CGRTYATIGA LAKHAKTHED PESGSKFNCK ICKKECSSLG

       490        500        510        520        530        540
ALRMHIRTHT LPCECHICGK AFSRTWLLQG HIRTHTGEKP YQCTVCSRAF ADRSNLRAHM

       550        560        570        580
QTHETVKRYS CVTCEKTFSR ISLLKRHQVH CETASQVAQR KTAS
```

Figure 29. Snail homolog (AF002987) sequence. The yellow highlighted aa was been recognized by MALDI-TOF analysis. The sequence coverage percentage is 39%. The portion highlighted in red was been determined by N-terminal sequence carried out by automatic Edman degradation.

	PEPTIDE SEQUENCE	N(+13)		NO(+29)		NO_2(+45)	
		Mw observed	Mw theotetical	Mw observed	Mw theotetical	Mw observed	Mw theotetical
Y139	^{133}SEPIDDYPASLTR^{145}			1.492,75	1.492,70	1.509,79	1.508,70
Y445	^{436}IPCTECGRTYATIGALAK^{453}	1.993,81	1.994,90				
Y445	^{444}TYATIGALAK^{453}			1.037,36	1.037,57		
Y370	^{355}DLPTMVSQTHDHTAFYGAQK^{374}			2.275,12	2.276,05	2.291,30	2.292,05
Y549	^{549}YSCVTCEKTFSR^{560}	1.550,70	1.550,68				

Table 2. Tyr nitration of snail. MS analysis of the tryptic peptide mixtures of nitrated snail Homolog in *C. Intestinalis*. The tryptic peptide mixture was analyzed by MS searching for tyrosine-containing peptides. Putative nitrated peaks were identified by an increase in mass corresponding to the addition of nitro (NO_2) (+45), nitroso (NO) (+29) and nitrene (N) (+13) species. Only peptides containing nitrated tyrosine residues are reported. The analysis of spectra, related to tryptic digestion, allowed to find peaks originated from the nitration of **Tyr 139**, **Tyr 445**, **Tyr 370** and **Tyr 549**.

The identification of snail as one of the target for nitration during larva metamorphosis prompted us to identify other proteins found nitrated at larva stage. The attention was focused on ERK/p-ERK on the basis of the strong immunopositivity to anti-nitrotyrosine antibodies in the expected molecular weight region and their reported signaling during *Ciona* metamorphosis [145]. ERK and p-ERK were detected by Western blot analysis on the late larva extract after immunoprecipitation (Figure 30 A). The extract was immunoprecipitated with anti-p-ERK antibodies and the immunocomplex p-ERK positive (Figure 30 A, 1) was found to be nitrated (Figure 30 A, 2). The p-ERK-free supernatant was treated with anti-ERK antibodies and the ERK-positive immunocomplex (Figure 30 A, 3) exhibited anti-nitrotyrosine reactivity (Figure 30 A, 4). The nitration of ERK and p-ERK was confirmed by 2-DE experiments which also revealed the presence of multiple immunopositive spots with analogous molecular weight and different pI, probably attributable to ERK in different nitration/phosphorylation patterns (Figure 30 B).

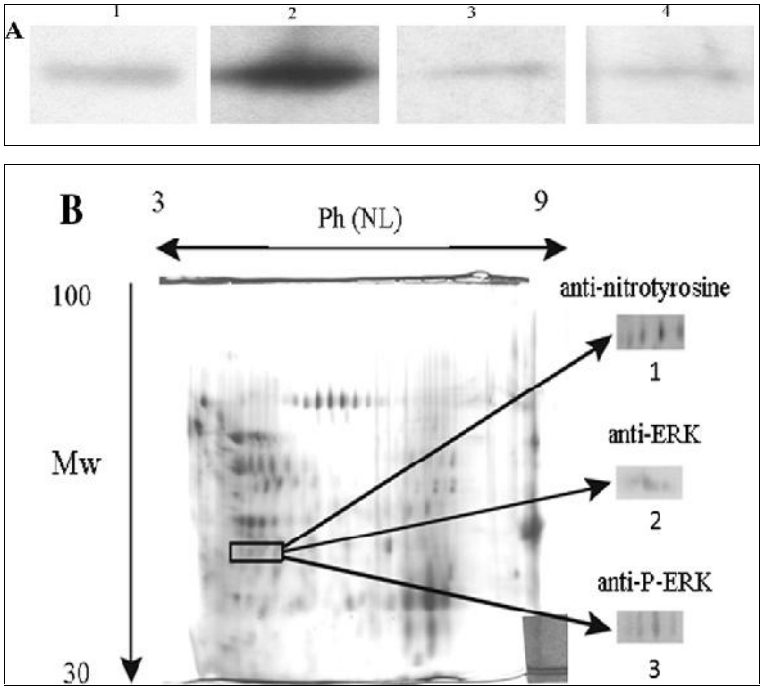

Figure 30. Identification of nitrated ERK and p-ERK. The protein extract from late larvae was examined after immunoprecipitation **(A)** and 2-DE **(B)**. **(A)** Western blots of p-ERK immunoprecipitate from late larvae performed with anti-p-ERK **(1)** and anti-nitrotyrosine **(2)** antibodies. Western blots of ERK immunoprecipitate from the p-ERK-free supernatant developed with anti-ERK **(3)** and anti-nitrotyrosine **(4)** antibodies. **(B)** The protein extract from late larvae was separated by 2-DE and stained by silver. ERK and p-ERK were detected by anti-ERK and anti-p-ERK antibodies, respectively **(2, 3)**. The same spots were also detected by anti-nitrotyrosine antibodies **(1)**.

Identification of nitrated snail and ERK represent an important outcome to yield interesting insights into the mechanisms regulating *Ciona* metamorphosis. Snail represents a superfamily of zinc-finger transcription factors involved in processes requiring pronounced cell movements during embryonic development and tumor progression [198, 199]. In *Ciona*, snail is linked to mesoderm subdivision in different territories, it establishes boundaries between the adjoining tissues of notochord and tail muscle lineages during embryonic development [200, 201]. No information is available about snail function and expression during larval development. The *Ciona* snail protein is

composed of 584 aminoacid residues and shares substantial homology with other members of the snail family [200]. In particular, the C-terminal 153 amino acid residues include five putative zinc fingers that are homologous to the corresponding zinc fingers of the *Drosophila* protein. Like other members of the family, *Ciona* snail contains particularly extensive homology in the second, third and fourth fingers involved in DNA binding. It is interesting to note that two out of the four tyrosine residues found nitrated in the present study (Tyr 445 and Tyr 549) belong to this C-terminal domain and are very well conserved in all the snail homolog proteins present in the data banks. It is tempting to speculate that nitration in this region may modulate the interaction with nucleic acids. The other two nitrated residues (Tyr 139 and Tyr 370) are located in the N-terminal region that is much more divergent and it is known to be phosphorylated in mammalian cells where phosphorylation regulates snail activity. In particular phosphorylation is relevant to the structure of snail: introduction of negative charges hinders the interaction of this region with the C-terminal zinc finger domain and induces a conformational change allowing, presumably, nuclear export of the protein. Phosphorylation just shifts the protein out of the nucleus, blocking its transcriptional activity. In this way phosphorylated snail is accumulated in the cytoplasm [202]. The possibility that nitration in the N-terminal region could affect snail phosphorylation is an issue which requires further investigation. In this context, the three spots with analogous molecular weight and different pI identified in late larvae of *C. intestinalis* as nitrated snail could probably correspond to isoforms of the protein in different nitration/phosphorylation patterns.

In addition to snail, also ERK and p-ERK appear to be nitrated in late larvae. This result is of biological interest in relation to the key role of ERK signaling in metamorphosis [145] and the reported relationship between ERK nitration and phosphorylation. In vascular smooth muscle cells nitration of ERK1/2 induces its phosphorylation [203], whereas in portal hypertensive gastric mucosa and murine peritoneal macrophages extensive ERK nitration leads to an impaired ERK signaling [204, 205]. It is relevant that aberrant activation of the ERK pathway has been correlated to many types of human tumors and the components of this signaling are becoming attractive targets for cancer chemotherapy [206].

Part 4- Conclusion

Investigation of protein tyrosine nitration has intensified over the last two decades leading to a better understanding of the role of this post-translational modification in cellular signaling.

Although initially considered to be a marker of oxidative stress, there is a growing body of experimental data suggesting that nitration of tyrosine fulfills the criteria of a physiological process. For example, tyrosine nitration has been detected under physiological conditions in most organ systems and in a number of cellular models.

On this regard, in the present work, two different experimental models have been used to explore the biological significance of protein tyrosine nitration in physiological processes associated with cells differentiation and ascidian development.

First, the discovery that NO signaling pathway is involved in larval development and metamorphosis of *Ciona intestinalis* prompted us to investigate the role of oxidative stress and NO-derived reactive nitrogen species (RNS) during ascidian metamorphosis. We provide evidence that NO regulates *Ciona* metamorphosis via a complex balance of signaling pathways that are critically dependent on local redox control and temporal changes of reactive oxygen species production. Our results demonstrate that NOS inhibitors along with scavengers of peroxynitrite and NO_2, two key NO-derived nitrative agents involved in protein nitration, markedly decrease the rate of *Ciona* metamorphosis. On the contrary, a NO donor as well peroxynitrite results in acceleration of the process. Increased protein nitration was observed at the late larvae stage, when larvae are competent, and proteomic methodologies identified nitrated tyrosine residues in ERK and snail proteins. Exposure of larvae to NO resulted in a marked decrease in ERK phosphorylation. Overall, the results strongly suggest the occurrence of two distinct pathways of NO signaling in *Ciona* development, one leading to apoptosis through caspase 3 and the other leading to extensive protein nitration in late larvae. Our finding that protein nitration occurred under normal physiological conditions associated with developmental processes, together with the identification of snail, ERK and p-ERK as nitration targets, reinforce the emerging notion of protein nitration as a signaling mechanism sui generis mediated by oxidative stress-like conditions and acting both directly and indirectly on other signaling pathways.

To reinforce the contention of NO signaling as a general mechanism of physiological significance, we characterized the effects of nanotopography on neuronal growth and differentiation using PC12 cell line as cellular model.

In studying neuronal proliferation and differentiation processes, it has been recently proposed that the physical properties of the substrates can be considered as a new kind of stimulus based on the finding that surface energy distribution and surface free-energy gradients trigger neuritogenesis of PC12 cells in the absence of nerve growth factor (NGF). However, the molecular mechanism of the triggered signaling cascade has not been identified yet. To characterize the process, at the molecular level, we studied the behavior of PC12 cells on nanostructured TiO_2 films of different roughness (20 and 29 rms) in the presence and in the absence of NGF. Since it has been demonstrated that NGF induces NO production by nitric oxide synthases (NOS) and that differentiation in PC12 cells grown on PLL-glass in the presence of NGF is associated to an increase in protein nitration, we detected whether increased protein nitration is also observed during PC12 differentiation triggered by nanostructured TiO_2 films in the absence of NGF. Our findings suggested that in PC12 cells grown in the absence of NGF, the topography of ns-TiO_2 triggers neuritogenesis by activating the expression of nitric oxide synthase (NOS) and the pERK1/2-NOS signaling. Differentiation is associated to an increase in protein nitration as described in PC12 cells grown on PLL-glass in the presence of NGF [72]. Beside adding new information on the mechanism through which PC12 cells respond to nano-roughness, our data further attest the biocompatibility of the nTiO_2 surface as cultures substrate since the behavior of cells grown on this material mimic the one described on PLL-coated glass without the need of a chemical stimulus such as NGF. This allow to address a major issue concerning the physiological role played by NO through nitration of cytoskeletal proteins in many cytoskeleton-mediated processes such as cell growth and division.

As compared to plant cells, where there are many evidences suggesting that protein nitration in plants is implicated in root formation and differentiation as well as seed germination [207], the NO mediated effect on mammalian cytoskeleton was found to be ambiguous. Although an increase in protein nitration has been found in many

neurological disorders such as Alzheimer or Parkinson, basal levels of Tyr nitration have been observed in proteins from various species under physiological conditions. An evident link between NO level and eukaryotic cytoskeleton organization has been described in different cells and organisms. Some of the most interesting examples are reported below.

The organization of mammalian actin was shown to be regulated by NO which causes F-actin disassembly and alteration of mesanglial cells shape [208]. The putative model for physiological axonal retraction was proposed based on NO-induced reconfiguration of microfilaments and microtubules during axonal retraction in chick sensory neurons [209]. Microtubule-associated protein-2 (MAP2) of rodents neurons is suggested to undergo Tyr nitration that may modulate MAP2 phosphorylation level. α-tubulin is defined as the main target of nitration in the nervous system of *Sepia officinalis* [78]. Besides that, differential nitration of cytoskeletal proteins such as decrease of actin and increase α-tubulin nitration during normal development of chicken embryo chorioallontoic membrane was observed [40].

In keeping with the previous observations, we demonstrated by western blot analysis and tandem mass spectrometry that nanotopography, in the absence of other inducers, triggers an increase in protein nitration during neuronal differentiation and that cytoskeleton becomes the main cellular fraction containing nitrated proteins.

Altogether, these findings suggest that tyrosine nitration is a physiological event not necessary related to pathological processes and that this NO-mediated post-translational modification of proteins may be regarded as a direct way to NO-signaling transduction. Our data showed for the first time that the NO signal cascade is involved in the differentiation process induced by nanotopography, adding new information on the mechanism and proteins involved in the neuritogenesis triggered by the surface properties.

Recently, in our laboratory, we aimed at defining whether protein nitration triggered by nanotopography was a general phenomenon no matter which kind of substrate utilized. To this aim, we checked by western blot analysis, the nitration of proteins on PC12 cells grown on ZrOx films. Lately, this material has received considerable attention for cell

culture due its well assessed biocompatibility and high adhesiveness for biomolecules. It has been proposed that zirconium dioxide might support normal growth and adhesion of mammalian cells without any surface modification using ECM proteins. In our preliminary results, we found that the pattern of nitration on ZrOx surfaces is equivalent to that detected on TiOx films. These results suggest that the surface nanoroughness represents the main driving force that actively influences neuronal differentiation of PC12 cells confirming our hypothesis that this phenomenon is independently of the physical and chemical properties of the substrates.

One of the main objectives of future works will be to continue the characterization of nitroproteome in neuron like-PC12 cells grown on ns-TiO2 surfaces. This will be a fundamental step to fully understand the role of focal adhesions in PC12 cells differentiation triggered by nanostructured TiO_2 films. An additional goal will be to use a new cell model such as stem cell line in order to study how roughness of the substrate guides stem cell differentiation. These finding will be highly significant for many applications, for the understanding of cell-nanostructured surface interaction and for the general understanding of the nano-bio interface.

Part of the work reported in this PhD thesis has been published in a manuscript entitled "Protein nitration as footprint of oxidative stress-related nitric oxide signaling pathways in developing *Ciona intestinalis. Nitric oxide* (2012), 27: 18-24". As far as the data concerning to tyrosine nitration and neuronal cells differentiation induced by the surface topography of nanostructured TiO_2, they are partially described in a submitted manuscript entitled "Nitric oxide synthase mediates PC12 differentiation induced by surface topography of nanostructured TiO_2".

Bibliography

1. Michel T., Feron O., Nitric oxide synthases: which, where, how, and why? *J. Clin. Invest.* (1997), 100: 2146-2152.
2. Palmer R.M., Rees D.D., Ashton D.S., Moncada S., L-arginine is the physiological precursor for the formation of nitric oxide in endothelium-dependent relaxation. *Biochem. Biophys. Res. Commun.* (1988), 153: 1251-1256.
3. Nagase S., Takemura K., Ueda A., Hirayama A., Aoyagi K., Kondoh M., Koyama A., A novel nonenzymatic pathway for the generation of nitric oxide by the reaction of hydrogen peroxide and D- or L-arginine. *Biochem. Biophys. Res. Commun.* (1997), 233: 150-153.
4. Maiese K., Boccone L., Neuroprotection by peptide growth factors against anoxia and nitric oxide toxicity requires modulation of protein kinase. C. *J. Cereb. Blood Flow Metab.* (1995), 15: 440-449.
5. Schild L., Reinheckel T., Reiser M., Horn T.F., Wolf G., Augustin W., Nitric oxide produced in rat liver mitochondria causes oxidative stress and impairment of respiration after transient hypoxia. *FASEB J.* (2002), 17: 2194-2201.
6. Schaul P.W., Regulation of nitric oxide synthase: location, location, location. *Ann. Rev. Physiol.* (2002), 64: 749-774.
7. Cork R.J., Perrone M.L., Bridges D., Wandell J., Scheiner C.A., Mize R.R., A web-accessible digital atlas of the distribution of nitric oxide synthase in the mouse brain. *Prog. Brain Res.* (1998), 118: 37-50.
8. Arbones M.L., Ribera J., Agullo L., Baltrons M.A., Casanovas A., Riveros-Moreno V., García A., Characteristics of nitric oxide synthase type I of a rat cerebellar astrocytes. *Glia* (1996), 18: 224-232.
9. Mungrue I.N., Bredt D.S., Stewart D.J., Husain M., From molecules to mammals: what's NOS got to do with? *Acta Physiol. Scand.* (2003), 179: 123-135.
10. Humbert P., Niroomand F., Fischer G., Mayer B., Koesling D., Hinsch K.D., Gausepohl H., Frank R., Schultz G., Böhme E., Purification of soluble guanylyl

cyclase from bovine lung by a new immunoaffinity chromatographic method. *Eur. J. Biochem.* (1990), 190: 273-278.

11. Stone J.R., Marletta M.A., Heme stoichiometry of heterodimeric soluble guanylate cyclase. *Biochemistry* (1995), 34: 14668-14674.
12. Beckman J.S., Koppenol W.H., Nitric oxide, superoxide, and peroxynitrite: the good, the bad, and the ugly. *Am J. Physiol.* (1996), 271: C1424-C1437.
13. Gaston B., Stamler J.S., Biochemistry of nitric oxide, nitric oxide and infection, *Kluwer Academic/Plenum Publisher*, Dordrecht/New York (1999), 37-55.
14. Matthews J.R., Botting C.H., Panico M., Morris H.R., Hay R.T., Inhibition of NF-κB DNA binding by nitric oxide. *Nucleic Acids Rev.* (1996), 2236-2242.
15. Klatt P., Molina E.P., Lamas S., Nitric oxide inhibits c-*Jun* DNA binding by specifically targeted S-glutathionylation. *J. Biol. Chem.* (1999), 274: 15857-15864.
16. Liu L., Hausladen A., Zeng M., Que L., Heitman J., Stamler J.S., A metabolic enzyme for S-nitrosothiol conserved from bacteria to humans. *Nature* (2001), 410: 490-494.
17. Huie R.E., Padmaja S., The reaction of NO with superoxide. *Free Radic. Res. Commun.* (1993), 18: 195-199.
18. Ischiropoulos H., Biological tyrosine nitration: a pathophysiological function of nitric oxide and reactive oxygen species. *Arch. Biochem. Biophys.* (1998), 356: 1-11.
19. Heppel L.A., Porterfield V.T., Metabolism of inorganic nitrite and nitrate esters; the coupled oxidation of nitrite by peroxide-forming systems and catalase. *J. Biol. Chem.* (1949), 178: 549-556.
20. Chance B., On the reaction of catalase peroxides with acceptors. *J. Biol. Chem.* (1949), 180: 649-658.
21. Cohen G., Martinez M., Hochstein P., Generation of hydrogen peroxide during the reaction of nitrite with oxyhemoglobin. *Biochemistry* (1964), 3: 901-903.
22. Ischiropoulos H., Zhu L., Chen J., Tsai M., Martin J.C., Smith C.D., Beckman J.S., Peroxynitrite-mediated tyrosine nitration catalyzed by superoxide dismutase. *Arch. Biochem. Biophys.* (1992), 298: 431-437.

23. Knowles M.E., McWeeny D.J., Couchman L., Thorogood M., Interaction of nitrite with proteins at gastric pH. *Nature* (1974), 247: 288-289.

24. Pfeiffer S., Lass A., Schmidt K., Maier B., Protein tyrosine nitration in cytokine-activated murine macrophages. Involvement of a peroxidase/nitrite pathway rather than peroxynitrite. *J. Biol*. *Chem.* (2001), 276: 34051-34058.

25. Szabo C., Multiple pathways of peroxynitrite cytotoxicity. *Toxicol. Lett.* (2003), 140-141: 105-112.

26. Greenacre S.A.B., and Ischiropoulos H., Tyrosine nitration: localization, quantification, consequences for protein function and signal transduction. *Free Radic. Res.* (2001), 34: 541-81.

27. Turko I.V., Murad F., Protein nitration in cardiovascular disease. *Pharmacol.* (2002), 54: 619-634.

28. Leeuwenburgh C., Hardy M.M., Hazen S.L., Wagner P., Oh-ishi S., Steinbrecher U.P., Heinecke J.W., Reactive nitrogen intermediates promotes low density lipoprotein oxidation in human atherosclerotic intima. *J. Biol. Chem.* (1997), 272: 1433-1436.

29. Zou M.H., Leist M., Ullrich V., Selective nitration of prostacyclin synthase and defective vasorelaxation in atherosclerotic bovine coronary arteries. *Am. J. Pathol.* (1999), 154: 1359-1365.

30. Aslan M., Ryan T.M., Townes T.M., Coward L., Kirk M.C., Barnes S., Alexander C.B., Rosenfeld S.S., Freeman B.A., Nitric oxide-dependant generation of reactive species in sickle cell disease: renal and hepatocellular actin tyrosine nitration. *J. Biol. Chem.* (2003), 278: 4194-4204.

31. Przedborki S., Chen Q., Vila M., Giasson B.I., Djaldatti R., Vukosavic S., Souza J.M., Jackson-Lewis V., Lee V.M., Ischiropoulos H., Oxidative post-translational modification of α-synuclein in the MPTP mouse model of Parkinson's disease. *J. Neurochem.* (2001), 76: 637-640.

32. Giasson B.I., Duda J.E., Murray I.V., Chen Q., Souza J.M., Hurtig H.I., Ischiropoulos H., Trojanowski J.Q., Lee V.M., Oxidative damage linked to neurodegeneration by

selective alpha-synuclein nitration in synucleinopathy lesions. *Science* (2000), 290: 985-989.

33. Bolan E.A., Gracy K.N., Chan J., Trifiletti R.R., Pickel V.M., Ultrastructural localization of nitrotyrosine within the caudate-putamen nucleus and the globus pallidus of normal rat brain. *J. Neurosci.* (2000), 20: 4798-4808.
34. Zhang H., Bhargava K., Keszler A., Feix j., Hogg N., Joseph J., Kalyanaraman B., Transmembrane nitration of hydrophobic tyrosyl peptides. Localization, characterization, mechanism of nitration and biological implications. *J. Biol. Chem.* (2003), 278: 8969-8978.
35. Souza J.M., Daikhin E., Yudkoff M., Raman C.S., Ischiropoulos H., Factor determining the selectivity of protein tyrosine nitration. *Arch. Biochem. Biophys.* (1999), 371: 169-178.
36. Berlett B.S., Friguet B., Yim M.B., Chock P.B., Stadtman E.R., Peroxynitrite-mediated nitration of tyrosine residue in *Escherichia coli* glutamine synthetase mimics adenylation: relevance to signal transduction. *Proc. Natl. Acad. Sci. USA* (1996), 93: 1776-1780.
37. Ischiropolous H., Biological selectivity and functional aspects of protein tyrosine nitration. *Biochem. Biophys. Res. Commun.* (2003), 305: 776-783.
38. Eiserich J.P., Estevez A.G., Bamberg T.V., Ye Y.Z., Chumley P.H., Beckman J.S., Freeman B., Microtubule dysfunction by post-translational nitrotyrosination of α-tubulin: A nitric oxide-dependent mechanism of cellular injury. *PNAS* (1999), 96: 6365-6370.
39. Shishehbor M., Aviles R.J., Brennan M.L., Goormastic M., Pearce G.L., Gokce N., Keaney J.F., Penn M.S., Sprecher D.L., Vita J.A., Hazen S.L., Association of nitrotyrosine levels with cardiovascular disease and modulation by statin therapy. *JAMA* (2003), 289: 1675-80.
40. Giannopoulou E., Katsoris P., Polytarchou C., Papadimitriou E., Nitration of cytoskeletal proteins in the chicken embryo chorioallantoic membrane. *Arch. Biochem. Biophys.* (2002), 400: 188-198.

41. Cappelletti G., Tedeschi G., Maggioni M.G., Negri A., Nonnis S., Maci R., The nitration of tau protein in neuron-like PC12 cells. *FEBS Lett.* (2004), 562: 35-39.
42. Lincoln J., Hoyle C.H.V., Burnstock G., Nitric oxide in health and disease. *Cambridge University Press.* (1997).
43. Alderton W.K., Cooper C.E., Knowles R.G., Nitric oxide Synthases: structure, function and inhibition. *Biochem. J.* (2001), 357: 593-615.
44. Bredt D.S., Endogenous nitric oxide synthesis: biological function and pathophysiology. *Free Radical Res.* (1999), 31: 577-596.
45. Kamijo R., Harada H., Matsuyama T., Bosland M., Gerecitano J., Shapiro D., Le J., Koh S.I., Kimura T., Green S.J., et al., Requirements for transcription factor IRF-1 in NOS induction in macrophages. *Science* (1994), 263: 1612-1615.
46. Bolaños J.P., Almeida A., Stewart V., Peuchen S., Land J.M., Clark J.B., Heales S.J., Nitric-oxide mediated mitochondrial damage in the brain: mechanisms and implications for neurodegenerative diseases. *J. Neurochem.* (1997), 68: 2227-2240.
47. Heales S.J.R., Bolaños J.P., Stewart V.C., Brookes P., Land J.M., Clark J.B., Nitric oxide, mitochondria and neurological disease. *Biochem. Biophys. Acta* (1999), 1410: 215-228.
48. Dawson V.L., Dawson T.M., Nitric oxide in neurodegeneration. *Prog. Brain Res.* (1998), 118: 3-11.
49. Contestabile A., Monti B., Ciani E., Brain nitric oxide and its dual role in neurodegeneration/neuroprotection: understanding molecular mechanisms to devise drug approaches. *Curr. Med. Chem.* (2003), 10: 2147-2174.
50. Dawson T.M., Dawson V.L., Snyder S.H., Nitric oxide as a mediator of neurotoxicity. *NIDA Res. Monogr.* (1993), 136: 258-271.
51. Le W.D., Colom L.V., Xie W.J., Smith R.G., Alexianu M., Appel S.H., Cell death induced by beta-amyloid 1-40 in MES 23.5 hybrid clone: the role of nitric oxide and NMDA-gated channel activation leading to apoptosis. *Brain Res.* (1995), 686: 49-60.

52. Liberatore G.T., Jackson-Lewis V., Vukosavic S., Mandir A.S., Vila M., McAuliffe W.G., Dawson V.L., Dawson T.M., Przedborski S., Inducible nitric oxide synthase stimulates dopaminergic neurodegeneration in the MPTP model of Parkinson disease. *Nat. Med.* (1999), 5: 1403-1409.

53. Lipton S.A., Choi Y.B., Sucher N.J., Chen H.S., Neuroprotective versus neurodestructive effects of NO-related species. *Biofactors* (1998), 8: 33-40.

54. Chiueh C.C., Neuroprotective properties of nitric oxide. *Ann. N.Y. Acad. Sci.* (1999), 890: 301-311.

55. Gibbs S.M., Truman J.W., Nitric oxide and cyclic GMP regulate retinal patterning in the optic lobe of *Drosophila*. *Neuron* (1998), 20: 83-93.

56. Huang C., Borchers C.H., Schaller M.D., Jacobson K., Phosphorylation of paxillin by p38MAPK is involved in the neurite extension of PC12 cells. *J. Cell Biol.* (2004), 26: 593-602.

57. Woo S., Gomez T.M., Rac1 and RhoA promote neurite outgrowth through formation and stabilization of growth come point contacts. *J. Neurosci.* (2006), 27: 730-742.

58. D'Arcandelo G., Halegoua S., A branched signaling pathway for nerve growth factor is revealed by Src-, Ras-, and Raf-mediated gene inductions. *Mol. Cell Biol*. (1993), 13: 3146-3155.

59. Klesse L.J., Meyers K.A., Marshall C.J., Para L.F., Nerve growth factor induces survival and differentiation through two distinct signaling cascades in PC12 cells. *Oncogene* (1999), 18: 2055-2068.

60. Rakhit S., Pyne S., Pyne N.J., Nerve growth factor stimulation of p42/p44 mitogen activated protein kinase in PC12 cells: Role of G(i/o), G protein-coupled receptor kinase 2, beta-arrestin I, and endocytic processing. *Mol. Pharmacol.* (2001), 60: 63-70.

61. Waetzig V., Herdegen T., The concerted signaling of ERK1/2 and JNKs is essential for PC12 cell neuritogenesis and converges at the level of target proteins. *Mol. Cell Neurosci.* (2003), 24: 238-249.

62. Greene L.A., Tischler A.S., Establishment of noradrenergic clonal line of rat adrenal pheochromocytoma cells which respond to nerve growth factor. *Proc. Natl. Acad. Sci.* USA (1976), 73: 2424-2428.
63. Ferrari A., Faraci P., Cecchini M., Beltram F., The effect of alternative neuronal differentiation pathways on PC12 cell adhesion and neurite alignment to nanogratings. *Biomaterials* (2010), 21: 2565-2573.
64. Fujii D.K., Massoglia S.L., Savion N., Gospodarowicz D., Neurite outgrowth and protein synthesis by PC12 cells as a function of substratum and nerve growth factor. *J. Neurosci*. (1982), 2: 1157-1175.
65. Lee J.H., Lee H.Y., Kim H.W., Adhesive proteins linked with focal adhesion kinase regulate neurite outgrowth of PC12 cells. *Acta Biomater.* (2012), 8: 165-172.
66. Aizawa M., Koyama S., Kimura K., Haruyama T., Yanagida Y., Kobatake E., Electrically stimulated modulation of cellular function in proliferation, differentiation, and gene expression. *Electrochemistry* (1999), 67:118-125.
67. Guo Y., Li M., Mylonakis A., Han J., MacDiarmid A.G., Chen X., Lelkes P.I., Wei Y., Electroactive oligoaniline-containing self-assembled monolayers for tissue engineering applications. *Biomacromolecules* (2007), 8: 3025-3034.
68. Peunova N., Enlkolopov G., Nitric oxide triggers a switch to growth arrest during differentiation of neuronal cells. *Nature* (1995), 375: 68-73.
69. Yamazaki M., Chiba K., Mohri T., Fundamental role of nitric oxide in neuritogenesis of PC12h cells. *Br. J. Pharmacol.* (2005), 146: 662-669.
70. Portier M.M., de Nè chaud B., Gros F., Peripherin, a new member of the intermediate filament protein family. *Dev. Neurosci.* (1994), 6: 335-344.
71. Escurat M., Djabali K., Gumpel M., Gros F., Portier M.M., Differential expression of two neuronal intermediate-filament proteins, peripherin and the low-molecular-mass neurofilament protein (NF-L), during the development of the rat. *J.Neurosci*. (1990), 10: 764-784.
72. Cappelletti G., Maggioni M.G., Tedeschi G., Maci R., Protein tyrosine nitration is triggered by nerve growth factor during neuronal differentiation of PC12 cells. *Exp. Cell Res.* (2003), 288: 9-20.

73. Tedeschi G., Cappelletti G., Nonnis S., Taverna F., , Negri A., Ronchi C., Ronchi S., Tyrosine nitration is a novel post-translational modification occurring on the neural intermediate filament protein peripherin. *Neurochem. Res.* (2007), 32: 433-441.

74. Nonnis S., Cappelletti G., Taverna F., Ronchi C., Ronchi S., Negri A., Grassi E., Tedeschi G., Tau is endogenously nitrated in mouse brain: identification of a tyrosine residue modified *in vivo* by NO. *Neurochem. Res.* (2008), 33: 518-525.

75. Sacksteder C.A., Qian W.J., Knyushko T.V., Endogenously nitrated proteins in mouse brain: links to neurodegenerative disease. *Biochemistry* (2006), 45: 8009-8022.

76. Chang W., Webster D.R., Salam A.A., Gruber D., Preasad A., Eiserich J.P., Bulinsky J.C., Alteration of tubulin's C-terminal amino acid specifically inhibits myogenic differentiation. *J. Biol.Chem* (2002), 277: 30690-30698.

77. Aulak K.S., Miyagi M., Yan L., West K.A., Massillon D., Crabb J.W., Stuehr D.J., Proteomic method identifies proteins nitrated *in vivo* during inflammatory challenge. *Proc. Natl. Acad. Sci. (*2001), 98: 12056-12061.

78. Palumbo A., Fiore G., Di Cristo C., Di Cosmo A., d'Ischia M., NMDA receptor stimulation induces temporary aplha-tubulin degradation signaled by nitric oxide-mediated tyrosine nitration in the nervous system of *Sepia officinalis*. *Biochem. Biophys. Res. Commun.* (2002), 293: 1536-1543.

79. Grune T., Blasing I.E., Sittle N., Roloff B., Haseloff R., Davies K.J., Peroxynitrite increases the degradation of aconitase and other cellular proteins by proteasome. *J. Biol. Chem*. (1998), 273: 10857-10862.

80. Souza J.M., Choi I., Chen Q., Weisse M., Daikhin E., Yudkoff M., Obin M., Ara J., Horwitz J., Ischiropoulos H., Proteolytic degradation of tyrosine nitrated proteins. *Arch. Biochem. Biophys*. (2000), 380: 360-366.

81. Monteiro H.P., Signal transduction by protein tyrosine nitration: competition or cooperation with tyrosine phosphorylation-dependent signaling events. *Free Radical Biol. Med*. (2002), 33: 765-773.

82. Cox M.E., Maness P.F., Tyrosine phosphorylation of α-tubulin is an early response to NGF and pp60v-src in PC12 cells. *J. Mol. Neurosci*. (1993), 4: 63-72.

83. Ley S.C., Verbi W.D., Pappin J.C., Druker B., Davies A.A., Crumpton M.J., Tyrosine phosphorylation of α-tubulin in human T lymphocytes. *Eur. J. Immunol*. (1994), 24: 99-106.

84. Wandosell F., Serrano L., Avila J., Phosphorylation of α-tubulin carboxyl-terminal tyrosine prevents its incorporation into microtubules. *J. Biol. Chem*. (1987), 262: 8268-8273.

85. Mandelkow E., Mandelkow E.M., Microtubules and microtubule-associated proteins. *Curr. Opin. Cell Biol*. (1995), 7: 72-81.

86. Teng K.K., Gerogieff I.S., Aletta J.M., Nunez J., Shelanski M.L., Greene L.A., Characterization of a PC12 cell sub-clone (PC12-C41) with enhanced neurite outgrowth capacity: implications for a modulatory role of high molecular weight tau in neuritogenesis. *J. Cell Sci*. (1993), 106: 611-626.

87. Horiguchi T., Uryu K., Giasson B.I., Ischiropoulos H., Light-Foot R., Bellmann C., Richter-Landberg C., Lee V.M-Y., Trojanowski J.Q., Nitration of tau protein is linked to neurodegeneration in tauopathies. *Am. J. Pathol*. (2003), 163: 1021-1031.

88. Rothe F., Possel H., Wolf G., Nitric oxide affects the phosphorylation state of microtubule-associate protein 2 (MAP-2) and neurofilament: an immunocytochemical study in the brain of rats and neuronal nitric oxide synthase (nNOS)-knockouts. *Nitric Oxide* (2002), 6: 9-17.

89. Kleinman H.K., Philp D., Hoffman M.P., Role of the extracellular matrix in morphogenesis. *Curr. Opin. Biotechnol*. (2003), 14: 526-532.

90. Dye J.F., Lawrence L., Linge C., Leach L., Firth J.A., Clark P., Distinct patterns of microvascular endothelial cell morphology are determined by extracellular matrix composition. *Endo. J. Endo. Cell Res.* (2004), 11: 151-167.

91. Shimizu Y., Rose D.M., Ginsberg M.H., Integrins in the Immune system. *Adv. Immunol.* (1999), 72: 325-380.

92. Schultz G.S., Wysocki A., Interactions between extracellular matrix and growth factors in wound healing. *Wound Repair Regen.* (2009), 17:153-162.

93. Bissell M.J., Modeling molecular mechanisms of breast cancer and invasion: Lessons from the normal gland. *Biochem. Soc. Trans.* (2007), 35:18-22.
94. van der Flier A., Sonnenberg A., Function and interactions of integrins. *Cell Tissue Res.* (2001), 305: 285-298.
95. Schwartz M.A., Integrin signaling revisited. *Trends Cell Biol*. (2001), 11: 466-470.
96. Mooney D., Hansen L., Vacanti J., Langer R., Farmer S., Ingber D., Switching from differentiation to growth in hepatocytes: Control by extracellular-matrix. *J. Cell Physiol.* (1992), 151: 497-505.
97. Zaman M.H., Trapani L.M., Sieminski A.L., Mackellar D., Gong H., Kamm R.D., Wells A., Lauffenburger D.A., Matsudaira P., Migration of tumor cells in 3D matrices is governed by matrix stiffness along with cell-matrix adhesion and proteolysis. *Proc. Natl. Acad. Sci.* (2006), 103: 10889-10894.
98. Engler A.J., Sen S., Sweeney H.L., Discher D.E., Matrix elasticity directs stem cell lineage specification. *Cell* (2006), 126: 677-689.
99. Khetani S.R., Bhatia S.N., Microscale culture of human liver cells for drug development. *Nat. Biotechnol.* (2008), 26: 120-126.
100. Tibbitt M.W., Anseth K.S., Hydrogels as extracellular matrix mimics for 3D cell culture. *Biotechnol. and Bioeng* (2009), 103: 655-663.
101. Petersen O.W., Ronnov-Jessen L., Howlett A.R., Bissell M.J., Interaction with basement membrane serves to rapidly distinguish growth and differentiation pattern of normal and malignant human breast epithelial cells. *Proc. Natl. Acad. Sci. USA* (1992), 89: 9064-9068.
102. Gieni R.S., Hendzel M.J., Mechanotransduction from the ECM to the genome: Are the pieces now in place? *J. Cell Biochem.* (2008), 104: 1964-1987.
103. Ashe H.L., Briscoe J., The interpretation of morphogen gradients. *Development* (2006), 133: 385-394.
104. Mahoney M.J., Anseth KS., Three-dimensional growth and function of neural tissue in degradable polyethylene glycol hydrogels. *Biomaterials* (2006), 27: 2265-2274.

105. Le Beyec J., Xu R., Lee S.Y., Nelson C.M., Rizki A., Alcaraz J., Bissell M.J., Cell shape regulates global histone acetylation in human mammary epithelial cells. *Exp. Cell Res.* (2007), 313: 3066-3075.

106. Chen C.S., Mrksich M., Huang S., Whitesides G.M., Ingber D.E., Geometric control of cell life and death. *Science* (1997), 276: 1425-1428.

107. Saha K., Pollock J.F., Schaffer D.V., Healy K.E., Designing synthetic materials to control stem cell phenotype. *Curr. Opin. Chem. Biol.* (2007), 11: 381-387.

108. Lutolf M.P., Hubbell J.A., Synthetic biomaterials as instructive extracellular microenvironments for morphogenesis in tissue engineering. *Nat. Biotechnol*. (2005), 23: 47-55.

109. Chen C., Jiang X., Microengineering the environment of mammalian cells in culture. *MRS Bull.* (2005), 30: 194-201.

110. Andersson A.S., Backhed F., Von Euler A., Richter-Dahlfors A., Sutherland D., Kasemo B., Nanoscale features influence epithelial cell morphology and cytokine production. *Biomaterials* (2003), 24: 3427-3436.

111. Dalby M.J., Riehle M.O., Sutherland D.S., Agheli H., Curtis A.S., Use of nanotopography to study mechanotransduction in fibroblasts-methods and perspectives. *Eur. J. Cell Biol.* (2004), 83: 159-69.

112. Yim E.K.F., Darling E.M., Kulangara K., Guilak F., Leong K.W., Nanotopography-induced changes in focal adhesions, cytoskeletal organization, and mechanical properties of human mesenchymal stem cells. *Biomaterials* (2010), 31: 1299-1306.

113. Abrams G.A., Goodman S.L., Nealey P.F., Franco M., Murphy C.J., Nanoscale topography of the basement membrane underlying the corneal epithelium of the rhesus macaque. *Cell Tissue Res.* (2000), 299: 39-46.

114. Ferrari A., Cecchini M., Serresi M., Faraci P., Pisignano D., Beltram F., Neuronal polarity selection by topography-induced focal adhesion control. *Biomaterials* (2010), 31: 4682-4694.

115. Foley A.D., Grunwald E.W., Nealey P.F., Murphy C.J., Cooperative modulation of neuritogenesis by PC12 cells by topography and nerve growth factor. *Biomaterials (*2005), 26: 3639-3644.

116. Fan Y.W., Cui F.Z., Hou SP., Xu Q.Y., Chen L.N., Lee I.S., Culture of neural cells on silicon wafers with nano-scale surface topograph. *J. Neurosci. Methods* (2002), 120: 17-23.

117. Schwarz U.S, Bischofs I.B., Physical determinants of cell organization in soft media. *Med. Eng. Phys.* (2005), 27: 763-772.

118. Lamour G., Journiac N., Souès S., Bonneau S., Nassoy P., Hamraoui A., Influence of surface energy distribution on neuritogenesis. *Colloids Surf B Biointerfaces* (2009), 72: 208-218.

119. Lamour G., Aftekhari-Bafrooei A., Borguet E., Souès A., Hamraoui A., Neuronal adhesion and differentiation driven by nanoscale surface free-energy gradients. *Biomaterials* (2010), 31: 3762-3771.

120. Wegner K., Piseri P., Vahedi Tafreshi H., Milani P., Cluster beam deposition: a tool for nanoscale science and technology. *J. Phys. D: Appl. Phys.* (2006), 39: R439-R459.

121. Carbone E., Marangi I., Zanardi A., Giorgetti L., Chierici E., Berlanda G., Biocompatibility of cluster-assembled nanostructured TiO_2 with primary and cancer cells. *Biomaterials* (2006), 27: 3221-3229.

122. Bellicchi M., Erratico S., Razini P., Meregalli M., Cattaneo A., Jacchetti E., Farini A., Villa C., Bresolin N., Porretti L., Lenardi C., Milani P., Torrente Y., *Ex vivo* expansion of human circulating myogenic progenitors on cluster-assembled nanostructured TiO_2. *Biomaterials* (2010), 31: 5385-5396.

123. Podestà A., Bongiorno G., Scopelliti P.E., Bovio S., Milani P., Semprebon G., et al., Cluster-assembled nanostructured titanium oxide films with tailored wettability. *J. Phys. Chem. C* (2009), 113: 18264-18269.

124. Carbone R., De Marni M., Zanardi A., Vinati S., Barborini E., Fornasari L., Milani P., Characterization of cluster-assembled nanostructured titanium oxide coatings as substrates for protein arrays. *Anal. Biochem.* (2009), 394: 7-12.

125. Scopelliti P.E., Borgonovo A., Indrieri M., Giorgetti L., Bongiorno G., Carbone R., Podestà A.,Milani P., The effect of surface nanometre-scale morphology on protein adsorption. *PLoS ONE* (2010), 5: e11862.

126. Giovine M., Pozzolini M., Favre A., Bavestrello G., Cerrano C., Ottaviani F., Chiarantini L., Cerasi A., Cangiotti M., Zocchi E., Scarfi S., Sara M., Benfatti U., Heat stress-activated, calcium dependent nitric oxide synthase in sponges. *Nitric Oxide* (2001), 5: 427-431.

127. Robertson J.D., Bonaventura J., Kohm A., Hiscat M., Nitric oxide is necessary for visual learning in *Octopus vulgaris*. *Proc. Biol. Sci.* (1996), 263: 1739-1743.

128. Robertson J.D., Bonaventura J., Kohm A.P., Nitric oxide is required for tactile learning in *Octopus vulgaris*. *Proc. Biol. Sci.* (1994), 256: 269-273.

129. Hanlon R.T., Messenger J.B.,. Defence. Cephalopod Behavior. Cambridge University Press, Cambridge (1996), 66-93.

130. Palumbo A., Melanogenesis in the ink gland of *Sepia officinalis*. *Pigment Cell Res*. (2003), 16: 517-522.

131. Kuo R.C., Baxter G.T., Thompson S.H., Stricker S.A., Patton C., Bonaventura J., Epel D., NO is necessary and sufficient for egg activation at fertilization. *Nature* (2000), 406: 633-636.

132. Leckie C., Empson R., Becchetti A., Thomas J., Galione A., Whitaker M., The NO pathway acts late during the fertilization response in sea urchin eggs. *J. Biol. Chem*.(2003), 278: 12247-12254.

133. Hyslop L.A., Carroll M., Nixon V.L., McDougall A., Jones K.T., Simultaneous measurement of intracellular nitric oxide and free calcium levels in chordate eggs demonstrates that nitric oxide has no role at fertilization. *Dev. Biol*. (2001), 234: 216-230.

134. Grumetto L., Wilding M., De Simone M.L., Tosti E., Galione A., Dale B.,. Nitric oxide gates fertilization channels in ascidian oocytes through nicotinamide nucleotide metabolism. *Biochem. Biophys. Res. Commun*. (1997), 239: 723-728.

135. Leise E.M., Kempf S.C., Durham N.R., Gifondorwa D.J., Induction of metamorphosis in the marine gastropod *Ilyanassa obsoleta*: 5HT, NO and programmed cell death. *Acta Biol. Hung*. (2004), 55: 293-300.

136. Bishop C.D., Bates W.R., Brandhorst B.P., Regulation of metamorphosis in ascidians involves NO/cGMP signaling and HSP90. *J. Exp. Zool*. (2001), 289: 374-384.

137. Bishop C.D., Brandhorst B.P., NO/cGMP signaling and HSP90 activity represses metamorphosis in the sea urchin *Lytechinus pictus*. *Biol. Bull*. (2001), 201: 394-404.

138. Millar R.H., The biology of ascidians. *Adv. Mar. Biol*. (1971), 9: 1-100.

139. Chiba S., Sasaki A., Nakayama A., Takamura K., Satoh N., Development of *Ciona intestinalis* juveniles (through 2nd ascidian stage). *Zool. Sci*. (2004), 21: 285-298.

140. Eri R., Arnold J.M., Hinman V.F., Green K.M., Jones M.K., Degnan B.M., Lavin M.F., Hemps, a novel EGF-like protein, plays a central role in ascidian metamorphosis. *Development* (1999), 126: 5809-5818.

141. Woods R.G., Roper K.E., Gauthier M., Bebell L.M., Sung K., Degnan B.M., Lavin M.F., Gene expression during early ascidian metamorphosis requires signaling by Hemps, an EGF-like protein. *Development* (2004), 131: 2921-2933.

142. Dehal P., Satou Y., Campbell R.K., Chapman J., Degnan B., De Tomaso A., Davidson B., Di Gregorio A., Gelpke M., Goodstein D.M., et al., The draft genome of *Ciona intestinalis*: insights into chordate and vertebrate origins. *Science* (2002), 298: 2157-2167.

143. Nakayama A., Satou Y., Satoh N., Isolation and characterization of genes that are expressed during *Ciona intestinalis* metamorphosis. *Dev. Genes Evol*. (2001), 211: 184-189.

144. Nakayama A., Satou Y., Satoh N., Further characterization of genes expressed during *Ciona intestinalis* metamorphosis. *Differentiation*. (2002), 70: 429-437.

145. Chambon J.P., Nakayama A., Takamura K., McDougall A., Satoh N., ERK- and JNK-signaling regulate gene networks that stimulate metamorphosis and apoptosis in tail tissues of ascidian tadpoles. *Development*. (2007), 134: 1203-1219.

146. Chambon J.P., Soule J., Pomies P., Fort P., Sahuquet A., Alexandre D., Paul-Henri Mangeat P.H., Baghdiguian S., Tail regression in *Ciona intestinalis* (Prochordate) involves a caspase-dependent apoptosis event associated with ERK activation. *Development*. (2002), 129: 3105-3114.

147. Tarallo R., Sordino P., Time course of programmed cell death in *Ciona intestinalis* in relation to mitotic activity and MAPK signaling. *Dev. Dyn*. (2004), 230: 251-262.

148. Garcia-Cardena G., Fan R., Shah V., Sorrentino R., Cirino G., Papapetropoulos A., Sessa W.C., Dynamic activation of endothelial nitric oxide synthase by Hsp90. *Nature*.(1998), 392: 821-824.

149. Bender A.T., Silverstein A.M., Demady D.R., Kanelakis K.C., Noguchi S., Pratt W.C., Osawa Y., Neuronal nitric-oxide synthase is regulated by the Hsp90-based chaperone system *in vivo*. *J. Biol. Chem*. (1999), 274: 1472-1478.

150. Comes S., Locascio A., Silvestre F., d'Ischia M., Russo G.L., Tosti E., Branno M., and Palumbo A., Regulatory roles of nitric oxide during larval development and metamorphosis in *Ciona intestinalis*. *Dev. Biol*. (2007), 306: 772-784.

151. Vahedi Tafreshi H., Piseri P., Benedek G., Milani P., The role of gas dynamics in operation conditions of a pulsed microplasma cluster source for nanostructured thin films deposition. *J. Nanosci. Nanotechnol.* (2006), 6: 1140-1149.

152. Piseri P., Vahedi Tafreshi H., Milani P., Manipulation of nanoparticles in supersonic beams for the production of nanostructured materials. *Curr. Opin. Solid State Mater. Sci.* (2004), 8: 195-202.

153. Barborini E., Kholmanov I.N., Conti A.M., Piseri P., Vinati S., Milani P., et al., Supersonic cluster beam deposition of nanostructured titania. *Eur. Phys. J. D.* (2003), 24: 277-282.

154. Karas M., Hillenkamp F., Laser desorption ionization of proteins with molecular mass exceeding 10000 daltons. *Anal. Chem* (1988), 60: 2299-2301.

155. Hillenkamp F., Karas M., Beavis R.C., and Chait B.T., Matrix-assisted laser desorption/ionization mass spectrometry of biopolymers. *Anal. Chem* (1991), 63: 1193A-1203A.

156. Fenn J. B., Mann M., Meng C. K., Wong S. F., Whitehouse C. M., Electrospray ionization for mass spectrometry of large biomolecules. *Science* (1989), 246: 64-71.

157. Makarov A., Denisov E., Kholomeev A., Balschun W., Lange O., Strupat K., Horning S., Performance Evalutation of a Hybrid Linear Ion Trap/ Orbitrap Mass Spectrometer. *Anal Chem* (2006), 78: 2113-2120.

158. Hu Q., Noll R. J., Li H., Makarov A., Hardman M., Graham Cooks R., The Orbitrap: a new mass spectrometer. *J. Mass Spectrom.* (2005) 40: 430-443.
159. Makarov A., Electrostatic axially harmonic orbitrap trapping: a high- performance technique of mass analysis. *Anal.Chem.* (2000), 72: 1156-1162.
160. Douglas D.J., Frank A.J., Mao D., Linear ion traps in mass spectrometry. *Mass. Spectrom. Rev*. (2005), 24: 1-29.
161. Hardman M., Makarov A., Interfacing the orbitrap mass analyzer to an electrospray ion source. *Anal. Chem*. (2003), 75: 1699-1705.
162. Guidarelli A., Cantoni O., Pivotal role of superoxides generated in the mitochondrial respiratory chain in peroxynitrite-dependent activation of phospholipase A2. *Biochem. J*. (2002), 366: 307-314.
163. Tedeschi G., Cappelletti G., Negri A., Pagliato L., Maggioni M.G., Maci R., Ronchi S., Characterization of nitroproteome in neuron-like PC12 cells differentiated with nerve growth factor: identification of two nitration sites in α-tubulin. *Proteomics* (2005), 5: 2422-2432.
164. Rabilloud T., Mechanisms of protein silver staining in polyacrylamide gels: a ten years synthesis. *Electrophoresis* (1990), 11**:** 785-794.
165. Sarver A., Scheffler N.K., Shetlar M.D., Gibson B.W., Analysis of peptides and proteins containing nitrotyrosine by matrix-assisted laser desorption/ionization mass spectrometry. *J. Am. Soc. Mass Spectrom*. (2001), 12: 439-448.
166. Turko I.V., Murad F., Mapping sites of tyrosine nitration by matrix-assisted laser desorption/ionization mass spectrometry. *Methods Enzymol.* (2005), 396: 266-275.
167. Barabasi A.L., Stanley H.E., Fractal concepts in surface growth. New York: Cambridge University Press, 1995.
168. Contestabile A., Ciani E., Role of nitric oxide in the regulation of neuronal proliferation, survival and differentiation. *Neurochem. Int.* (2004), 45: 903-914.
169. Hindley S., Juurlink B.H., Gysbers J.W., Middlemiss P.J., Herman M.A., Rathbone M.P., Nitric oxide donors enhance neutrophin-induced neurite outgrowth through a cGMP-dependent mechanism. *J. Neurosci. Res.* (1997), 45: 427-439.

170. Yamazaki M., Chiba K., Mohri T., Hatanaka H., Cyclic GMP-dependent neurite outgrowth by genipin and nerve growth factor in PC12h cells. *Eur. J. Pharmacol.* (2004), 488: 35-43.

171. Fostermann U., Boissel J.P., Kleimert H., Expressional control of the"constitutive" isoforms of nitric oxide synthase (NOS I and NOS III). *FASEB J*. (1998), 12: 773-790.

172. Su Y., Kondrikov D., Block E.R., Cytoskeletal regulation of nitric oxide synthase. *Cell Biochem Biophys* (2005), 43: 439-449.

173. Cappelletti G., Maggioni M.G., Ronchi C., Maci R., Tedeschi G., Protein tyrosine nitration is associated with cold- and drug- resistant microtubules in neuronal-like PC12 cells. *Neurosci. Lett.* (2006), 401: 159-164.

174. Vaudry A., Stork P.J.S., Lazarovici P., Eiden L., Signaling pathways for PC12 cell differentiation: making the right connections. *Science* (2002), 296: 1648-1649.

175. Zhang Z., Tarone G., Turner D.C., Expression of integrin alpha 1 beta 1 is regulated by nerve growth factor and dexamethasone in PC12 cells. Functional consequences for adhesion and neurite outgrowth. *J. Biol. Chem.* (1993), 268: 5557-5565.

176. Danker K., Mecahi N., Lucka L., Reutter W., Horstkorte R., The small GTPase ras is involved in growth factor-regulated expression of alpha 1 integrin subunit in PC12 cells. *Biol. Chem.* (2001), 382: 969-972.

177. Ivankovic-Dikic I., Gronroos E., Blaukat A., Barth B.U., Dikic I., Pyk2 and FAK regulate neurite outgrowth induced by growth factors and integrins. *Nat. Cell. Biol*. (2000), 2: 574-581.

178. Cucina A., Sterpetti A.V., Pupelis G., Fragale A., Lepidi S., Cavallaro A., Giustiniani Q., Santoro D'Angelo L., Shear stress induces changes in the morphology and cytoskeleton organization of arterial endothelial cells. *Eur. J. Vasc. Endovasc. Surg.* (1995), 9: 86-92.

179. Kondrikov D., Fonseca F.V., Elms S., Fulton D., Black S.M., Block E.R., Su Y., β-Actin association with endothelial nitric-oxide synthase modulates nitric oxide and superoxide generation from the enzyme. *J. Biol. Chem.* (2009), 285: 4319-4327.

180. Witteck A., Yao Y., Fechir M., Forstermann U., Kleinert H., Rho protein-mediated changes in the structure of the actin cytoskeleton regulate human inducible NO synthase gene expression. *Exp. Cell Res.* (2003), 287: 106-115.
181. Zeng C., Morrison A.R., Disruption of the actin cytoskeleton regulates cytokine-induced iNOS expression. *Am. J. Physiol. Cell. Physiol.* (2001), 281: C932-C940.
182. Hattori Y., Kasai K., Disruption of the actin cytoskeleton up-regulates iNOS expression in vascular smooth muscle cells. *J. Cardiovasc. Pharmacol.* (2004), 43: 209-213.
183. Marczin N., Jilling T., Papapetropoulos A., Go C., Catravas J.D., Cytoskeleton-dependent activation of the inducible nitric oxide synthase in cultured aortic smooth muscle cells. *Br. J. Pharmacol*. (1996), 118: 1085-1094.
184. Ory S., Destaing O., Jurdic P., Microtubule dynamics differentially regulates Rho and Rac activity and triggers Rho-independent stress fiber formation in macrophage polykaryons. *Eur. J. Cell Biol*. (2002), 81: 351-362.
185. Jung H.I., Shin I., Park Y.M., Kang K.W., Ha K.S., Colchicine activates actin polymerization by microtubule depolymerization. *Mol. Cells* (1997), 7: 431-437.
186. Kajstura J., Sowa G., Wronska D., Induction of DNA synthesis by microtubule depolymerization is mediated by actin filaments. *Cytobios* (1993), 76: 67-74.
187. Zhang J.S., Kraus W.E., Turskey G.A., Stretch-induced nitric oxide modulates mechanical properties of skeletal muscle cells. *Am. J. Physiol. Cell Physiol.* (2004), 287: C292-C299.
188. Marechal G., Gailly P., Effects of nitric oxide on the contraction of skeletal muscle. *Cell Mol. Life Sci*. (1999), 55: 1088-1102.
189. Gupta S.K., Vlahakis E., Integrin α9β1 mediates enhanced cell migration through nitric oxide synthase activity regulated by Src tyrosine kinase. *J. Cell Sci.* (2009), 122: 2043-2054.
190. Maa M.C., Chang M.Y., Li J., Li Y.Y., Hsieh M.Y., Yang C.J., et al., The iNOS/Src/FAK axis is critical in Toll-like receptor-mediated cell motility in macrophages. *Biochim. Biophys. Acta* (2011), 1813: 136-147.

191. Handy R.L., Moore P.K., Mechanism of the inhibition of neuronal nitric oxide synthase by 1-(2-trifluoromethylphenyl) imidazole (TRIM). *Life Sci.* (1997), 25: PL389-94.

192. Handy R.L., Harb H.L, Wallace P., Gaffen Z., Whitehead K.J., Moore P.K., Inhibition of nitric oxide synthase by 1-(2-trifluoromethylphenyl) imidazole (TRIM) *in vitro*: antinociceptive and cardiovascular effects. *Br. J. Pharmacol*. (1996), 119: 423-431.

193. Inoue M., Sato E.F., Nishikawa M., Hiramoto K., Kashiwagi A., Utsumi K., Free radical theory of apoptosis and metamorphosis. *Redox Rep*. (2004), 9: 237-47.

194. Rudneva I.I., Antioxidant system of Black Sea animals in early development. *Comp. Biochem. Physiol*. (1999), 265-271.

195. Dandapat J., Chainy G.B., Rao K.J., Lipid peroxidation and antioxidant defence status during larval development and metamorphosis of giant prawn, *Macrobrachium rosenbergii*. *Comp. Biochem. Physiol*. (2003), 221-233.

196. Menon J., Rozman R., Oxidative stress, tissue remodeling and regression during amphibian metamorphosis. *Comp. Biochem. Physiol*. (2007), 625-631.

197. Amoresano A., Chiappetta G., Pucci P., d'Ischia M., Marino G., Bidimensional tandem mass spectrometry for selective identification of nitration sites in proteins. *Anal. Chem*. (2007), 79: 2109-2117.

198. Nieto M.A., The snail superfamily of zinc-finger transcription factors. *Nat. Rev*. *Mol*. *Cell Biol*. (2002), 3: 155-166.

199. Barrallo-Gimeno A., Nieto M.A., The snail genes as inducers of cell movement and survival: implications in development and cancer. *Development* (2005), 13: 23151-3161.

200. Corbo J.C., Erives A., Di Gregorio A., Chang A., Levine M., Dorsoventral patterning of the vertebrate neural tube is conserved in a protochordate. *Development* (1997), 124: 2335-2344.

201. Fujiwara S., Corbo J.C., Levine M., The snail repressor establishes a muscle/notochord boundary in the *Ciona* embryo. *Development* (1998), 125: 2511-2520.

202. Dominguez D., Montserrat-Sentis B., Virgos-Soler A., Guaita S., Grueso J., Porta M., Puig I., Baulida J., Franci C., Garcia de Herreros A., Phosphorylation regulates the subcellular location and activity of the snail transcriptional repressor. *Mol. Cell Biol*. (2003), 23: 5078-5089.

203. Pinzar E., Wang T., Garrido M.R., Xu W., Levy P., Bottari S.P., Angiotensin II induces tyrosine nitration and activation of ERK1/2 in vascular smooth muscle cells. *FEBS Lett*. (2005), 579: 5100-5104.

204. Narang H., Dhariwala F.A., Krishna M., Effect of nitric oxide donor and gamma irradiation on modifications of ERK and JNK in murine peritoneal macrophages. *J. Cell Commun. Signal*. (2007), 1: 219-226.

205. Kinjo N., Kawanaka H., Akahoshi T., Yamaguchi S., Yoshida D., Anegawa G., Konishi K., Tomikawa M., Tanoue K., Tarnawski A., Hashizume M., Maehara Y., Significance of ERK nitration in portal hypertensive gastropathy and its therapeutic implications. *Am. J. Physiol. Gastrointest. Liver Physiol*. (2008), 295: G1016-G1024.

206. Kohno M., Pouyssegur J., Targeting the ERK signaling pathway in cancer therapy. *Ann. Med*. (2006), 38: 200-211.

207. Yemets A.I., Krasylenko Y.A., Lytvyn D.I., Sheremet Y.A., Blume Y.B., Nitric oxide signaling *via* cytoskeleton in plants. *Plant Science* (2011), 181: 545-554.

208. Sandau K.B., Gantner F., Brune B., Nitric oxide-induced F-actin disassembly is mediated via cGMP, cAMP and protein kinase A activation in rat mesangial cells. *Exp. Cell. Res.* (2001), 271: 329-336.

209. He Y., Yu W., Baas P.W., Microtubule reconfiguration during axonal retraction induced by nitric oxide. *J. Neurosci.* (2002), 22: 5982-5991.

Ringraziamenti

Desidero ringraziare la Prof.ssa Gabriella Tedeschi, mia relatrice di tesi, e il Professore Armando Negri per la disponibilità dimostratami, e per avermi dato la possibilità di proseguire ulteriormente il mio percorso di studi. Li ringrazio vivamente per avermi dato fiducia durante questi anni permettendomi di conoscere l'importanza dell'impegno e della perseveranza necessari a svolgere le attività di ricerca scientifica.

Vorrei inoltre ringraziare i miei genitori e la mia famiglia (gatti inclusi) per il costante supporto e per essermi stati sempre vicini.

Un grazie ai miei amici-colleghi di laboratorio per questi anni che avete reso speciali.

Un GRAZIE particolare a Moira, Flavia, Silvia e a tutti gli amici che mi sono stati vicino e per i weekend imprevedibili passati insieme. Loro sanno perché.

Infine ringrazio Fabio per aver scelto di intraprendere insieme questa lunga strada. Grazie.